P.PORTO

ESCOLA SUPERIOR DE SAÚDE

M MESTRADO

BIOQUÍMICA EM SAÚDE

Deciphering the influence of CD276 glycocode in colorectal cancer immunomodulation

Mariana Moura Magalhães

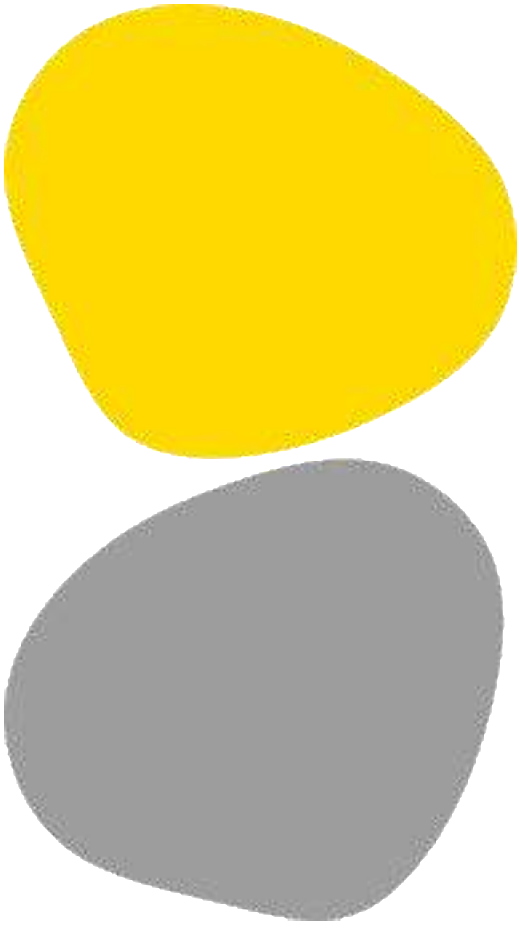

07/**2025**

Deciphering the Influence of CD276 glycocode in colorectal cancer immunomodulation

Autor

Mariana Magalhães

Orientador(es)

PhD/Andreia Peixoto/CI-IPOP; RISE; i3s

PhD/José Alexandre Ferreira/ CI-IPOP

MD, PhD /Lúcio Lara Santos/ ICBAS-UP; UFP; CI-IPOP

PhD/Ricardo Ferraz/ESS-IPP

Dissertação/Projeto/Relatório de Estágio apresentada(o) para cumprimento dos requisitos necessários à obtenção do grau de Mestre em ***Bioquímica em Saúde – Bioquímica Clínica e Metabólica*** *pela Escola Superior de Saúde do Instituto Politécnico do Porto.*

Financial support

Dissertation carried out with the financial support of the principal researcher contract 2022.08311.CEECIND (José Alexandre Ferreira), junior researcher contract 2023.06366.CEECIND (Andreia Peixoto), and the Portuguese Oncology Institute of Porto—Research Centre (CI-IPOP-29–2014; CI-IPOP-58–2015).

Contribution to the planning and execution of the following research activity throughout the year in which this Master's Thesis was developed.

Poster presentation

Magalhães, M., Dourado-Gonçalves, M., Ferreira, D., Relvas-Santos, M., Miranda, A., Afonso, LP., Santos, LL., Peixoto, A. and Ferreira, JA. Deciphering the Influence of CD276 glycocode in Gastric Cancer Immunoregulation. 2nd Young Research's Day, IPO-PORTO

Oral communication

Magalhães, M., Dourado-Gonçalves, M., Santos, LL., Peixoto, A. and Ferreira, JA. Deciphering the Influence of CD276 glycocode in Gastric Cancer Immunoregulation. IJUP 2025: Encontro de Investigação Jovem, Universidade do Porto

Co-authorship in an original article submitted to the 'Advanced Science' journal (Annex I)

Soares, J., Ferreira, D., Gonçalves, M., Miranda, A., Relvas-Santos, M., Brandão, A., Paulo, P., Cotton, S., Freitas, R., Magalhães, M., Ferreira, E., Santos, B., Afonso, LP., Silva, AMN., Palmeira, C., Amado, F., Peixoto, A., Santos, LL., and Ferreira, JA. CD276 immature glycosylation drives colorectal cancer aggressiveness and T-cell mediated immune escape. Preprint, submitted at 3rd august 2025, https://doi.org/10.1101/2025.08.01.668091

Preliminary Note

I hereby declare that the preliminary functional assays concerning proliferation and invasion capacity of SW480 and SW620 cell lines with CD276 silencing were originally performed and presented by Eliana Soares to the University of Porto as part of her PhD in Biomedical Sciences. These preliminary results are included in this thesis with her knowledge and consent, as well as from her main PhD supervisor and the corresponding author of the envisioned publication. My contribution consisted in replicating these experiments and increasing the sample size (N) in order to obtain statistically significant results suitable for publication. The results presented in this thesis reflect both the original data and the expanded data generated in the course of my master's research.

Agradecimentos

Termino esta etapa com um profundo sentimento de realização e uma enorme felicidade. Foi um longo caminho cheio de altos e baixos, mas reconheço que um caminho assim não se faz sozinho. Muitas pessoas fizeram parte desta minha caminhada e a todas sou imensamente grata por terem estado lá.

Em primeiro lugar, gostaria de agradecer à minha orientadora, a Doutora Andreia Peixoto, por todo o apoio e dedicação ao longo deste ano. Obrigada por toda a paciência, pelos conselhos valiosos e pelos conhecimentos transmitidos, que foram fundamentais para o meu crescimento académico e para o meu desenvolvimento enquanto cientista.

Ao meu coorientador, José Alexandre Ferreira, agradeço pelo valioso conhecimento partilhado ao longo deste ano e pela confiança depositada em mim e nas minhas capacidades. Obrigada por todo o apoio, orientação e inspiração ao longo desta etapa.

Ao Prof. Doutor Lúcio Lara Santos, agradeço enquanto coordenador do Grupo de Patologia e Terapêutica Experimental (GPTE), por me ter acolhido e proporcionado a oportunidade de realizar este projeto e esta tese.

A todos os meus colegas do GPTE, quero expressar um sincero agradecimento pelo acolhimento e dedicação desde o primeiro dia. Obrigada por me terem recebido tão bem, pelo apoio constante e pelo exemplo de profissionalismo e companheirismo que demonstraram ao longo deste ano. Obrigada, Eduardo, pela disponibilidade e ajuda da sala de culturas; Dylan, por me esclareceres todas as dúvidas que surgiam sempre com paciência e disponibilidade; Rafa, que mesmo tendo estado menos tempo, foi uma ajuda preciosa; Bia, por todo o apoio e constante disponibilidade para ajudar em qualquer dúvida; Roberto por toda a ajuda com a parte estatística e toda a boa disposição; Janine, pela partilha de conhecimento e disponibilidade para ajudar; e Mariana, que, mesmo não tendo um trabalho relacionado, estiveste sempre pronta para ajudar. Obrigada, também aos meus colegas Daniela, Renato, Susana e ao Doutor Luís Lima. Em geral, obrigada por toda a boa disposição, companheirismo e bom ambiente que existiu todos os dias no laboratório.

Não me posso deixar de mencionar aqueles que se cruzaram comigo, por menos tempo e no início desta etapa: Rui e Martina. Obrigada a ambos pelo conhecimento transmitido. Obrigada, em especial a ti, Martina, foste uma verdadeira mentora para mim, partilhando ensinamentos essenciais a vida no laboratório, que levarei sempre comigo. A tua simpatia, disponibilidade e preocupação marcaram, sem dúvida, esta experiência.

Às minhas amigas e colegas, as duas Maria João, quero agradecer por todo o apoio incondicional que me deram ao longo deste ano. A vossa amizade foi um presente inesperados e essencial nesta etapa. Foi um

privilégio partilhar convosco tantos momentos, desafios e conquistas. Obrigada por me ouvirem sempre, mesmo nos meus desabafos quando as coisas não corriam como esperado. Gostei imenso de vos conhecer e espero levar-vos comigo além desta etapa.

Obrigada a todos os meus amigos, em especial à minha Ritinha, que tem sido uma presença constante e insubstituível desde o início da minha vida universitária. Mesmo quando seguimos caminhos diferentes no mestrado, nunca deixou de estar ao meu lado, apoiando-me de forma incondicional. Obrigada por todo o teu carinho, pela tua compreensão e por nunca hesitares em ajudar mesmo nos dias mais difíceis. Sou grata por ter alguém como tu ao meu lado, partilhando não só as dificuldades, mas também todas as alegrias.

Por último, quero agradecer à minha família: mãe, pai, Inês e Tiago. Obrigada por me aturarem com tanta paciência ao longo desta caminhada e por todo o apoio incondicional que sempre me deram. Sei que nem sempre é fácil lidar com as minhas ansiedades, dúvidas e momentos de stress, mas nunca deixaram de acreditar em mim e de me incentivar a seguir em frente. A vossa compreensão, carinho e presença foram fundamentais para que eu conseguisse ultrapassar cada desafio e chegar até aqui.

Um grande obrigada a todos, sem vocês isto não seria possível.

Resumo

O cancro colorretal (CCR) é uma das principais causas de morbilidade e mortalidade oncológica a nível mundial, sendo que os subtipos mais agressivos apresentam frequentemente resistência às terapias convencionais. A proteína de checkpoint imunitário CD276 (B7-H3) encontra-se altamente expressa no CCR e está associada a um pior prognóstico, progressão tumoral e evasão imunitária. O CD276 sofre uma extensa glicosilação, uma modificação que influencia a estabilidade, a localização e as interações imunitárias da proteína, mas a função específica da sua glicosilação no CCR não é clara.

Este estudo avalia o impacto da *O*-glicosilação imatura do CD276 na agressividade do CCR. Para representar a glicosilação aberrante típica de células cancerígenas, foi realizado o *knockout* da enzima *C1GALT1* em células de CCR, resultando numa *O*-glicosilação de cadeia curta. Foi também verificado os efeitos do *knockdown* do CD276 através do silenciamento por RNA de interferência (siRNA) na proliferação e invasão através de ensaios de BrdU ELISA e invasão com Matrigel, respetivamente. Além disso, foram realizados ensaios de proteómica e fosfoproteómica para explorar a forma como o CD276 influencia as vias de sinalização oncogénica.

Os nossos resultados revelam que a *O*-glicosilação aberrante e imatura do CD276 promove a proliferação e invasão de células de CCR através da manutenção de networks biossintéticas e de fosforilação oncogénicas. Por outro lado, a ausência do CD276 neste contexto, ativou respostas de stress que envolvem o processamento do RNA, reparação do DNA e reorganização mitocondrial, destacando o CD276 como um condutor dependente da glicosilação da agressividade do CCR e um potencial alvo terapêutico.

Palavras-chave: Cancro colorretal; CD276; *O*-glicosilação; checkpoint imunitário.

Abstract

Colorectal cancer (CRC) remains a major contributor to cancer-related illness and death worldwide, with aggressive subtypes often resistant to conventional therapies. The immune checkpoint protein CD276 (B7-H3) is highly expressed in CRC and is associated with poor prognosis, tumour progression, and immune evasion. CD276 undergoes extensive glycosylation, a modification that influences protein stability, localisation, and immune interactions, yet the specific roles of its glycosylation in CRC are not well understood.

This study examines how immature *O*-glycosylation of CD276 affects CRC aggressiveness. To model the altered glycan landscape typical of cancer cells, *C1GALT1*-knockout CRC cells, which lack the enzyme necessary for *O*-glycan elongation, were used. The effects of CD276 knockdown using small interfering RNA (siRNA) on cell proliferation and invasion were assessed by BrdU ELISA and Matrigel invasion assays, respectively. Additionally, proteomic and phosphoproteomic analyses were conducted to explore how CD276 influences oncogenic signalling pathways.

Our findings reveal that aberrant, immature *O*-glycosylation of CD276 promotes CRC cell proliferation and invasion by sustaining oncogenic biosynthetic and phosphorylation networks. Conversely, CD276 depletion activates stress responses involving RNA processing, DNA repair, and mitochondrial reorganisation, highlighting CD276 as a glycosylation-dependent driver of CRC aggressiveness and a potential therapeutic target.

Keywords: Colorectal cancer; CD276; *O*-glycosylation; immune checkpoint

Abbreviations/Acronyms

ACN	Acetonitrile
ADC	Antibody-drug conjugate
AGC	Automatic Gain Control
AKT	Protein Kinase B
ATCC	American Type Culture Collection
ATP	Adenosine triphosphate
B3GnT/C3GnT	Core 3 synthase
BrdU	5-bromo-2'-deoxyuridine
C2GnT	Core 2 synthase
CAR-T	Chimeric antigen receptor T cell
cDNA	Complementary DNA
CEA	Carcinoembryonic Antigen
CIMP	CpG Island Methylator Phenotype
CRC	Colorectal cancer
CTL	Cytotoxic T Lymphocyte
DAPI	4',6-diamidino-2-phenylindole
DC	Dendritic cell
DC-SIGN	Dendritic cell-specific ICAM-3-grabbing non-integrin
DNA	Deoxyribonucleic acid
DTT	Dithiothreitol
EDTA	Ethylenediaminetetraacetic acid
EGFR	Epidermal growth factor receptor
EMT	Epithelial-mesenchymal transition
ER	Endoplasmic reticulum
ERK	Extracellular signal-regulated kinase
ESCC	Esophageal Squamous Cell Carcinoma
FAP	Familial adenomatous polyposis
FBLN2	Fibulin-2
FBS	Fetal bovine serum
FDR	False Discovery Rate
FdUMP	5-fluoro-2'-deoxyuridine 5'-monophosphate
FGFR2	Fibroblast Growth Factor Receptor 2
FOBT	Faecal occult blood test
FUT8	Fucosyltransferase 8
Gal	Galactose
GalNAc	N-acetylgalactosamine
GALNT2	Polypeptide N-acetylgalactosaminyltransferase 2
GAPDH	Glyceraldehyde-3-Phosphate Dehydrogenase
GlcNAc	N-acetylglucosamine
GO	Gene ontology
HCD	High-energy collision dissociation
ICI	Immune checkpoint inhibitor
IFN-γ	Interferon gamma
IL	Interleukin
kNN	k-Nearest Neighbours
KO	Knockout

KSEA	Kinase-Substrate Enrichment Analysis
LC-MS/MS	Liquid Chromatography-Tandem Mass Spectrometry
LS	Lynch syndrome
mAb	Monoclonal antibody
MGAT3	N-acetylglucosaminyltransferase III
MGL	Macrophage Galactose-type Lectin
MMR	Mismatch repair
MMRd	Mismatch repair deficiency
mRNA	Messenger RNA
MS	Mass spectrometry
MSI	Microsatellite instability
MSS	Microsatellite stability
mTOR	Mechanistic target of rapamycin
MUC1	Mucin 1
MUC2	Mucin 2
$Na_4P_2O_7$	Tetrasodium pyrophosphate
NADH	Nicotinamide Adenine Dinucleotide (reduced)
NaF	Sodium Fluoride
$NaVO_3$	Sodium metavanadate
NF-kB	Nuclear Factor kappa B
NK cell	Natural killer cell
OGT	O-GlcNAc transferase
OSCC	Oral Squamous Cell Carcinoma
PBS	Phosphate Buffered Saline
PCA	Principal component analysis
PD-1	Programmed cell death protein 1
PD-L1	Programmed cell death ligand 1
PET	Polyethylene terephthalate
PFA	Paraformaldehyde
PI3K	Phosphoinositide 3-kinase
PMSF	Phenylmethylsulfonyl fluoride
PPI	Protein-protein interaction
RT-PCR	Reverse transcription polymerase chain reaction
RNA	Ribonucleic acid
SDC	Sodium Deoxycholate
SDS-PAGE	Sodium Dodecyl Sulphate Polyacrylamide Gel Electrophoresis
siRNA	Small interfering RNA
snRNA	Small nuclear RNA
TACAs	Tumour-associated carbohydrate antigens
TAM	Tumour-associated macrophage
TBS	Tris-buffered saline
TBS-T	Tris-buffered saline with Tween-20
TFA	Trifluoroacetic Acid
TNBC	Triple-negative breast cancer
TNF-α	Tumour Necrosis Factor alpha
TNM	Tumour-node-metastasis
TREML2	Trem-like transcript 2
UHPLC	Ultra-High-Performance Liquid Chromatography

VEGF	Vascular endothelial growth factor
WT	Wild type

Table of contents

1. Introduction

1.1. Colorectal Cancer

1.1.1. Epidemiology and risk factors

Cancer remains one of the most significant global health challenges, with incidence rates rising in recent years. In 2022, approximately 20 million new cancer cases and 9.7 million cancer-related deaths were reported worldwide. According to GLOBOCAN data, lung cancer was the most common and deadliest cancer type (1). Other leading cancers by incidence and mortality include breast (female), colorectal, prostate, gastric, liver, thyroid, cervical, and bladder cancers. These numbers are projected to increase further due to population growth and ageing (1).

Colorectal cancer (CRC) is the third most commonly diagnosed cancer (9.6%) and the second leading cause of cancer-related death (9.3%) globally (Figure 1, 'High incidence and Mortality') (1). In Portugal, CRC was the most common malignancy in 2022, with approximately 10,575 new cases. The disease also remains a major cause of cancer mortality in the country, with a mortality rate (14.2%) exceeding the European average (12.5%) (2).

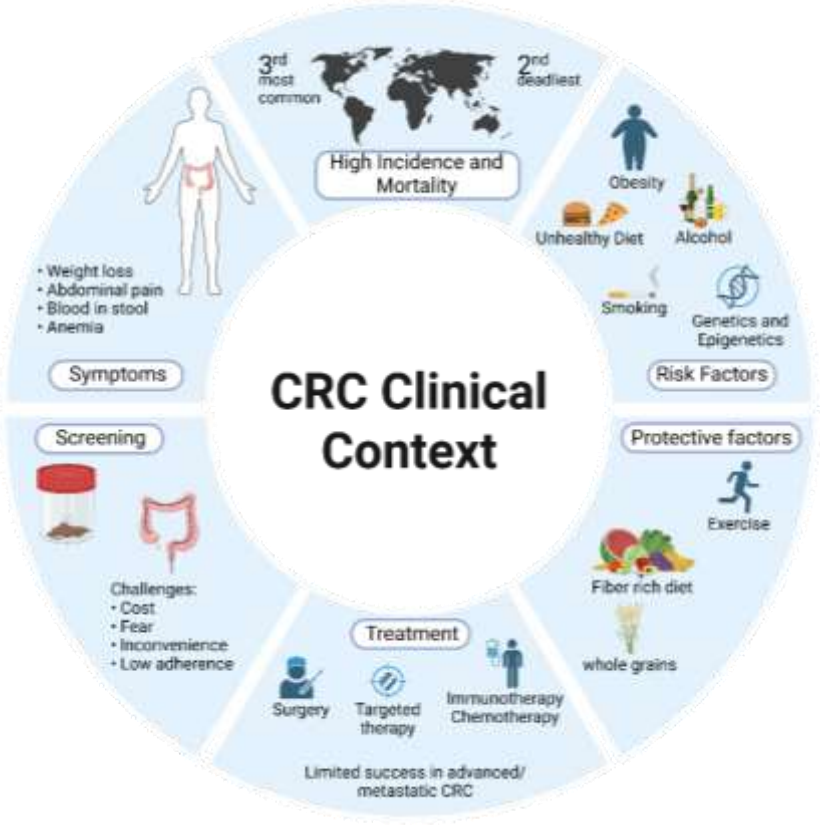

Figure 1. The clinical context of CRC. CRC poses a significant health challenge due to high prevalence, various risk factors, late diagnosis, and limited treatment success in advanced stages. Despite advances in prevention and screening, persistent barriers highlight the urgent need for innovation in detection and management. (Created in https://BioRender.com)

The most common clinical manifestations of CRC include unintended weight loss, decreased appetite, abdominal discomfort, tenesmus (the sensation of incomplete bowel evacuation), alterations in stool morphology or bowel habits, haematochezia (blood in stools), and rectal bleeding (Figure 1, 'Symptoms'). In younger individuals, chronic occult gastrointestinal bleeding may remain undetected, frequently resulting in anaemia (3).

Key risk factors for CRC include overweight and obesity, which are frequently related to sedentary behaviour and higher intake of animal-based foods, along with smoking and alcohol consumption. Conversely, physical activity and a diet rich in dairy products, fibre, and whole grains are associated with reduced CRC risk (Figure 1, 'Risk factors') (1, 4).

There has been an increasing incidence of CRC among young adults in high-income countries, a trend likely linked to rising rates of physical inactivity, obesity, and antibiotic use. In response, the recommended age for initial CRC screening has been lowered in some regions, now set at 45 years in the United States (1, 3).

The screening of CRC is a multi-step process that begins with non-invasive stool-based tests or direct visualisation procedures. These tests are designed to detect hidden blood in faeces, abnormal DNA, or suspicious lesions in asymptomatic individuals. If any test yields a positive or abnormal result, a follow-up colonoscopy is performed for definitive diagnosis, possible removal of polyps, or tissue sampling, with ongoing surveillance as needed. Early-phase screening is crucial for identifying lesions that may have been missed in previous testing rounds but have not yet progressed to advanced disease, thereby reducing the CRC incidence (5, 6). Notably, CRC incidence and mortality have declined in recent years, primarily due to population-based screening programs that enable the detection and removal of precancerous lesions (7, 8). Despite these advances, several challenges to screening adherence persist. These include a sense of personal invulnerability, cost, fear of diagnosis, lack of perceived benefit, aversion to handling stool samples, and the inconvenience of the process (Figure 1, 'Screening') (7).

Furthermore, CRC can have a genetic and/or epigenetic basis. Activation of oncogenes and inactivation of tumour suppressor genes are central mechanisms driving molecular diversity in cancer, rather than random mutation accumulation throughout cancer

progression (9). The CpG island methylator phenotype (CIMP) has been proposed as a distinct driver of CRC, but recent analyses suggest that somatic hypermethylation in tumours occurs gradually, and on an age-dependent basis (10). CpG island methylation can be observed in normal colonic cells as a function of ageing or in cancerous tissues associated with CIMP (11). In this context, the mutator phenotype, characterised by genetic alterations such as microsatellite instability (MSI) due to mismatch repair deficiency (MMRd), appears to play a more dominant role than epigenetic changes in influencing the phenotypic features of colon cancer (10–12).

While the majority of CRC cases are sporadic, resulting from acquired mutations and environmental risk factors, only a small percentage are due to inherited genetic syndromes (13). There are two main types of hereditary CRC: Familial Adenomatous Polyposis (FAP) and Lynch Syndrome (LS). Mutations in the *APC* gene, which impair its gatekeeper function and result in the development of multiple adenomatous polyps, are the main cause of FAP. When untreated, these polyps have a high risk of progressing to invasive lesions, like cancer. Individuals with FAP typically develop CRC at a young age, needing regular surveillance and, in some cases, surgical intervention (14, 15). Mutations in MMR genes, such as *MLH1* and *MSH2*, are associated with LS, resulting in an increased mutation rate in tumour cells and accelerated tumour progression (16). Individuals with LS often develop CRC directly from the accumulation of mutations in the colonic epithelium, with a more rapid progression to malignancy (17).

1.1.2. Diagnosis and Therapy

The faecal occult blood test (FOBT) is widely used as a non-invasive initial screening tool for CRC, as it detects hidden blood in stool through biochemical assays (5, 7). When FOBT has a positive result, further diagnostic evaluation is required. Colonoscopy is the gold standard diagnostic procedure in this context, as it allows direct visualisation of the colonic mucosa, enables polyp resection, and facilitates tissue biopsy for definitive histopathological analysis (5). Although colonoscopy is highly effective, it is an operator-dependent procedure that can be associated with patient discomfort, particularly in anatomically challenging regions (18). Sedation can help reduce discomfort but introduces logistical complexities. Alternative strategies, such as carbon dioxide insufflation or the use

of ultrathin scopes, may also minimise discomfort without compromising detection rates. The diagnostic accuracy of colonoscopy is closely linked to the expertise of the endoscopist. The information obtained through diagnostic procedures not only confirms the presence and extent of CRC but also serves as the foundation for selecting the most appropriate therapeutic strategies tailored to each patient's clinical and molecular profile. While early detection is crucial, surgical resection remains the primary therapeutic modality for localised CRC that has not metastasised (3). In cases where the tumour has penetrated the intestinal wall or metastasised to regional lymph nodes, systemic therapies, including chemotherapy and molecularly targeted agents, are frequently employed as adjuvant or neoadjuvant treatments (3, 19, 20). The management of metastatic CRC, particularly with unresectable liver metastases, has evolved to include diverse therapeutic strategies (Figure 1, 'Treatment'). Systemic chemotherapy now incorporates agents such as irinotecan and oxaliplatin, used in regimens like FOLFOX and FOLFIRI, often in combination with biologic agents like bevacizumab (anti-VEGF) and cetuximab (anti-EGFR) to enhance efficacy and improve survival rates (21-23). Following surgical resection of liver metastases, adjuvant chemotherapy is routinely recommended, though evidence supporting its benefits remains limited, with typical regimens lasting 4-6 months. Intra-arterial therapies, including hepatic arterial infusion and transarterial chemoembolization, provide localised treatment options, although their optimal use is still under investigation (20). The role of biologic therapies in the adjuvant setting remains uncertain and requires further evaluation in ongoing clinical trials (20, 24, 25).

For a subset of advanced CRC cases, particularly those with MMRd or MSI, immunotherapy has emerged as a highly effective treatment option, demonstrating significant clinical benefit. Recent studies have shown that immune checkpoint inhibitors (ICIs) can achieve a median overall survival of 65.4 months and a median progression-free survival of 37.9 months in patients with MMRd/MSI advanced CRC (19). However, immunotherapies targeting the PD-1/PD-L1 axis in CRC are only successful in MSI tumours, which account for 15% of all CRC patients (17). Conversely, immunotherapy is not effective for microsatellite-stable (MSS) and proficient MMR (Figure 1, 'Treatment') (26-28). Therefore, it is essential to find novel immune evasion targets to develop new targeted therapies.

1.2. CD276 in tumour biology and its therapeutic potential

In cancer, the interplay between tumour cells and the immune system is a decisive factor in disease progression and therapeutic response (26). As mentioned before, despite advances in immunotherapy, many patients with CRC do not benefit from current ICIs, especially those with MSS tumours. This highlights the urgent need to identify additional immunoregulatory molecules that contribute to immune evasion and tumour aggressiveness. Among the emerging candidates, CD276 has attracted significant attention due to its high expression in colorectal tumours, association with poor prognosis, and multifaceted roles in both immune regulation and tumour biology (29). Understanding the functions and therapeutic potential of CD276 is therefore highly relevant to the quest for improving outcomes in CRC.

1.2.1. CD276 (B7-H3): a multifaceted player in colorectal cancer progression

CD276, also called B7-H3, is a member of the B7 family and functions as a type I transmembrane glycoprotein encoded by the *CD276* gene on chromosome 15. It plays an essential role in T cell-mediated immune responses (30, 31). Structurally, CD276 comprises three domains: an extracellular domain, a transmembrane domain and a short intracellular domain. The extracellular domain defines the two isomers of CD276 by the number and arrangement of immunoglobulin-like domains they possess. The 4Ig-B7-H3 isomer contains four Ig-like domains, organised as two tandem IgV-IgC pairs, resulting from exon duplication in the human gene. In contrast, the 2Ig-B7-H3 isomer has only two Ig-like domains, one IgV-like and one IgC-like, which is the predominant form in mice and also present in humans (32). Despite extensive research, the precise mechanism of action of CD276 remains unclear, and findings in the literature are often conflicting.

High CD276 expression is associated with an increased risk of distant metastasis, tumour recurrence, and poor survival of CRC patients (29, 33). This glycoprotein was strongly associated with tumour invasion and advanced TNM stages, suggesting that it reflects aggressive pathological characteristics of this cancer (34). Furthermore, CRC patients exhibit higher circulating levels of soluble CD276 compared to healthy individuals (35).

Recurrent tumours frequently show increased CD276 expression, which not only raises the risk of relapse but also impairs the effectiveness of DNA-damaging agents, potentially through mechanisms such as CD276-mediated aerobic glycolysis (33).

Beyond its immunological functions, CD276 is implicated in several non-immunological processes that contribute to tumour progression. Recent studies have elucidated the multifaceted oncogenic roles of CD276 in various experimental models. Specifically, CD276 has been shown to enhance tumour cell metabolism by promoting the Warburg effect in breast cancer cell lines (36). Additionally, CD276 facilitates angiogenesis and promotes epithelial-mesenchymal transition (EMT) in CRC cell lines (37, 38). Its involvement in supporting tumour cell invasion and migration has also been reported in CRC cell lines (39). Furthermore, an association between CD276 expression and resistance to apoptosis has been observed in patient-derived samples of renal cell carcinoma (40), suggesting a multifaceted role in cancer.

1.2.2. Diverse oncogenic and immune-evasive roles of CD276

A complex regulatory network of immunological checkpoints delivers both activating and inhibitory signals, modulating immune responses crucial for the elimination of cancer cells. Among these, CD276 is recognised as an immune checkpoint molecule and is implicated in tumour immune evasion (Figure 2) (31, 41). However, the mechanisms underlying its aberrant expression and function remain largely unknown (42).

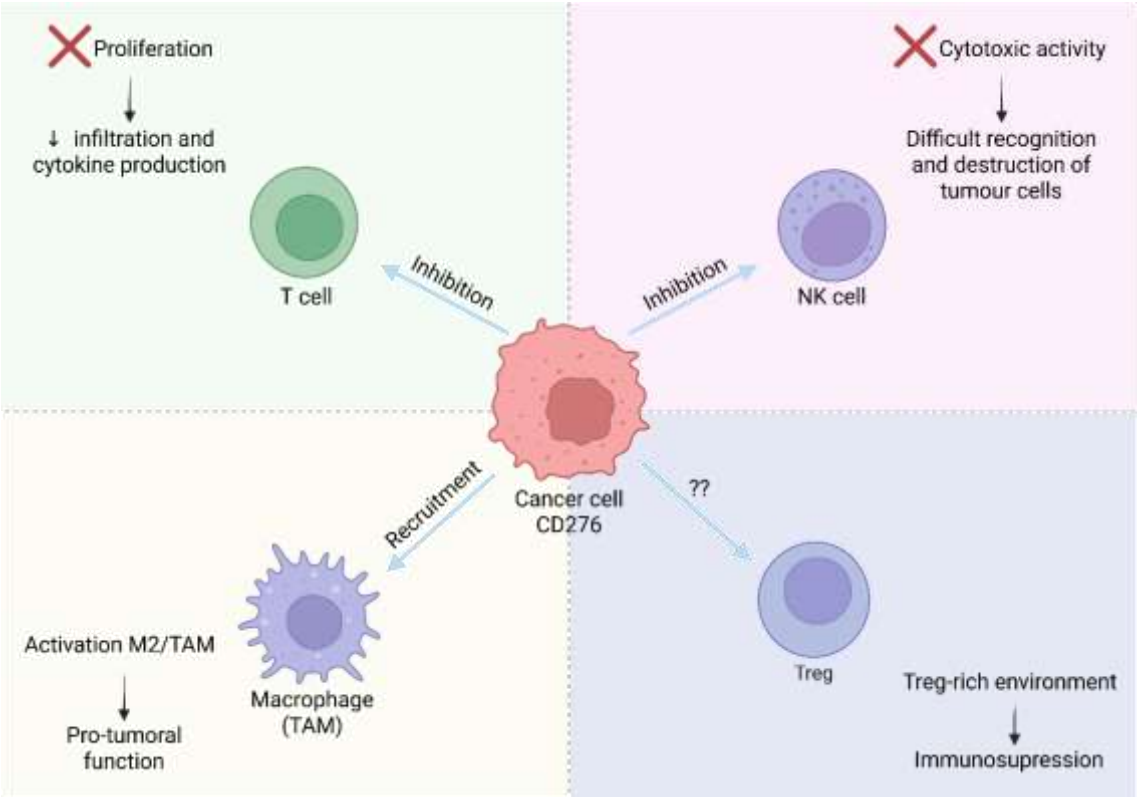

Figure 2. CD276 as an immune checkpoint. CD276 orchestrates an immunosuppressive tumour microenvironment by interacting with immune cells. CD276 inhibits T cell proliferation, leading to reduced

infiltration and cytokine production, thereby weakening the anti-tumour immune response. CD276 suppresses NK cell cytotoxic activity, making it more difficult for these cells to recognise and destroy tumour cells. CD276 promotes the recruitment and polarisation of macrophages toward a pro-tumour (M2/TAM) phenotype, enhancing tumour growth and immune suppression. Although the precise mechanism remains unclear, high CD276 expression is associated with higher Treg infiltration, suggesting an indirect role in promoting immunosuppression.
(Created in https://BioRender.com)

Unlike other B7 family members, the natural, definitive receptor for human CD276 remains elusive and controversial. While CD276 is established as a co-stimulatory or co-inhibitory ligand, its precise receptor on immune cells, especially human T cells, has not been clearly defined, in contrast to the well-characterised PD-1/PD-L1 interaction. Early studies proposed TREML2 as a candidate receptor, with evidence from mouse models indicating that CD276-TREML2 interaction could enhance IL-2 and IFN-γ production in T cells (43). However, subsequent research, including studies in human systems, has failed to confirm this interaction, and biophysiological assays have not detected binding between CD276 and TREML2, suggesting species- and context-specific discrepancies and highlighting the importance of model specificity (44). More recently, IL20RA has been identified through high-throughput screening as a potential CD276 binding partner, but this finding is preliminary and requires further validation in human cells (45).

The lack of a consistently identified, broadly accepted receptor for CD276 contributes significantly to the complexity and sometimes contradictory nature of its functional roles. This ambiguity may explain why CD276 can exert both immunostimulatory and immunosuppressive effects, possibly depending on cellular context, tumour type, or the presence of multiple, less-defined binding partners (44, 46). It also raises the possibility that some effects attributed to CD276 may result from indirect signalling pathways or non-immune mechanisms, rather than direct receptor engagement.

Functionally, CD276 has been shown, in some contexts, to enhance tumour immunogenicity by stimulating $CD8^+$ T cell responses and promoting the rapid expansion of P1A-specific cytotoxic T lymphocytes (CTLs) *in vivo* in the mouse P815 tumour line, particularly during the expansion phase of T cell responses (46). However, more recent findings, in pancreatic and colorectal cancers, indicate that CD276 facilitates immune escape by suppressing the production of IFN-γ, IL-2, IL-10, and IL-13 within the tumour microenvironment, leading to reduced $CD4^+$ and $CD8^+$ T cell responses and correlating with decreased $CD8^+$ T cell infiltration and poorer patient survival (41, 47). CD276 appears to interact with inhibitory receptors on human T cells, resulting in a marked downregulation of

T cell responses, where costimulatory molecules are typically scarce, further supporting an immunosuppressive role for CD276 (44). Furthermore, it functions as a negative regulator in tumour immunity by inhibiting the cytotoxic activity of natural killer (NK) cells and $CD8^+$ T cells, supporting its role in tumour immune evasion and suggesting that targeting the CD276 checkpoint, either alone or in combination with PD-1 blockade, may represent a novel immunotherapeutic strategy against cancer (48). Moreover, an *in vivo* study demonstrated that IFN-γ upregulated CD276 expression on antigen-presenting cells, while CD276 engagement with its receptor established a negative feedback mechanism during the amplification phase of T helper 1 responses (49).

Beyond direct immune modulation, CD276 is also involved in non-immune pathways that promote tumour progression. For example, miR-34a has been shown to upregulate CD276, which in turn stimulates TNF-α production, promoting tumour immune evasion and growth in CRC (42). CD276 also plays a pivotal role in the recruitment of tumour-associated macrophages (TAMs), supporting tumour progression and suppressing anti-tumour T cell activity, in part by modulating plasminogen activator inhibitor-1 (PAI-1) within the tumour microenvironment (50).

Additionally, CD276 contributes to therapeutic resistance in cancer. For instance, *Sun et al.* (51) demonstrated that IL-8 upregulates PD-L1 expression in gastric cancer cells, thereby conferring drug resistance. This IL-8-mediated effect concurrently enhances CD276 expression, which promotes cell migration via activation of the AKT/c-Myc/mTOR pathway (52, 53). In CRC, *Lu et al.* (29) observed CD276 and PD-L1 co-expression in 5.7% of patients, a dual checkpoint signature associated with tumour microenvironment remodelling, immune evasion, and diminished efficacy of anti-PD1/PD-L1 ICIs.

Mechanistically, CD276 induces chemoresistance through multiple pathways. It stimulates the PI3K-AKT signalling cascade, increasing production of the DNA repair protein XRCC1, which enhances resistance to oxaliplatin in CRC cells (54). Additionally, CD276 activates the EGFR/ERK signalling axis to drive chemoresistance (33).

In summary, the controversy surrounding the receptor for CD276, combined with its context-dependent effects on both immune pathways, highlights the complexity of its role in cancer biology. This underscores the necessity for model-specific interpretation and further research to clarify its mechanisms and therapeutic potential.

1.2.3. Therapeutic strategies targeting CD276 in cancer

CD276 has emerged as a critical therapeutic target due to its dual role in promoting tumour progression and facilitating immune evasion. This glycoprotein is implicated in multiple oncogenic processes, including tumour growth, metastatic dissemination, resistance to immunotherapies and modulation of the tumour microenvironment. Its capacity to suppress adaptive immunity, by reducing T cell activation and proliferation in non-malignant tissues and attenuating immune responses against tumour antigens in malignant tissues (30), highlights its multifaceted involvement in both immune and non-immune oncogenic mechanisms.

The widespread and differential expression of CD276 on tumour cells positions it as an attractive target for novel therapeutic interventions, with the potential applicability to an extensive spectrum of cancer patients, including those with CRC. Despite the absence of approved CD276-targeted therapies and the lack of knowledge of its receptor, accumulating evidence underscores its therapeutic target potential (29, 37, 55). Preclinical studies demonstrate that antibody-mediated CD276 blockade enhances CD8+ T cell infiltration and activation, reducing tumour progression and metastasis, particularly in MSS CRC models (41, 56).

Antibody-based therapies, particularly monoclonal antibodies (mAbs), are under development to neutralise CD276 immunosuppressive signalling and restore anti-tumour immunity (57). Preclinical studies reveal that such blockade reactivates CD8+ T cells and NK cells, restoring immune surveillance (48, 58). Building on this approach, antibody-drug conjugates (ADCs), which leverage anti-CD276 mAbs to deliver cytotoxic agents directly to tumour cells, have shown efficacy in preclinical models of CRC and non-small cell lung cancer. These ADCs inhibit tumour proliferation, reactivate immune cells within the tumour microenvironment and minimise systemic toxicity (59, 60).

Chimeric antigen receptor T (CAR-T) cell therapy further expands the therapeutic landscape by engineering patient-derived T cells to express CD276-specific receptors, enabling selective targeting and elimination of CD276-positive tumour cells. This approach has shown potent activity in preclinical models of solid tumours, underscoring its translational potential (61).

Indirect targeting strategies focus on modulating CD276 expression or post-translational modifications. For example, inhibition of fucosyltransferase 8 (FUT8), an enzyme responsible for the core fucosylation of CD276, reduces its membrane stability and

promotes lysosomal degradation. The small-molecule inhibitor FDW028 exemplifies this approach, suppressing CRC progression by destabilising CD276 (62).

Combination therapies are being explored to maximise therapeutic efficacy. Co-targeting CD276 and PD-1/PD-L1 pathways enhances anti-tumour immunity, while synergistic effects with angiogenesis inhibitors, such as bevacizumab, or NF-kB inhibitors, such as BAY11-7082, exploit CD276's role in the NF-kB/VEGFA signalling axis (37). Additionally, CD276 deficiency potentiates chemotherapy agents like paclitaxel and immunotherapy in ovarian cancer models, although complex biological interactions remain to be fully elucidated (63). Also, radiotherapy upregulates CD276 expression in CRC, and its blockade amplifies radiation-induced neoantigen-specific T cell responses (56). Furthermore, innovative delivery platforms, such as lipid nanoparticles co-encapsulating apigenin, FdUMP and anti-CD276 antibodies, demonstrate enhanced tumour growth inhibition and biosafety in CRC models (64).

Collectively, these strategies underscore the central role of CD276 in cancer biology and its promise as a therapeutic target. Further research into CD276 glycoproteoforms, their functional impact on immunomodulation, and clinical validation of emerging therapies will be essential to translate preclinical insights into effective, personalised CRC treatments.

1.3. Glycosylation: a fundamental post-translational modification in cancer biology

Glycosylation, the enzymatic addition of diverse glycan structures to proteins and lipids, is one of the most common and structurally complex post-translational modifications, estimated to affect approximately half of all eukaryotic proteins (65, 66). This intricate process is broadly categorised into two primary types based on their linkage: *N*-glycosylation and *O*-glycosylation. *N*-glycans are covalently attached to the nitrogen atom of asparagine residues within a specific Asn-X-Ser/Thr consensus sequence, where "X" is any amino acid except proline. In contrast, *O*-glycans are linked via the oxygen atom of serine or threonine residues (66). While *N*-glycosylation is generally more extensively characterised, *O*-glycosylation, owing to its greater structural diversity and the absence of a universal consensus sequence, remains comparatively less understood.

Glycosylation plays a crucial role in myriad biological processes, including protein folding, stability, intracellular trafficking, cell-cell recognition, cellular signalling, and immune responses (65, 67, 68). Consequently, defects or alterations in either *N*-glycosylation or *O*-

glycosylation are frequently associated with a wide range of pathologies, notably impacting cancer progression and invasiveness (65, 69, 70). Within the context of CRC, aberrant glycosylation patterns are now recognised as a fundamental molecular hallmark, profoundly influencing tumour biology, immune interactions, and clinical manifestations (71, 72). Among the glycoproteins affected, CD276 undergoes extensive glycosylation (73), a modification known to influence protein stability, localisation, and immune interactions. However, the specific roles of its *O*-glycosylation in CRC are not yet fully elucidated.

1.3.1. Aberrant *N*-glycosylation in colorectal cancer

N-glycosylation is consistently and significantly altered in CRC, contributing to diverse aspects of tumour progression and immune evasion. Tumour tissues frequently exhibit distinct *N*-glycan profiles, including reduced levels of bisecting *N*-acetylglucosamine (GlcNAc) and increased expression of sialylated Lewis epitopes, sulphated glycans, and paucimannosidic structures (71, 74). These modifications can destabilise protein structure and function, and actively remodel the extracellular matrix, promoting malignancy. For example, the loss of an *N*-glycosylation site in Fibulin 2 (FBLN2) due to alternative splicing leads to protein misfolding, reduced secretion and the development of a pro-metastatic fibronectin-rich matrix (75). Similarly, aberrant glycosylation, such as decreased *N*-glycosylation at APMAP-N196, has been shown to accelerate CRC progression (74).

Beyond its direct effects on tumour cell behaviour, altered *N*-glycosylation also plays a critical role in impairing CRC responsiveness to immune surveillance. Notably, defective glycosylation of the IFN-γ receptor α subunit destabilises the receptor and promotes its degradation, leading to cellular resistance to immune-mediated cytotoxicity. This specific defect, characterised by the presence of high-mannose rather than complex glycan structures, often arises from the downregulation of MGAT3 and is recognised as a prevalent mechanism of immune escape in CRC. Crucially, restoration of MGAT3 function can rescue receptor stability and IFN-γ responsiveness, thereby offering a potential strategy to enhance immunotherapeutic efficacy (76).

Furthermore, systemic *N*-glycosylation patterns can serve as biomarkers in CRC. For instance, the glycosylation profiles of IgG subclasses in plasma are altered in CRC patients, demonstrating decreased galactosylation, fucosylation, and sialylation, particularly in the IgG2-Fc structure. These systemic changes may directly affect immune effector functions

and hold promise as potential biomarkers for CRC progression (77). Colorectal cancer is also marked by significant alterations in fucosylation patterns. Suppressed α-1,2 fucosylation, mediated by FUT2, is associated with poor patient survival (78). Conversely, tumour tissues often display elevated levels of fucosylated Lewis antigens, such as Lewis^b and Lewis^Y, which are particularly enriched on metastatic cells. Highly fucosylated carcinoembryonic antigen (CEA) has been specifically observed in liver metastases, further underscoring the critical role of fucosylation in organ-specific dissemination (79).

1.3.2. Aberrant *O*-glycosylation in colorectal cancer: biosynthesis, truncation, and functional impact

O-glycosylation is a fundamental post-translational modification in CRC, serving as a significant hallmark of the disease and profoundly influencing tumour biology, immune interactions, and clinical outcomes (72, 80). Mucins, which are heavily *O*-glycosylated proteins, play a central role in this process in the colorectal epithelium, where their glycan chains typically provide crucial protection and lubrication to epithelial surfaces (81).

Under physiological conditions, the biosynthesis of mucin-type *O*-glycans initiates with the addition of *N*-acetylgalactosamine (GalNAc) to serine or threonine residues, forming the Tn antigen. In healthy tissues, this Tn antigen is typically extended to form various core structures. Core 1 (T antigen) is generated by the addition of galactose. Core 2 is subsequently formed by adding GlcNAc to core 1. Additionally, GlcNAc addition to Tn can form core 3, which can be further elongated to core 4. These extensions result in a diverse array of linear or branched glycans. Sialylation of Tn and T antigen produces sialyl-Tn (STn) and sialyl-T (ST) structures, respectively (Figure 3). In normal cells, these nascent or truncated forms are rarely exposed on the cell surface, as further elongation and modification typically mask them (81).

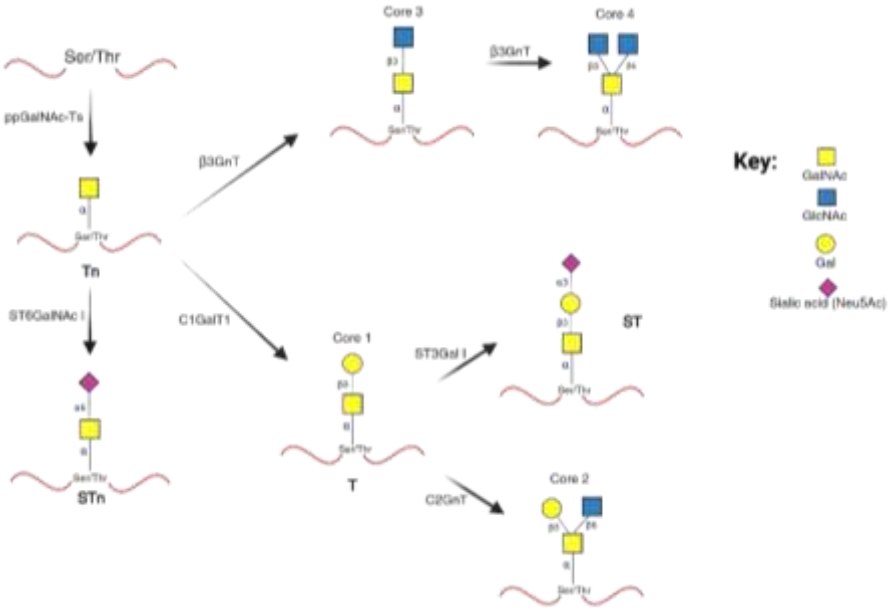

Figure 3. Biosynthetic Pathways of Mucin-Type *O*-Glycosylation. The *O*-glycosylation begins with the addition of *N*-acetylgalactosamine (GalNAc) to serine or threonine residues, forming the Tn antigen. Further modifications yield diverse core structures: addition of galactose (Gal) produces the T antigen (core 1), which can be extended to core 2 by the addition of *N*-acetylglucosamine (GlcNAc). Alternatively, GlcNAc addition to Tn forms core 3, which can be further elongated to core 4. Sialylation of Tn or T antigen generates the STn and ST structures, respectively. Created in https://BioRender.com

In stark contrast to physiological conditions, *O*-glycosylation is markedly dysregulated in CRC, leading to the abundant expression of truncated *O*-glycans, which are normally cryptic but become exposed due to biosynthetic defects (65, 82). Prominently, the Tn antigen, along with its sialylated derivative, STn, are detected in over 85% of CRC patients and are especially enriched in poorly differentiated and mucinous carcinomas (72, 83, 84). Additionally, a significant increase in *O*-GlcNAcylation is observed in CRC tumour tissues, correlating with elevated expression of *O*-GlcNAc transferase (OGT), a robust marker of proliferative cancer cells (80).

The accumulation of these aberrant glycans arises from several converging molecular mechanisms that disrupt normal *O*-glycosylation biosynthesis. These include defective activity of key enzymes like T-synthase and its essential chaperone, Cosmc, often due to mutations or hypermethylation of the *Cosmc* gene (72, 82, 85, 86). Furthermore, the downregulation of core synthases, such as core 3 synthase (B3GNT6/C3GnT) and core 2 synthase (C2GnT-M), impairs glycan elongation (87, 88). Conversely, overexpression of specific glycosyltransferase, such as C1GALT1, which increased malignancy and poor prognosis by altering the glycosylation of key proteins like FGFR2 (85).

These profound glycosylation abnormalities have far-reaching consequences for CRC biology. The presence of truncated *O*-glycans, exemplified by Tn antigen, promotes various aspects of malignancy, including tumorigenesis, tumour growth, invasion, metastasis, resistance to apoptosis, and chemoresistance (89, 90). Moreover, aberrant *O*-glycosylation directly alters the function of key proteins crucial for CRC progression. This includes mucins (e.g., MUC1, MUC2) (91, 92), receptor tyrosine kinases (e.g., FGFR2, MET) (85, 93), and structural proteins (94), affecting their stability, localisation, and biological activity in ways that drive malignancy.

Crucially, these glycan changes dramatically reshape the tumour microenvironment and facilitate immune escape (95). Tumour-associated carbohydrate antigens (TACAs), such as Tn, STn, T and Lewis antigens, modulate immune interactions by inducing immune tolerance or suppression. They engage C-type lectin receptors, including DC-SIGN and MGL, on antigen-presenting cells (e.g., dendritic cells, DCs), thereby skewing T-cell responses and making it more difficult for the immune system to fight the tumour effectively (82, 96). DC-SIGN interacts with Lewis antigens on tumour CEA, while MGL binds GalNAc moieties on tumour-associated MUC1. These interactions can influence how dendritic cells present tumour antigens and may lead to abnormal T cell responses, ultimately making it more difficult for the immune system to fight the tumour effectively (96). Soluble mucins secreted by CRC cells, particularly those bearing sialyl-Lewis^a epitopes, can directly inhibit NK cell-mediated cytotoxicity in a dose-dependent manner. Even poorly glycosylated MUC1 has been shown to protect against NK cell attack, indicating that both the presence and type of glycan modification modulate innate immune recognition (92). Furthermore, circulating galectins are elevated in CRC patients, especially in metastatic disease. These galectins enhance tumour cell adhesion to the vascular endothelium by binding to the T antigen on MUC1, thus facilitating metastasis. While high galectin-2 levels are associated with increased mortality, the presence of anti-T autoantibodies can mitigate this risk, likely through competitive inhibition of galectin binding (97).

The dysregulated *O*-glycosylation patterns in CRC also offer promising avenues for clinical application. Aberrant *O*-glycan structures, including Tn, STn and T antigen, alongside increased *O*-GlcNAcylation, are being actively investigated as diagnostic and prognostic biomarkers (98-100). For instance, immunotherapeutic approaches targeting TACAs, such as sialyl-Tn-containing mucins or T antigen peptides, are currently under investigation for

their potential to overcome tumour immune escape (101, 102). Therapeutic strategies currently under development or investigation include restoring normal glycosylation pathways, directly targeting specific glycosyltransferases such as C1GALT1, and modulating mucin expression and glycosylation to limit tumour progression and improve patient outcomes (103–105).

In summary, *O*-glycosylation is fundamentally altered in CRC, with specific defects in its biosynthesis leading to the accumulation of truncated glycan structures. These aberrant glycans critically drive tumour progression, metastasis and immune evasion by modulating protein function and immune cell interactions. These comprehensive insights highlight the profound importance of glycan-based biomarkers and therapeutic targets in the ongoing fight against CRC.

1.3.3. CD276 glycosylation for target therapy in CRC

CD276 undergoes predominantly *N*-linked glycosylation. In humans, CD276 contains eight *N*-glycosylation sites organised into four pairs (N91/N309, N104/N322, N189/N407 and N215/N433) resulting from tandem duplication of its IgV-IgC domain (106). These modifications are indispensable for protein stability and membrane localisation (106, 107), as inhibition of *N*-glycosylation at conversed NXT motifs destabilises CD276 and enhances its proteasomal degradation (106). Structural analyses reveal that *N*-glycans at the N91/N309 and N104/N322 pairs are essential for efficient transport through the endoplasmic reticulum (ER)-to-Golgi apparatus. Mutations at these sites cause ER retention and subsequent degradation by the ER-associated degradation pathway (107).

Glycosylated CD276 exerts immunosuppressive effects by impairing T cells proliferation and CTLs activity, with *N*-glycosylation at N91/N309 and N104/N322 being mechanistically essential. *In vivo* models demonstrated that glycosylated CD276 disrupts tumour infiltration by T and NK cells, facilitating immune evasion (106, 107).

Aberrant glycosylation of CD276 is observed in several cancers. In oral squamous cell carcinoma (OSCC), CD276 is significantly overexpressed and displays altered glycosylation, with more diverse *N*-glycans, higher fucosylation and the presence of terminal α-galactose (B antigen), which enhances interactions with immune cells via receptors such as DC-SIGN and Langerin (108). In triple-negative breast cancer (TNBC), aberrant CD276 glycosylation, mediated by the fucosyltransferase FUT8, is a predictor of poor prognosis and is essential

for maintaining high CD276 expression and its immunosuppressive function (106). In oesophageal squamous cell carcinoma (ESCC), elevated fucosylation levels of CD276 contribute to disease development and suggest its utility as a biomarker. In cervical cancer, the prognostic value of CD276 is influenced by co-expression with the *O*-glycosylation enzyme GALNT2, with high co-expression correlating with poorer overall survival (109).

Therapeutic strategies targeting CD276 glycosylation show translational promise. Pharmacological inhibition of FUT8 in TNBC disrupts CD276-mediated immune suppression (106), while glycosylation-specific antibodies like Ab-82 induce antibody-dependent cellular cytotoxicity by selectively binding *N*-glycosylated epitopes (107). Preclinical studies of Ab-82 demonstrate synergistic efficacy with ADCs, achieving tumour regression through dual mechanisms of immune activation and targeted payload delivery (107, 110).

In summary, CD276 is a multifaceted therapeutic target due to its central role in oncogenic processes and its aberrant *N*-glycosylation in several malignancies, including CRC. Notably, all documented glycosylation of CD276 to date is *N*-linked, and there are no published data on *O*-glycosylation of CD276. This unexplored dimension of CD276 biology represents a significant knowledge gap and could address existing limitations in CRC treatment, where immune checkpoint resistance remains prevalent. Further investigation into this area may reveal novel strategies to overcome immune evasion and improve clinical outcomes in CRC and other cancers.

2. Aims and scopes

Colorectal cancer remains a leading cause of cancer-related morbidity and mortality worldwide, with tumour aggressiveness and immune evasion representing major obstacles to effective therapy. Recent evidence suggests that post-translational modifications, particularly glycosylation patterns, play a crucial role in modulating tumour cell behaviour and interactions with the immune system. CD276 is an immune checkpoint molecule frequently overexpressed in CRC, and its glycosylation status, especially immature or aberrant forms, may critically influence both tumour progression and immune escape mechanisms.

Therefore, this project aims to understand the impact of CD276 immature glycosylation on CRC aggressiveness. More specifically, the objectives of the project are:

i. Investigate short-chain *O*-glycosylation and CD276 functional impact in CRC cells;
ii. Understand the impact of aberrantly glycosylated CD276 on the CRC cell proteome remodelling;
iii. Dissect the functional consequences of aberrantly glycosylated CD276 in CRC.

By focusing on CD276 *O*-glycosylation, this project aims to advance the understanding of how specific glycan modifications regulate CRC aggressiveness, potentially identifying novel biomarkers and therapeutic targets for improved cancer treatment.

3. Materials and Methods

3.1. Cell culture

Human CRC cell lines SW480 and SW620, obtained from the American Type Culture Collection (ATCC), were maintained at 37 °C in a 5% CO_2 humidified atmosphere and atmospheric oxygen, using complete RPMI 1640 GlutaMAX™ medium (Gibco™, Thermo Fisher Scientific) supplemented with 10% heat-inactivated foetal bovine serum (FBS; Gibco™, Thermo Fisher Scientific) and 1% penicillin-streptomycin (10,000 Units/mL penicillin; 10,000 mg/mL streptomycin; Gibco™, Thermo Fisher Scientific).

3.2. CD276 siRNA silencing

CD276 was silenced in SW480 and SW620 glycoengineered cell models by siRNA reverse transfection with Silencer® Select siRNAs (s37289 [exon 10] and s37288 [exon 7]; Invitrogen™, Thermo Fisher Scientific) or negative control siRNA (4390843, Invitrogen™). Cells (600,000/well in 6-well plates) were transfected using Lipofectamine RNAiMAX (Invitrogen™) in Opti-MEM reduced serum medium (Gibco™), following the manufacturer's protocol. siRNA-lipid complexes were incubated for 5 minutes at room temperature before addition to cells, which were then incubated for 72 h at 37°C. The control groups consist of the negative control siRNA, to diminish the off-target effects of the further experiments, and a group transfected only with Lipofectamine without siRNA, which was an internal control for Lipofectamine cytotoxicity. Five independent experiments were performed, each in duplicate. Knockdown efficiency was confirmed by Western blot (B7-H3 polyclonal antibody, PA5-80426, Invitrogen™) and RT-PCR.

3.3. RT-PCR

Total RNA was extracted from SW480 and SW620 cells using TriPure isolation reagent (Roche Diagnostics) and quantified by NanoDrop spectrophotometry. Complementary DNA (cDNA) was synthesised using a High-Capacity cDNA Reverse Transcriptase Kit (4368814, Thermo Fisher Scientific). CD276 mRNA levels were quantified by TaqMan RT-PCR (CD276: Hs00987207_m1; Thermo Fisher Scientific) on a 7500 Sequence Detector (Applied Systems). Glyceraldehyde-3-phosphate dehydrogenase (GAPDH; Hs03929097_g1; Thermo Fisher Scientific) and β-Actin (ACTB; Hs99999903_m1; Thermo

Fisher Scientific) served as endogenous controls. All reactions were run in duplicate, and relative expression was calculated using the $2^{-\Delta Ct}$ method.

3.4. Western blot

Protein lysates from CRC cells were extracted using RIPA buffer (25 mM Tris-HCl pH 7.2, 150 mM NaCl, 5 mM $MgCl_2$, 1% NP-40, 5% glycerol) supplemented with protease inhibitors (aprotinin, leupeptin, PMSF, NaF, $NaVO_3$, $Na_4P_2O_7$). The proteins were quantified by the BCA method, and equal amounts of protein (50 µg) were separated on 4–20% SDS-PAGE gels (Bio-Rad) and transferred to nitrocellulose membranes. Transfer efficiency was verified by Ponceau S staining. Membranes were blocked with 5% non-fat dry milk in TBS-T for 1 h at room temperature, then incubated overnight at 4ºC with B7-H3 polyclonal antibody (PA5-80426, Invitrogen™; 2 µg/mL in 3% milk). After washing, membranes were incubated with goat anti-rabbit IgG (H+L) secondary antibody (65-6120, Invitrogen™; 1:60,000 in 3% milk) for 30 minutes at room temperature. Detection was performed using Amersham ECL Prime Western Blotting Detection Reagent (GE Healthcare), and bands were quantified using Image Lab Software (Bio-Rad) on a ChemiDoc XRS system (Bio-Rad).

3.5. Cell proliferation assay

Cell proliferation was assessed using a colorimetric BrdU-based ELISA (Cell Proliferation ELISA, Roche Diagnostics). This validated assay detects bromodeoxyuridine (BrdU), a thymidine analogue that is incorporated into nascent DNA strands during S-phase progression, through specific antibody-mediated colorimetric detection. Glycoengineered (*C1GALT1* knockout) SW480 and SW620, as well as their silencing derivatives, were seeded at 10,000 per well in a 96-well plate, 24h before the assay. The next day, cells were labelled with BrdU for 2h. Absorbance was measured at 450 nm using an iMARK™ microplate absorbance reader (Bio-Rad Laboratories). For this assay, a background control (cell without BrdU exposure), a blank (all components except the cells) and an internal control of death (cells treated with Triton X-100, inducing cell lysis and establishing the minimal expected signal) were used. All conditions were tested in 3 replicates, and results were normalised to the background control.

3.6. Cell invasion assay

The invasive capacity of CRC glycoengineered cell lines with CD276 silencing and respective control was evaluated using Falcon® Permeable Supports (24-well plate, 8.0 μm PET membranes; Corning). Inserts were coated with 25 μL Corning® Matrigel® Basement Membrane Matrix and incubated at 37ºC until solidified. Subconfluent cells, detached with trypsin/EDTA (Thermo Fisher Scientific), were seeded at 50,000 cells/mL in the upper chamber, while 750 μL of complete medium was added to the lower chamber. After 24 h incubation at 37ºC, 5% CO_2, the inserts were washed with PBS, and non-invasive cells were gently removed from the upper membrane surface using a PBS-moistened cotton bud. Invasive cells on the underside of the membrane were fixed in 4% paraformaldehyde (PFA, Sigma-Aldrich) for 15 minutes at room temperature, washed with PBS, stained with DAPI (VECTASHIELD®, Vector Laboratories) and counted under a fluorescence microscope (Zeiss Axiovert 200M, 20x magnification). Results were normalised to proliferation rates and expressed as fold-change relative to controls. Three independent experiments were performed, each with five replicates.

3.7. Proteomics assay

Protein lysates after CD276 silencing in the SW620 cell line were obtained using RIPA buffer as described for Western Blot. After quantification, 50 μg of total protein from each sample was aliquoted. The protein was diluted (1:2) in 50 mM Tris-HCl buffer, pH 8.0, and the final volume of the samples was adjusted with 50 mM ammonium bicarbonate to ensure consistent buffer conditions across samples. Disulfide bonds were reduced by adding Dithiothreitol (DTT) to a final concentration of 20 mM, followed by incubation at 60ºC for 1 hour. Alkylation was performed with iodoacetamide at 40 mM for 30 minutes in the dark at room temperature, and the reaction was quenched with DTT to a final concentration of 10 mM. Proteins were digested overnight at 37ºC with a 1:50 (enzyme:substrate, w/w). Digestion was stopped by adding formic acid to a final concentration of 2%. The sample was centrifuged at 14,000g for 15 minutes at 4ºC, the supernatant was collected, and the solution was dried using a speed vacuum. Peptides were desalted using Pierce™ C-18 Spin Columns (Thermo Fisher Scientific) following the manufacturer's protocol. After drying, peptides were resuspended in 2% Trifluoroacetic acid (TFA) in 20% acetonitrile (ACN), loaded onto a prepared C18 spin column, and centrifuged, with the flow-through reapplied for maximum peptide binding; the column was washed with 0.5% TFA in 5% ACN, peptides

were eluted with 70% ACN, and the eluate was dried again. Prior to LC-MS/MS, the peptides were resuspended in 0.1% formic acid to a final concentration of approximately 0.5 µg/µL, followed by centrifugation at 10,000 rpm for 10 minutes to remove particulates, and 15 µL of supernatant was transferred to an MS vial for injection. This approach minimises peptide loss and ensures compatibility with reverse-phase LC-MS/MS.

Proteomic data were processed using Proteome Discoverer software (Thermo Fisher Scientific) with the workflow explained in the LC-MS/MS data processing section and a comprehensive protein database. Normalised abundance values were exported, and data quality was ensured by filtering for proteins with high and medium FDR confidence. Lists of present proteins in each group were compared using Venn diagrams generated by online tools (Interactivenn, https://www.interactivenn.net). Principal component analysis (PCA) was performed in R software (version 4.5.0; R Foundation) after imputing missing values using k-nearest neighbours (kNN) imputation. Only proteins detected in at least three samples per group were included to ensure robustness of analysis. A volcano plot was constructed by calculating $\log_2$-transformed fold changes and $-\log_{10}$-transformed p-values from Student's t-tests. Functional enrichment analyses were conducted using the ClueGo plugin from Cytoscape (http://www.cytoscape.org/) (111, 112), STRING (https://string-db.org/) and g:Profiler (https://biit.cs.ut.ee/gprofiler/gost) online platforms.

3.8. Nano-LC-MS/MS for proteomics

A Vanquish Neo UHPLC system (Thermo Fisher Scientific) was directly coupled to a Q Exactive Plus mass spectrometer (Thermo Scientific) equipped with an EASY-Spray nanoelectrospray ion source. (Thermo Scientific). For chromatographic separation, 0.1% aqueous formic acid was used as eluent A, while eluent B consisted of 0.1% formic acid in 80% acetonitrile. Each sample was injected in a 10 µL volume onto a C18 PepMap Neo trapping column (5 µm particle size) and washed isocratically with 97.5% eluent A and 2.5% eluent B at a flow rate of 0.200 µL/min. After 3 minutes, the flow was switched to an EASY-Spray C18 PepMap analytical column (100 Å, 75 µm x 150 mm ID and 3 µm particle size), maintained at 35ºC, with a constant flow of 0.200 µL/min. Peptide separation was achieved using a linear gradient: starting at 2.5% eluent B at 3 minutes, increasing to 12% at 10 minutes, 46% at 120 minutes, and reaching 99% at 125 minutes. The column was held at

99% eluent B for 10 minutes, followed by re-equilibration at 2.5% eluent B until the 150 minutes. The mass spectrometer operated in positive ion mode, with a spray voltage of 1.9 kV and a capillary temperature of 275ºC. Full MS scans were acquired at a resolution of 140,000 over an m/z range of 300–2000, with an AGC target of $3x10^6$ and a maximum injection time of 200 ms. The instrument performed data-dependent acquisition, selecting the top 15 most intense ions for high-energy collision dissociation (HCD). MS^2 scans were acquired at a resolution of 17,500 (at m/z 200), using a stepped normalised collision energy of 28%, an AGC target of $1x10^5$, and a maximum injection time of 100 ms. A 4.0 m/z isolation window was selected to maximise sensitivity, and this parameter was chosen based on instrument recommendations, optimal duty cycle and sample complexity. Additional data-dependent settings included a minimum AGC target of $7x10^3$, peptide match preferred, dynamic exclusion set to 30 seconds, exclusion of unassigned and singly charged ions, as well as those with charge states equal to 1 and above 8, and isotope exclusion enabled. Data acquisition was carried out using Xcalibur software version 4.5 (Thermo Fisher Scientific).

3.9. Proteomics LC–MS/MS data processing

Data analysis was performed automatically using the SequestHT search engine, with protein identifications validated by the Percolator algorithm (Proteome Discoverer; Thermo Scientific). Database searches were conducted against the human SwissProt database, with trypsin specified as the proteolytic enzyme (up to 3 missed cleavage sites), a precursor ion mass tolerance of 10 ppm, and a product ion tolerance of 0.02 Da. Carbamidomethylation of cysteine residues was defined as a static modification, while oxidation of methionine (+15.995 Da) was included as a dynamic modification. No additional variable modifications for serine or threonine were considered. Normalisation was carried out based on the total peptide amount within each fraction. For all analyses, a significance threshold of p-value < 0.05 was applied. Prediction of putative *O*-glycosylation sites was not performed.

Normalised abundance values were exported, and data quality was ensured by filtering for proteins with high and medium FDR confidence and a minimum of three valid values per group. Lists of present proteins in each group were compared using Venn diagrams generated by online tools (Interactivenn, https://www.interactivenn.net). PCA was performed after kNN imputation of missing values in R software (version 4.5.0; R

Foundation), and volcano plots were constructed by calculating $\log_2$-transformed fold changes and $-\log_{10}$-transformed p-values from Student's t-tests. Functional enrichment analyses were conducted using the ClueGo plugin from Cytoscape (http://www.cytoscape.org/) (111, 112) and STRING (https://string-db.org/) and g:Profiler (https://biit.cs.ut.ee/gprofiler/gost) online platforms.

3.10. Phosphoproteomics assay

For phosphoproteomics analysis, three confluent wells per cell model in a 6-well plate were placed on ice, washed with ice-cold TBS and lysed using a denaturing buffer containing 1% sodium deoxycholate (SDC), 10 mM tris(2-carboxyethyl)phosphine hydrochloride (TCEP.HCl), 100 mM Tris pH 8.5 and 40 mM chloroacetamide, supplemented with a protease and phosphatase inhibitor cocktail (78440, Thermo Fisher Scientific). After aspirating the culture, cells were gently rinsed with TBS, lysed *in situ* and collected by scraping. The lysate was heat-treated at 95ºC for 5 minutes, subjected to three cycles of ultrasonication at 40ºC for 5 minutes each, with cooling on ice between cycles, and clarified by centrifugation at 14,000g for 15 minutes at 4ºC. Protein was quantified, and 200 µg aliquots were prepared for downstream processing. Proteins were reduced, alkylated and digested with sequencing-grade trypsin at a 1:50 (w/w) enzyme-to-protein ratio in 50 mM ammonium bicarbonate overnight at 37ºC. The resulting peptides were acidified with formic acid to a final concentration of 2%, centrifuged, and the supernatant was dried using a SpeedVac concentrator. The phosphopeptides were enriched using the High-Select™ TiO2 Phosphopeptide Enrichment Kit (A32993, Thermo Fisher Scientific) under acidic conditions. A pH below 3 was achieved by adding formic acid to a final concentration of 10%, as recommended by the manufacturer's protocol for the High-Select™ TiO2 Phosphopeptide Enrichment Kit to ensure optimal binding and phosphate loss. The enriched samples were finally dried by SpeedVac before LC-MS/MS analysis. Each experimental condition was analysed using five biological replicates for controls and three biological replicates for each siRNA treatment group, supporting statistical robustness and reproducibility of the phosphoproteomic analyses.

3.11. Nano-LC-MS/MS for phosphoproteomics

Approximately 1 µg of enriched phosphopeptides in 10 µL volume was injected onto a PepMap Neo C18 trap column (5 µm, 300 µm x 5 mm, Thermo Fisher Scientific) and separated on an EASY-Spray PepMap C18 analytical column (5 µm, 75 µm x 150 mm, Thermo Fisher Scientific) at 35ºC, using a Vanquish Neo UHPLC coupled to a Q Exactive Plus mass spectrometer (Thermo Fisher Scientific). Chromatographic separation was performed at 200 µL/min with mobile phase A (0.1% formic acid in water) and mobile phase B (0.1% formic acid in 80% ACN) using a segmented gradient: 9% eluent B at 7 minutes, held until 12 minutes, increased to 36% at 102 minutes, ramped to 99% at 107 minutes, held for 11 minutes and re-equilibrated at 2.5% until 125 minutes.

The mass spectrometer operated in positive ion mode (spray voltage 1.9 kV, capillary temperature 275ºC). Full MS scans were acquired at 70,000 resolution (m/z 375–1600, AGC target $3x10^6$, max injection 120 ms). The top 10 most intense precursor ions were selected for HCD fragmentation (stepped NCE 28%, resolution 17,500, AGC target $1x10^5$, max injection time 100 ms, isolation window 1.4 m/z, fixed first mass 100 m/z), with an apex trigger set to 2–4 seconds. Unassigned and singly charged ions, as well as precursors with charge states 1 or above 8, were excluded from selection. Dynamic exclusion was set to 16.0 seconds. Peptide match was preferred, and isotope exclusion was enabled. Ions that were unassigned, singly charged or had charge states of 1 or greater than 8 were excluded. Additionally, the apex trigger was set to 2–4 seconds. Data were acquired using Xcalibur software version 4.5 (Thermo Fisher Scientific).

3.12. Phosphoproteomics LC–MS/MS data processing

Data analysis was performed automatically using the MaxQuant version 1.6.17.0 (113) search engine. A maximum of 5 modifications and 2 missed cleavages were allowed. Carbamidomethylation was designated as a fixed modification, whereas methionine oxidation, protein *N*-terminal acetylation, and phosphorylation of serine, threonine, and tyrosine were designated as variable modifications. Both protein and peptide false discovery rates were controlled at below 1%, and the match between runs feature was enabled. For downstream analysis, only class 1 phosphosites with localisation probabilities greater than 0.75, as defined by MaxQuant, were included. Phosphosites were required to have at least two valid detections in at least one experimental group. Missing values were

imputed using a normal distribution with a downshift of 1.8, and the resulting data were further analysed using Phosphomatics (114).

3.13. Statistical analysis

Statistical analyses were performed using the GraphPad Prism software (Dotmatics) and R software (version 4.5.0; R Foundation). For proliferation and invasion assays, one-way ANOVA followed by Tukey's multiple comparisons test was applied. Proteomic data were analysed using two-tailed Student's t-test in Microsoft® Excel® (version 2505 Build 16.0.18827.20102). Due to the exploratory nature and limited sample size, a significance threshold of $p<0.05$ was used. Fold changes were calculated as the ratio of mean protein expression between the siRNA-treated and the control groups. For visualisation, fold changes were $\log_2$-transformation to normalise distribution, and p-values were converted to $-\log_{10}$ values for volcano plot representation, enabling systematic identification of differentially expressed proteins. Phosphoproteomic data analysis followed the same workflow, with all analyses conducted using the Phosphomatics platform.

4. Results

To address the functional consequences of specific *O*-glycosylation patterns in colorectal cancer (CRC), a robust and well-characterised cellular model system was selected. This study utilises *C1GALT1*knockout (KO) CRC cell lines, previously established in both SW480 (epithelial-like, derived from a primary tumour) and SW620 (mesenchymal-like, from a lymph node metastasis of the same patient) cell lines using CRISPR-Cas9 technology. These *C1GALT1*KO models are particularly relevant as they exhibit a complete suppression of core 1 *O*-glycan structures and a robust overexpression of Tn and STn antigens, thereby faithfully representing the aberrant glycosylation characteristic of advanced CRC. These cell models were used as the experimental platform to investigate the impact of CD276 immature glycosylation on CRC aggressiveness.

4.1. Truncated *O*-glycosylation drives CD276-mediated aggressiveness in a cell line-dependent manner

To investigate the functional impact of CD276 and its altered glycosylation in CRC cells, transient knockdown strategies were employed using two different siRNAs (si1 and si2). For these experiments, SW480 (epithelial-like, derived from a primary tumour) and SW620 (mesenchymal-like, from a lymph node metastasis of the same patient) wild-type (WT) cell lines were used, alongside their respective *C1GALT1* knockout (KO) counterparts, which model aberrant *O*-glycosylation. CD276 expression was successfully reduced by siRNA-mediated knockdown in all tested cell lines, as confirmed by RT-PCR (Figure 4A and B) and Western blot (Figure 4C).

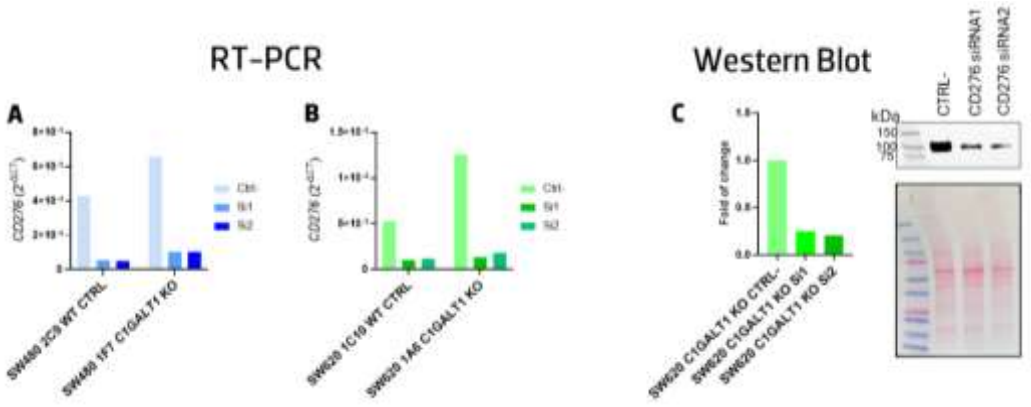

Figure 4. RT-PCR and Western blotting confirmed CD276 knockdown. After *C1GALT1* KO and CD276 silencing, the silencing of CD276 was validated. (**A**) There was an approximate 85% decrease in CD276 expression for both SW480 wild-type (WT) control for the *C1GALT1*KO 2C9 clones and SW480 *C1GALT1*KO 1F7 clones. (**B**) Notably, for SW620, there was a decreased expression of CD276 of approximately 80% for

SW620 WT control for *C1GALT1*KO 1C10 clones and an approximate 90% decrease of CD276 expression for SW620 *C1GALT1* KO 1A6 clones. (**C**) The CD276 protein expression was verified for the SW620 cell line, showing a decrease of 75% decrease for siRNA1 and an 80% decrease for siRNA2. These results demonstrate effective silencing of CD276 at both mRNA and protein levels, validating the efficiency of the siRNA-mediated knockdown approach.

The proliferative capacity of the SW480 cell line demonstrated minimal sensitivity to CD276 depletion across most experimental conditions (Figure 5A). A modest decrease in proliferation was observed only in *C1GALT1*KO SW480 cells treated with CD276 siRNA1 ($p = 0.0053$); however, this effect was not observed with the second siRNA. In contrast, the SW620 cell line exhibited distinct responses. CD276 knockdown resulted in significant proliferation suppression specifically in *C1GALT1*KO SW620 cells ($p = 0.0016$ for si1 and $p = 0.0135$ for si2 treatments). No significant proliferative changes were detected in wild-type SW620 cells following CD276 depletion (Figure 5B). Furthermore, CD276 silencing significantly reduced invasion in both SW480 C1GALT1 KO (Figure 5C) and SW620 *C1GALT1* KO (Figure 5D) cell lines. Notably, *C1GALT1* knockout independently enhanced invasive capacity in SW620 cells, an effect that was abolished by CD276 silencing.

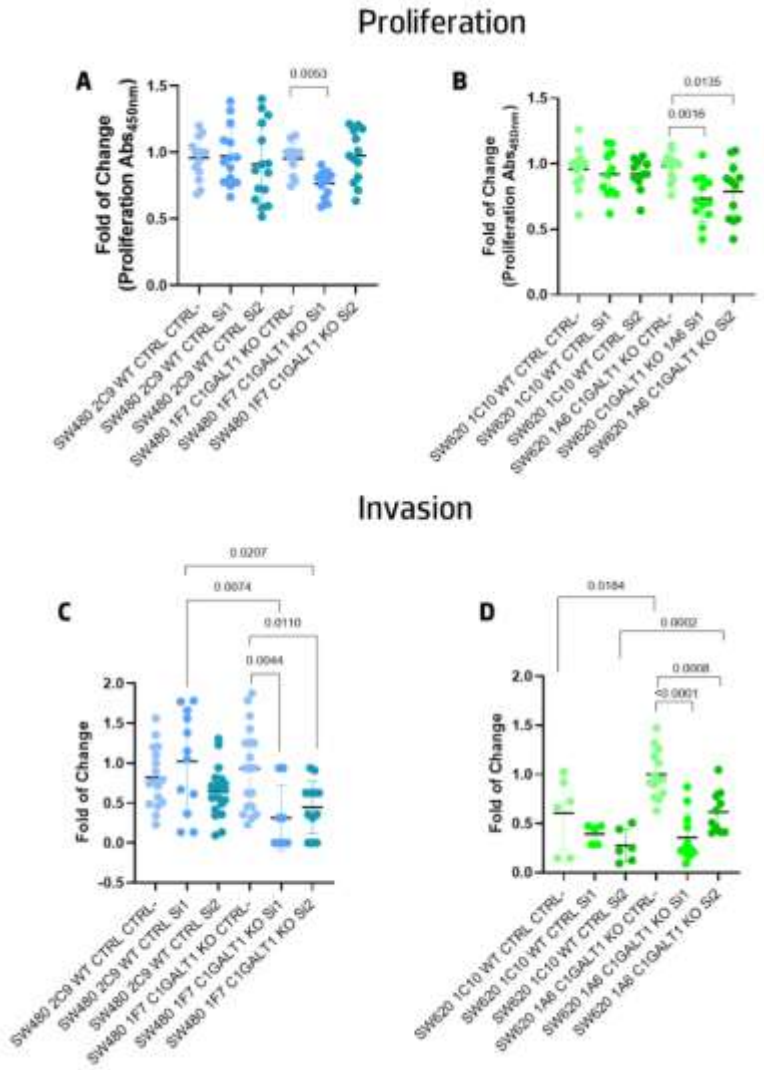

Figure 5. Aberrant *O*-glycosylation and CD276-mediated cellular aggressiveness. After *C1GALT1*KO and CD276 silencing, both cell lines (SW480 and SW620) were submitted to functional assays. In these experiments, the SW480 2C9 and SW620 1C10 cells correspond to the WT control clones of the *C1GALT1*KO, while the SW480 1F7 and SW620 1A6 clones correspond to the KO of *C1GALT1*. CD276 exhibited limited proliferative regulatory function in SW480, even with altered glycosylation (**A**). No significant changes occurred in wild-type SW620 cells upon CD276 downregulation (**B**). In the invasion assay, the downregulation of CD276 decreased the invasion capacity of SW480 (**C**) and SW620 (**D**) cell lines.

These experimental results collectively establish that CD276 influences both proliferative and invasive cellular processes through glycosylation-dependent and cell context-specific mechanisms. The tumour-promoting activities of CD276 are most pronounced in the SW620 cell line. The findings demonstrate a functional connection between aberrant *O*-glycosylation patterns and CD276-mediated cellular aggressiveness, validating SW620 cells as an optimal experimental platform for comprehensive mechanistic investigations, including detailed proteomic and phosphoproteomic analytical approaches.

4.2. CD276 both promotes biosynthetic pathways and suppresses stress-response mechanisms

To investigate the proteomic landscape altered by aberrant glycosylation of CD276 in CRC cells, quantitative proteomic profiling was conducted on SW620 *C1GALT1* KO cells following CD276 silencing (using siRNAs si1 and si2) and compared to non-silenced controls. CD276 knockdown was verified by RT-PCR and immunoblotting prior to proteomic analysis (Figure 4).

This analysis identified a total of 1309 high/medium FDR confidence proteins across all groups, with 1277 proteins detected in controls, 1278 in si1, and 1258 in si2. A Venn diagram illustrates the proteomic overlap and group-specific protein identifications (Figure 6A). Specifically, 12 proteins were identified as unique to both CD276-silenced groups (si1 and si2), while 16 proteins were unique to the non-silenced control group. Initial network analysis of these 28 unique proteins in Cytoscape revealed no significant interactions. Subsequent STRING database evaluation of proteins unique to the control group showed non-significant connectivity (protein-protein interaction enrichment p-value of 0.0693; Figure 6B). However, g:Profiler functional enrichment analysis of two clusters within the control-unique proteins identified one cluster (ACO1, IDH2, NDUFS3, MCCC2) associated with aerobic respiration, tricarboxylic acid, small molecule, and purine-containing compound metabolic processes. The second cluster (AHCTF1, PABPC3) did not show enriched functional terms. In contrast, proteins unique to the siRNA-silenced groups formed a cohesive network (Figure 6C), and g:Profiler analysis of these proteins highlighted associations with rRNA processing, cellular component biogenesis, and organisation, including RNA helicase activity.

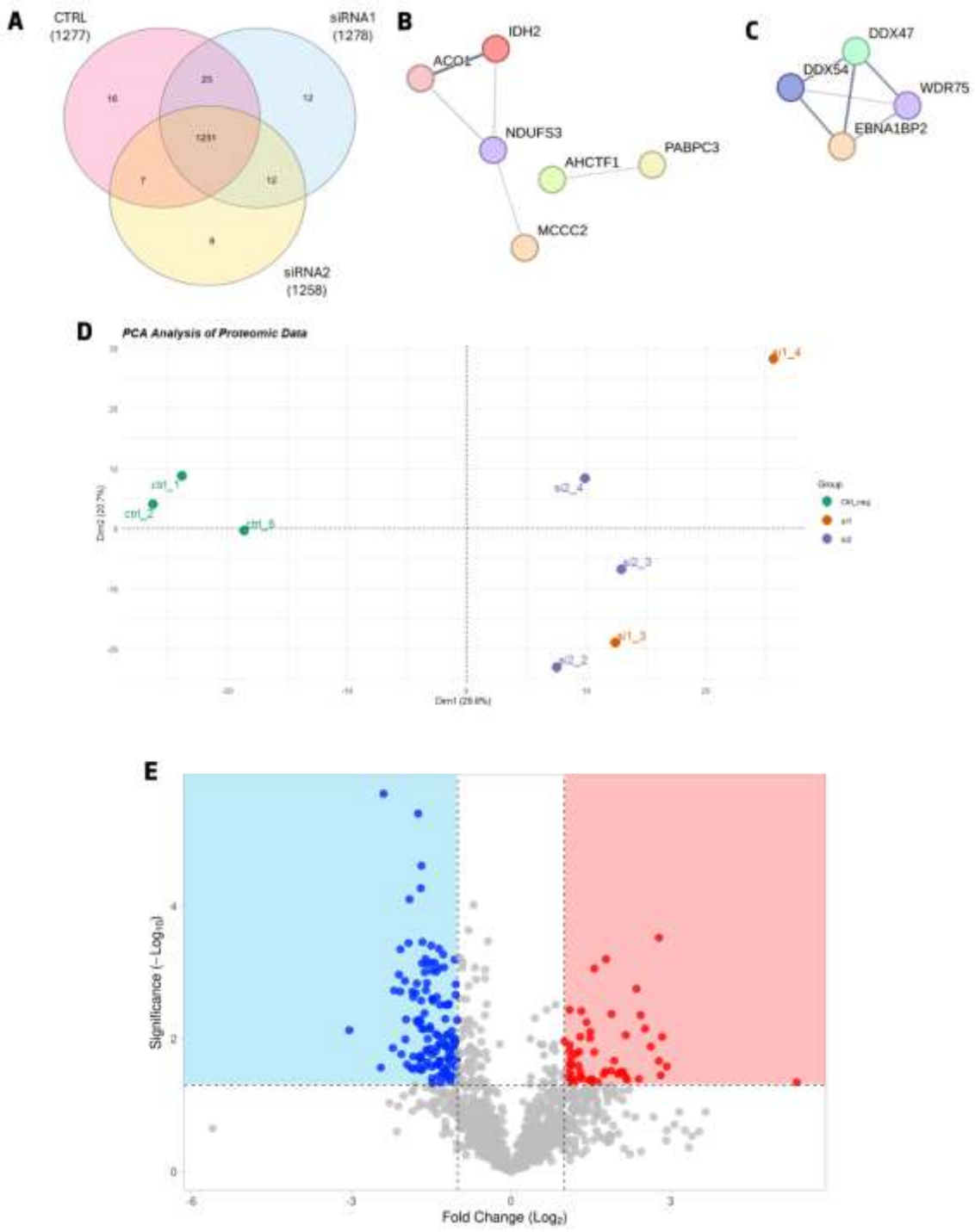

Figure 6. Comprehensive proteomic analysis of siCD276 with aberrant glycosylation in SW620 cells. (**A**) The Venn diagram illustrates the overlap of identified proteins among all experimental groups. Network maps depict protein-protein interaction networks from STRING analysis by significance of control exclusive proteins (**B**) and siRNA exclusive proteins (**C**). (**D**) PCA shows the clustering and variance among samples, without outlier samples, based on global proteomic profiles, indicating similarities and differences between experimental groups. (**E**) Volcano plot visualises differentially expressed proteins, with significance plotted against fold change, highlighting proteins with statistically significant changes between control and siRNA groups. In blue are the overexpressed proteins in the control, and in red are the overexpressed proteins in the siRNA.

The PCA of filtered datasets demonstrated clear segregation between control and the siRNA (si1 and si2) clusters with minimal intra-group variance (Figure 6D). Volcano plot analysis of shared proteins across all groups (Figure 6E) identified 124 proteins significantly more abundant in CD276-expressing control cells compared to CD276-silenced cells, and 53 proteins significantly more abundant in CD276-silenced cells compared to controls (Table 1).

Table 1. Differentially expressed proteins from the volcano plot. 124 proteins were downregulated and 53 were upregulated, when compared with the control siRNA group with the control group.

Downregulated				Upregulated	
ID	Protein	ID	Protein	ID	Protein
P15374	UCHL3_HUMAN	P54709	AT1B3_HUMAN	P27694	RFA1_HUMAN
P20810	ICAL_HUMAN	Q9UHD8	SEPT9_HUMAN	O76021	RL1D1_HUMAN
P02786	TFR1_HUMAN	Q9NYF8	BCLF1_HUMAN	Q96ST2	IWS1_HUMAN
Q9Y262	EIF3L_HUMAN	P60866	RS20_HUMAN	O60784	TOM1_HUMAN
P13861	KAP2_HUMAN	Q00325	S25A3_HUMAN	Q00796	DHSO_HUMAN
P63220	RS21_HUMAN	P55084	ECHB_HUMAN	Q99729	ROAA_HUMAN
Q9BVA1	TBB2B_HUMAN	Q96FW1	OTUB1_HUMAN	P26368	U2AF2_HUMAN
Q09028	RBBP4_HUMAN	P26447	S10A4_HUMAN	P09012	SNRPA_HUMAN
Q06203	PUR1_HUMAN	P49589	SYCC_HUMAN	P35249	RFC4_HUMAN
Q9H6T3	RPAP3_HUMAN	O15260	SURF4_HUMAN	O75367	H2AY_HUMAN
P63173	RL38_HUMAN	P08697	A2AP_HUMAN	Q9P2D7	DYH1_HUMAN
O15143	ARC1B_HUMAN	P39687	AN32A_HUMAN	P51572	BAP31_HUMAN
Q92890	UFD1_HUMAN	P49755	TMEDA_HUMAN	Q02218	ODO1_HUMAN
Q99627	CSN8_HUMAN	Q8WWI1	LMO7_HUMAN	O15212	PFD6_HUMAN
P19404	NDUV2_HUMAN	P00966	ASSY_HUMAN	P43897	EFTS_HUMAN
P63151	2ABA_HUMAN	P40429	RL13A_HUMAN	Q6P2Q9	PRP8_HUMAN
O14776	TCRG1_HUMAN	P31930	QCR1_HUMAN	Q9NX63	MIC19_HUMAN
P13073	COX41_HUMAN	Q96PK6	RBM14_HUMAN	Q13151	ROAO_HUMAN
P09960	LKHA4_HUMAN	P11717	MPRI_HUMAN	Q92530	PSMF1_HUMAN
P63162	RSMN_HUMAN	P43490	NAMPT_HUMAN	P62266	RS23_HUMAN
P62258	1433E_HUMAN	Q8IX12	CCAR1_HUMAN	P36871	PGM1_HUMAN
O60884	DNJA2_HUMAN	Q9BWF3	RBM4_HUMAN	Q99714	HCD2_HUMAN
O14929	HAT1_HUMAN	P07814	SYEP_HUMAN	P21281	VATB2_HUMAN
P50416	CPT1A_HUMAN	O43852	CALU_HUMAN	P46783	RS10_HUMAN
P46776	RL27A_HUMAN	Q9Y2Q3	GSTK1_HUMAN	Q9Y570	PPME1_HUMAN
Q15181	IPYR_HUMAN	P43034	LIS1_HUMAN	O75170	PP6R2_HUMAN
P53634	CATC_HUMAN	P62241	RS8_HUMAN	Q9BTC0	DID01_HUMAN
P62829	RL23_HUMAN	Q13177	PAK2_HUMAN	Q9BRP8	PYM1_HUMAN
O60568	PLOD3_HUMAN	P35613	BASI_HUMAN	P58876	H2B1D_HUMAN
Q9UBE0	SAE1_HUMAN	P61088	UBE2N_HUMAN	P05204	HMGN2_HUMAN
Q16352	AINX_HUMAN	Q9H910	JUPI2_HUMAN	P16104	H2AX_HUMAN
Q9Y3B7	RM11_HUMAN	P15559	NQO1_HUMAN	P62995	TRA2B_HUMAN
P61204	ARF3_HUMAN	P01023	A2MG_HUMAN	A1L0T0	HACL2_HUMAN
Q9Y617	SERC_HUMAN	P35221	CTNA1_HUMAN	Q8NHQ9	DDX55_HUMAN
O15085	ARHGB_HUMAN	P61353	RL27_HUMAN	O00186	STXB3_HUMAN
O95881	TXD12_HUMAN	P32322	P5CR1_HUMAN	Q8IVD9	NUDC3_HUMAN
P18085	ARF4_HUMAN	P35268	RL22_HUMAN	Q14978	NOLC1_HUMAN
Q9H0Q0	CYRIA_HUMAN	P10599	THIO_HUMAN	P37108	SRP14_HUMAN
Q9BQE3	TBA1C_HUMAN	O15819	UB2V2_HUMAN	P46108	CRK_HUMAN
Q16629	SRSF7_HUMAN	P63165	SUMO1_HUMAN	Q9BQ39	DDX50_HUMAN
P35250	RFC2_HUMAN	P18124	RL7_HUMAN	Q08380	LG3BP_HUMAN

P50552	VASP_HUMAN	Q99536	VAT1_HUMAN	P31942	HNRH3_HUMAN
P26639	SYTC_HUMAN	P30519	HMOX2_HUMAN	043252	PAPS1_HUMAN
P23229	ITA6_HUMAN	Q9NYB0	TE2IP_HUMAN	Q9NS69	TOM22_HUMAN
014715	RGPD8_HUMAN	P18621	RL17_HUMAN	Q13126	MTAP_HUMAN
Q9Y3U8	RL36_HUMAN	Q02543	RL18A_HUMAN	Q9BYD6	RM01_HUMAN
P60891	PRPS1_HUMAN	Q15185	TEBP_HUMAN	P28838	AMPL_HUMAN
P52565	GDIR1_HUMAN	P09496	CLCA_HUMAN	P55957	BID_HUMAN
P11279	LAMP1_HUMAN	P27144	KAD4_HUMAN	Q13838	DX39B_HUMAN
P05976	MYL1_HUMAN	P02768	ALBU_HUMAN	Q9H4L4	SENP3_HUMAN
P49454	CENPF_HUMAN	P42766	RL35_HUMAN	Q92575	UBXN4_HUMAN
P10515	ODP2_HUMAN	P20340	RAB6A_HUMAN	094826	TOM70_HUMAN
Q96HE7	ERO1A_HUMAN	Q01469	FABP5_HUMAN	P43246	MSH2_HUMAN
P24539	AT5F1_HUMAN	P28482	MK01_HUMAN		
015347	HMGB3_HUMAN	Q99460	PSMD1_HUMAN		
Q86SX6	GLRX5_HUMAN	P41091	IF2G_HUMAN		
Q9NZZ3	CHMP5_HUMAN	Q13442	HAP28_HUMAN		
P61254	RL26_HUMAN	P27348	1433T_HUMAN		
P17655	CAN2_HUMAN	Q9H074	PAIP1_HUMAN		
Q9Y3I0	RTCB_HUMAN	P18754	RCC1_HUMAN		
Q15293	RCN1_HUMAN	000299	CLIC1_HUMAN		
Q92769	HDAC2_HUMAN	Q16718	NDUA5_HUMAN		

A total of 177 differentially expressed proteins, identified by the volcano plot, were subjected to further functional enrichment analysis. Cytoscape analysis of biological processes detected significant interactions only within the proteins that were less abundant upon CD276 silencing (Figure 7A). For molecular functions, Cytoscape identified interactions in both groups (Figure 7B).

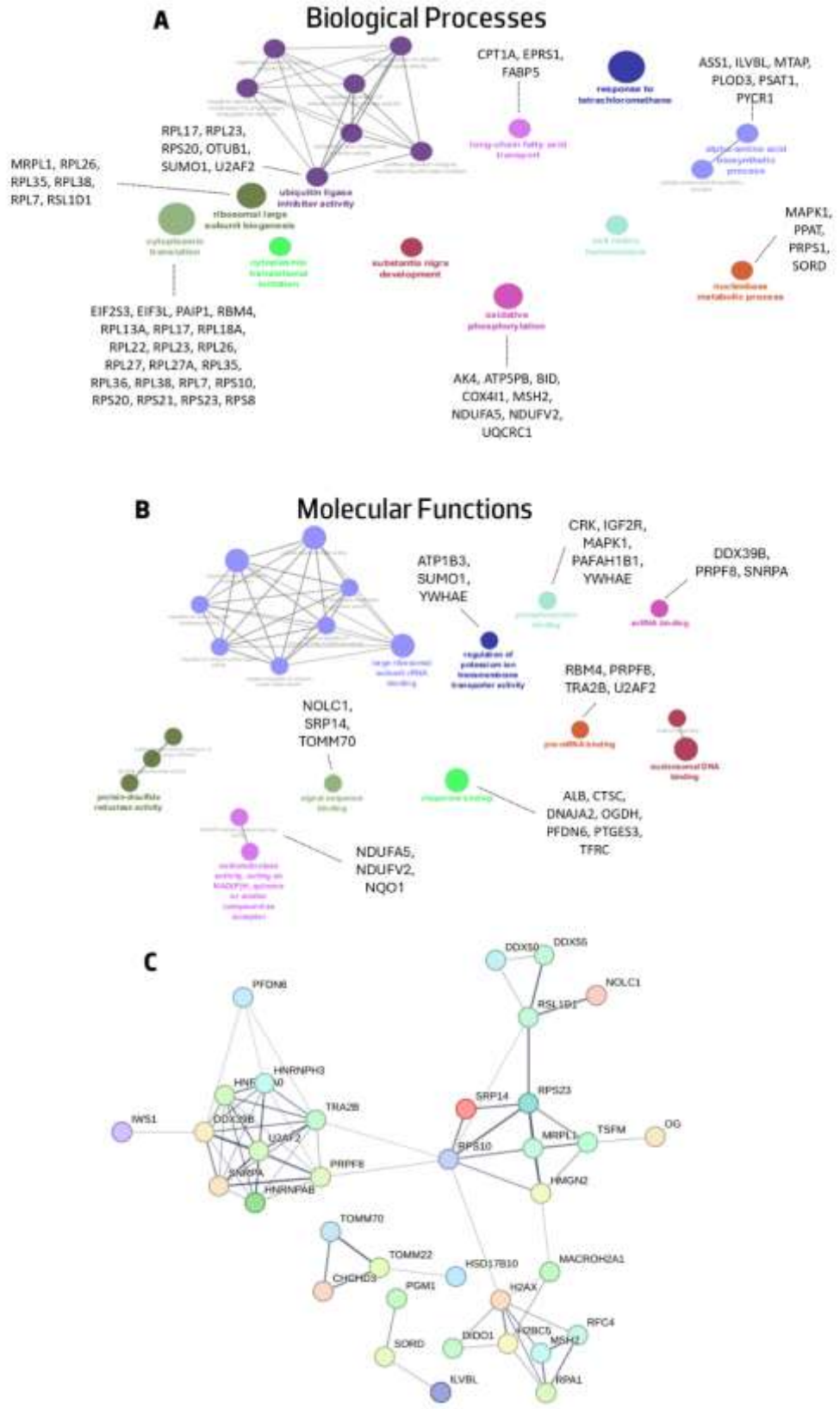

Figure 7. Comprehensive networks of differentially expressed proteins. Cytoscape analysis of differentially expressed proteins for biological processes (**A**) and molecular functions (**B**). (**C**) STRING analysis by significance for the overexpressed proteins from the volcano plot (overexpressed in siRNA groups), PPI enrichment p-value = 6.9×10^{-7}.

Proteins that were significantly less abundant following CD276 silencing were associated with fundamental cellular machinery, including cytoplasmic translation and ribosomal biogenesis. Energy metabolism was similarly affected, particularly oxidative phosphorylation and long-chain fatty acid transport. Additionally, proteins associated with amino acid and nucleobase biosynthesis were more abundant in CD276-expressing control cells. This group of proteins also included those related to ubiquitin ligase regulation, chaperone binding, phosphoprotein binding, regulation of potassium ion transport, and various glycosylation processes.

For proteins that were significantly more abundant following CD276 silencing (i.e., less abundant in controls), Cytoscape did not identify specific GO terms or pathways for biological processes. However, STRING analysis revealed a significant network for this protein group (PPI enrichment p-value of 6.9×10^{-7}; Figure 7C). This network included proteins involved in oxidative phosphorylation, ATP metabolism, mitochondrial respiratory chain complex assembly, NADH dehydrogenase activity, and mitochondrial organisation. The Cytoscape analysis for molecular functions showed that these increased proteins in CD276-silenced cells were involved in signal sequence binding, snRNA binding, and pre-mRNA binding.

Further g:Profiler analysis of individual clusters within the proteins less abundant upon CD276 silencing (Table 2) identified enriched GO terms related to RNA metabolism and processing, including RNA binding, snRNA binding, mRNA metabolic processes, RNA helicase activity, and various RNA methyltransferase activities. For proteins that were more abundant upon CD276 silencing, enriched GO terms included those associated with genome maintenance and chromatin organisation, specifically DNA repair, telomere maintenance, DNA binding, and structural constituents of chromatin. This group of proteins was also associated with mitochondrial organisation, protein transmembrane transport, and a range of metabolic enzyme activities.

Table 2. Molecular functions and biological processes with the respective GO term from g:Profiler analysis of overexpressed siRNA proteins.

	Molecular Function		Biological Process	
HNRNPH3, TRA2B, PRPF8, HNRNPAB, SNRPA, DDX39B, HNRNPA0, U2AF2	GO:0003723	RNA binding	GO:0016071	mRNA metabolic process
	GO:0030619	U1 snRNA binding		
TOMM70, TOMM22, HSD17B10, CHCHD3	GO:0008320	Protein transmembrane transporter activity	GO:0007005	Mitochondrial organisation

	GO:0106281	Chenodeoxycholate 7-alpha-dehydrogenase	GO:0071806	Protein transmembrane transport
	GO:0106282	Isoursodeoxycholate 7-beta-dehydrogenase		
	GO:0008709	Cholate 7-alpha-dehydrogenase activity		
	GO:0106283	Ursodeoxycholate 7-beta-dehydrogenase		
	GO:0047015	3-hydroxy-2-methylbutyryl-CoA dehydrogenase activity		
PGM1, SORD, ILVBL	GO:0047833	D-sorbitol dehydrogenase (acceptor) activity	GO:0044283	Small-molecule biosynthetic process
	GO:0046526	D-xylulose reductase activity	GO:0032787	Monocarboxylic acid metabolic process
	GO:0003984	Acetolactate synthase activity		
	GO:0003939	L-iditol 2-dehydrogenase activity		
	GO:0050255	Ribitol 2-dehydrogenase activity		
	GO:0000721	(R, R)-butanediol dehydrogenase activity		
DIDO1, H2AX, MACROH2A1, RFC4, RPA1, MSH2, H2BC5	GO:0030527	Structural constituent of chromatin	GO:0006281	DNA repair
	GO:0046982	Protein heterodimerisation activity	GO:1901988	Negative regulation of cell cycle phase transition
	GO:0003677	DNA binding		
RPS10, SRP14, MRPL1, HMGN2, RPS23, TSFM, OGDH	GO:0003723	RNA binding		
DDX50, DDX55, RSL1D1, NOLC1	GO:0003724	RNA helicase activity		

4.3. Quantitative phosphoproteomic profiling of SW620 *C1GALT1* KO cells reveals CD276-dependent phosphorylation changes

Quantitative phosphoproteomic profiling was performed on SW620 *C1GALT1* knockout CRC cells following CD276 knockdown and compared to non-silenced control cells. PCA revealed clear separation between CD276-silenced and control glycoengineered cells, revealing distinct global phosphoproteomic profiles (Figure 8A). Kinase-substrate enrichment analysis (KSEA) showed significantly negative Z-scores for ATR, ATM, AKT1 and CHEK1 (Figure 8B). Pathway enrichment analysis identified significant changes in phosphorylation-dependent programs related to spliceosome assembly, chromatin remodelling, junction integrity, and cytoskeletal regulation (Figure 8C).

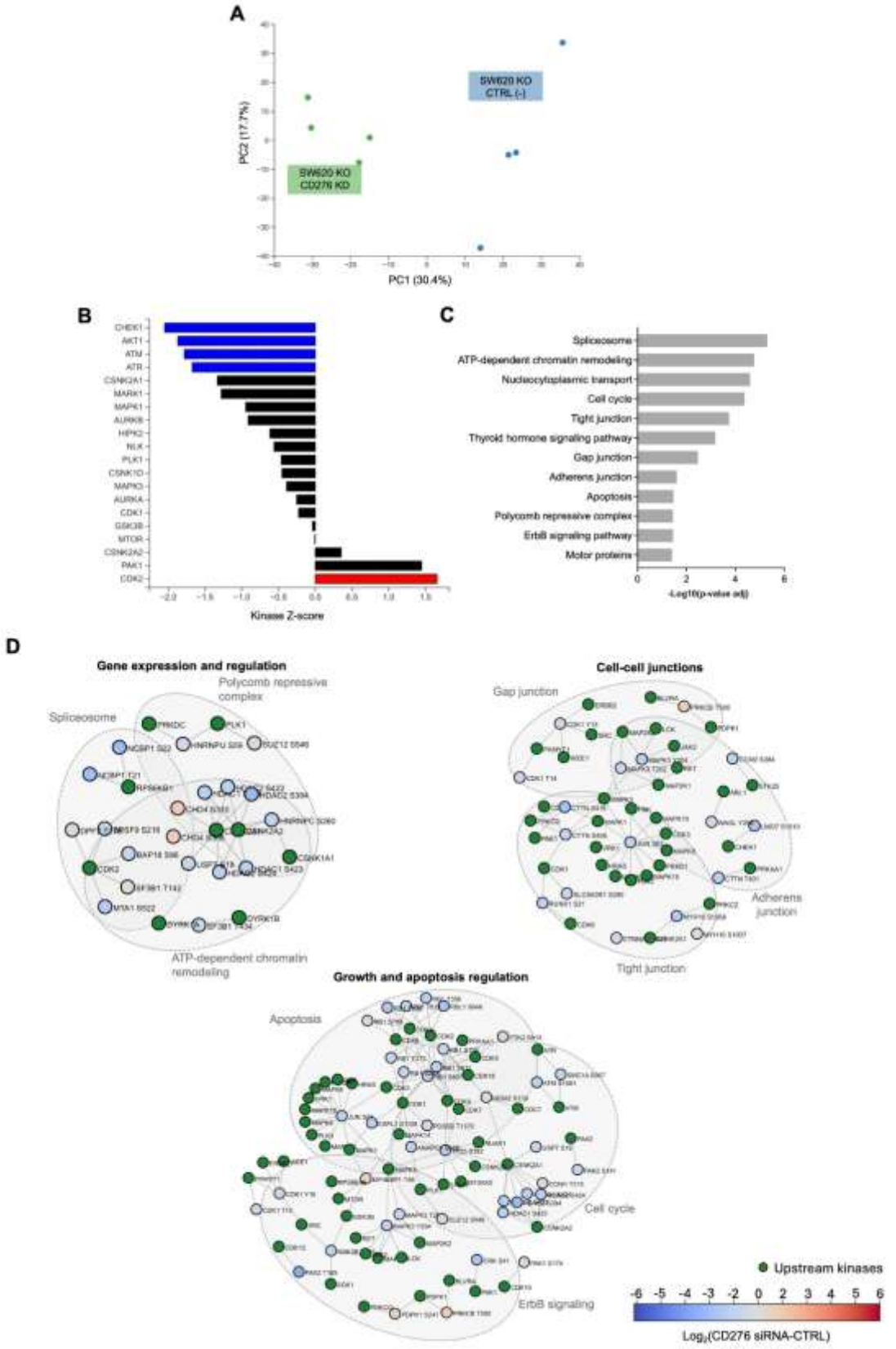

Figure 8. Comprehensive phosphoproteomics analysis. (**A**) PCA of global phosphoproteomic data from SW620 *C1GALT1* KO cells with CD276 knockdown (green) and control siRNA (blue). Distinct clustering indicates separation of phospho-signalling profiles between CD276-silenced and control cells. (**B**) Kinase activity analysis showing Z-scores for kinases differently regulated upon CD276 knockdown. Blue bars indicate kinases with significantly reduced activity (negative Z-score), red indicates increased activity

(positive Z-score), and black denotes minimal changes. (**C**) Pathway enrichment analysis of phosphorylated proteins following CD276 knockdown. Bar graph displays the top pathways ($-\log_2$ adjusted p-value), including spliceosome assembly, chromatin remodelling and cell junction organisation. (**D**) Network analysis of phosphorylation events mapped to functional modules. Nodes represent phosphoproteins grouped by biological processes: gene expression and regulation (top left), cell-cell junctions (top right), and growth/apoptosis regulation (below). Node colour indicates $\log_2$ fold change in phosphorylation (CD276 siRNA vs control), with blue for decreased and red for increased phosphorylation. Green circles denote upstream kinases.

Network analysis of phosphorylation events demonstrated reduced phosphorylation across key nuclear and chromatin-associated proteins, including CHD4, HDAC2 and MTA1, which are core components of the NuRD complex (Figure 8D). Specifically, CD276 knockdown led to reduced phosphorylation at HDAC2 S394 and loss of MTA1 S522 phosphorylation. Increased phosphorylation was observed at CHD4 S308 and S310. At the cytoskeletal level, phosphorylation of targets involved in adherens junctions, tight junctions and gap junctions, such as CTTN, MYH10 and LMO7, was markedly reduced (Figure 8D). Reduced phosphorylation was also detected on several RB1 residues and JUN S63. In contrast, hyperphosphorylation of MAPK3, also known as ERK1, was observed. In CD276-expressing control cells, altered phosphorylation was observed on proteins related to cell cycle checkpoints, metabolic processes, and alternative splicing (Figure 8B, D).

5. Discussion

5.1. Aberrant *O*-glycosylation of CD276 amplifies pro-tumorigenic functions in CRC cells

This study investigated the functional impact of CD276 and its altered glycosylation in CRC cells. The findings demonstrate that aberrant *O*-glycosylation, specifically induced by *C1GALT1* KO, fundamentally alters CD276's functional role, particularly amplifying its pro-tumorigenic functions in metastatic, mesenchymal-like contexts. These results highlight that disrupted *O*-glycosylation enhances CD276's proliferative signalling capabilities in a cell line-dependent fashion. The overarching findings align with prior evidence that glycosylation modulates immune checkpoint molecules and their downstream signalling in cancer cells, impacting both proliferation and invasion (39, 55).

The differential response to CD276 knockdown between the epithelial-like SW480 cells and the mesenchymal-like SW620 cells underscores the critical importance of cellular context. In the SW480 cell line, CD276 depletion resulted in minimal proliferative capacity. This indicates that while aberrant *O*-glycosylation is present, CD276's contribution to proliferation in this primary tumour-derived cell line may be less pronounced or context-dependent. In contrast, the SW620 cell line, derived from a lymph node metastasis and exhibiting a mesenchymal-like phenotype, displayed a markedly different and more pronounced response. CD276 knockdown led to significant proliferation suppression specifically in the *C1GALT1* KO SW620 cells, while wild-type SW620 cells showed no significant proliferative changes. This observation is consistent with reports that metastatic CRC cells exhibit a heightened dependence on immune checkpoint signalling for their survival and proliferation (115). The unique metabolic and signalling adaptations of metastatic cells might render them more susceptible to changes in CD276's glycosylation and subsequent function. This amplification of CD276's proliferative signalling capabilities in the metastatic context, particularly when its *O*-glycosylation is truncated, suggests a critical role for CD276 in maintaining the aggressive phenotype of disseminated CRC cells.

Furthermore, the pronounced reduction in invasion upon CD276 silencing in both *C1GALT1* KO cell lines (SW480 KO and SW620 KO) strongly supports a direct role for aberrantly glycosylated CD276 in sustaining invasive cellular behaviour. A particularly noteworthy finding emerged in SW620 cells, where *C1GALT1* knockout independently enhanced

invasive capacity. Crucially, this pro-invasive effect of *C1GALT1* deficiency was completely abolished by CD276 silencing. This observation directly reinforces CD276's functional importance within the context of immature *O*-glycosylation, implying that CD276 acts as a key effector or mediator of the pro-invasive phenotype driven by *C1GALT1* deficiency in metastatic CRC cells. These findings corroborate broader studies that implicate CD276 in promoting EMT and metastasis, now providing a glycosylation-specific mechanism for this role.

5.2. Aberrant CD276 orchestrates a dual proteomic reprogramming in glycosylation-deficient CRC cells

The quantitative proteomic profiling of glycoengineered SW620 cells, following CD276 silencing, revealed distinct global proteomic alterations that shed light on CD276's mechanistic role in CRC aggressiveness. The analysis indicates that aberrantly glycosylated CD276 orchestrates a dual regulatory role in CRC progression, broadly influencing fundamental biosynthetic pathways and simultaneously modulating cellular stress responses.

In the presence of aberrantly glycosylated CD276 (i.e., in control *C1GALT1*KO SW620 cells), the overexpression of proteins associated with core cellular machinery, including cytoplasmic translation, ribosomal biogenesis, amino acid and nucleobase biosynthesis, as well as oxidative phosphorylation and long-chain fatty acid transport, was observed. This suggests that aberrantly glycosylated CD276 supports a highly anabolic and metabolically active state, crucial for sustaining the observed aggressive proliferative and invasive phenotypes. Furthermore, the increased abundance of proteins associated with ubiquitin ligase regulation, chaperone binding, phosphoprotein binding, and potassium ion transport in CD276-expressing cells indicates that aberrant CD276 contributes to maintaining cellular quality control mechanisms that may be essential for navigating the stress of a highly anabolic cancerous state.

Conversely, CD276 silencing in glycoengineered SW620 cells triggered a coordinated proteomic shift, revealing both suppression of certain pathways and activation of distinct adaptive responses. Pathways analysis identified a significant downregulation of proteins involved in fundamental biosynthetic processes, including cytoplasmic translation, ribosomal biogenesis, and aspects of energy metabolism (oxidative phosphorylation and

long-chain fatty acid transport). This broad suppression of core anabolic and metabolic functions in the absence of CD276 supports its role as a critical factor in sustaining the highly active state of glycosylation-deficient metastatic cells.

Critically, concomitant with these suppressions, CD276 depletion in *C1GALT1* KO SW620 cells led to the activation of compensatory cellular mechanisms. Pathways enriched in CD276-silenced cells included heightened mitochondrial energy metabolism, ATP synthesis, and electron transport, suggesting that the normal presence of CD276 may exert a disruptive influence on cellular energy balance, with its absence triggering a compensatory bioenergetic enhancement. Additionally, CD276 depletion significantly amplified mechanisms responsible for targeting newly synthesised proteins to their correct cellular locations (indicated by increased signal sequence binding proteins, crucial for directing proteins to the secretory pathway or cellular membranes (116)) and profoundly altered RNA processing events. Increased abundance of snRNA and pre-mRNA binding proteins, key players in RNA maturation and splicing (117, 118), alongside enriched RNA helicase activity and various RNA methyltransferase activities, points towards a robust upregulation of ribonucleoprotein assembly and RNA metabolism. Furthermore, proteins involved in genome maintenance and chromatin organisation, including DNA repair, telomere maintenance, and DNA binding, were also found to be more abundant upon CD276 silencing.

Collectively, these patterns indicate that silencing aberrantly glycosylated CD276 in the context of *C1GALT1* knockout induces a dual cellular response. It leads to a broad suppression of fundamental biosynthetic and metabolic pathways that CD276 normally promotes, while selectively enhancing cellular mechanisms for protein targeting, RNA processing fidelity, and genome integrity maintenance. This reprogramming highlights CD276's function as a metabolic and proteostatic gatekeeper; its loss under glycosylation deficiency induces adaptive stress responses centred on RNA/DNA fidelity and energy plasticity. These findings align with established roles of CD276 in cancer metabolic reprogramming and stress adaptation (36) and are reminiscent of adaptive responses to immune checkpoint blockade observed previously, where cancer cells rewire their RNA processing machinery to maintain growth and survival (119).

5.3. Aberrant *O*-Glycosylation of CD276 Sustains Oncogenic Phosphorylation Networks Driving CRC Aggressiveness

Phosphoproteomic analyses provided crucial mechanistic insight into how aberrant *O*-glycosylation of CD276 contributes to CRC progression. The distinct phospho-signalling profile observed following CD276 knockdown in glycoengineered SW620 cells underscores the pivotal role of aberrantly glycosylated CD276 in orchestrating oncogenic kinase networks. The pronounced reduction in global phosphorylation and specific kinase activities, particularly those implicated in cell motility, chromatin remodelling and immune modulation, suggests that CD276 is essential for maintaining the phosphorylation landscape that supports tumour cell plasticity (120–122).

KSEA revealed a significant downregulation of ATR, ATM, AKT1, and CHEK1 activity. These kinases are involved in critical cellular processes, including DNA damage response, cell adhesion, survival, and immune evasion (123). Specifically, the decreased activity of ATR, ATM, and CHEK1, central to the DNA damage response and checkpoint regulation, suggests that CD276's presence normally maintains a phosphorylation state that supports checkpoint adaptation. Their downregulation upon CD276 silencing could impair cell cycle arrest and DNA repair capacity, potentially sensitising cells to genotoxic stress. Simultaneously, the reduction in AKT1 activity likely compromises pro-survival signalling and cytoskeletal dynamics, which in turn affect cellular adhesion and migration, thereby indicating that aberrantly glycosylated CD276 sustains pro-migratory signalling pathways (124). Collectively, these KSEA findings suggest that CD276 depletion leads to a coordinated downregulation of key kinases and downstream signalling modules controlling DNA damage response, survival, adhesion, and gene expression, which could collectively reduce tumour cell plasticity and resilience, consistent with the observed reduction in proliferation and invasion.

Network analysis of phosphorylation events provided further details on these regulatory changes. Reduced phosphorylation of core components of the NuRD complex, including HDAC2 and MTA1, was observed (125, 126). Notably, CD276 knockdown led to dephosphorylation at HDAC2-S394, a site whose hypo-phosphorylation is known to impair HDAC2 deacetylase activity and promote transcription of growth-inhibitory genes like *p21* (127, 128). Concurrently, the loss of MTA1 S522 phosphorylation is associated with diminished capability to respond to cellular stress and reduced adaptability to new microenvironments. These changes collectively highlight the role of aberrant glycosylated

CD276 in enhancing the plasticity and metastatic potential of the tumour cells through direct modulation of chromatin remodelling complexes.

Interestingly, increased phosphorylation was observed at CHD4 S308 and S310 residues upon CD276 silencing. These modifications are involved in DNA damage responses and checkpoint control (129), suggesting a compensatory activation of chromatin remodelling and DNA repair pathways in the absence of aberrantly glycosylated CD276. This aligns with the proteomic data, which also showed an upregulation of DNA repair proteins upon CD276 silencing, further supporting a shift from a pro-proliferative to a state prioritising genome integrity in the absence of CD276.

At the cytoskeletal level, phosphorylation of critical regulators of lamellipodia formation and microtubule remodelling, such as CTTN, MYH10 and LMO7, was markedly reduced. Their dephosphorylation is directly aligned with the observed reduction in invasive capacity following CD276 silencing (130). These findings strongly support a role for aberrantly glycosylated CD276 in maintaining an invasive phenotype through cytoskeletal plasticity. The disruption of these pathways upon CD276 knockdown reflects a coordinated collapse of the invasive and proliferative signalling axes that CD276 normally sustains.

Further, reduced phosphorylation of several RB1 residues and reduced JUN S63 were observed, both known to control the cell cycle and resistance to apoptosis when phosphorylated. In contrast, hyperphosphorylation of MAPK3 (ERK1), a member of the ErbB signalling pathway, was noted. Control cells, expressing aberrantly glycosylated CD276, exhibited phosphosite signatures characteristic of a stress-adaptive, invasive phenotype. These phosphorylation patterns and kinase activities are known to support checkpoint adaptation, metabolic rewiring, and alternative splicing programs (131-134), all features strongly associated with EMT and invasive behaviour. The reversal of many of these "stress-adaptive" phosphorylation patterns upon CD276 silencing reinforces that aberrantly glycosylated CD276 acts as a central regulator of invasive reprogramming within CRC cells.

Collectively, the phosphoproteomic data reveal that aberrantly glycosylated CD276 orchestrates a kinase-driven signalling program that profoundly promotes proliferation, invasion, and potentially resistance to apoptosis in CRC. This study provides a mechanistic framework linking aberrant *O*-glycosylation to the specific kinase activities and phosphorylation events that sustain aggressive CRC phenotypes.

6. Conclusion

The present results provide compelling mechanistic evidence that aberrant *O*-glycosylation of CD276 is not merely a passive bystander, but an active driver of oncogenic signalling in CRC. These findings significantly extend previous observations that CD276 expression correlates with poor prognosis and metastasis in CRC and other cancers. Importantly, the presented multi-omics data collectively support a novel model in which glycosylation-dependent modulation of CD276 amplifies kinase-driven signalling cascades, thereby integrating key metabolic, proliferative, invasive and immune-evasive mechanisms within aggressive CRC cells.

This project also highlights the substantial utility of SW620 *C1GALT1* knockout cells as a robust *in vitro* model for dissecting the intricate interplay between glycosylation and immune checkpoint signalling in metastatic CRC. The comprehensive proteomic and phosphoproteomic datasets generated here provide a valuable resource for deciphering the complex biology of glycosylated CD276 and for identifying novel therapeutic targets within its signalling axis.

While the study establishes a clear functional link between aberrant glycosylation, CD276, and aggressive CRC phenotypes, the precise molecular mechanisms by which specific glycan structures on CD276 modulate its interactions and downstream signalling warrant further investigation. Future studies employing site-specific glycoengineering approaches and validated *in vivo* models will be crucial to rigorously validate these findings and to explore the efficacy of therapeutic interventions specifically targeting glycosylated CD276.

In conclusion, the findings presented here unequivocally establish that CD276 glycosylation status is a decisive factor in shaping its oncogenic potential in CRC. Aberrant *O*-glycosylation profoundly enhances the ability of CD276 to drive tumour-promoting signalling pathways, particularly in aggressive and metastatic cell contexts. These insights elevate CD276 glycosylation not only as a biomarker for disease progression but also as a highly promising therapeutic target. Specifically, strategies aimed at targeting CD276 and its associated glycosylation machinery, potentially in combination with conventional immune checkpoint inhibition, may offer novel opportunities to disrupt the fundamental survival, invasion, and immune evasion mechanisms that underpin advanced CRC.

7. References

1. Bray F, Laversanne M, Sung H, Ferlay J, Siegel RL, Soerjomataram I, et al. Global cancer statistics 2022: GLOBOCAN estimates of incidence and mortality worldwide for 36 cancers in 185 countries. CA Cancer J Clin. 2024;74(3):229-63.
2. Cancer IAfRo. Cancer Today Globocan 2022 Portugal. World Health Organization; 2022.
3. Society AC. Cancer Facts & Figures 2025. American Cancer Society journal, CA: A Cancer Journal for Clinicians. 2025.
4. Glade MJ. Food, nutrition, and the prevention of cancer: a global perspective. American Institute for Cancer Research/World Cancer Research Fund, American Institute for Cancer Research, 1997. Nutrition. 1999;15(6):523-6.
5. Winawer SJ, Fletcher RH, Miller L, Godlee F, Stolar MH, Mulrow CD, et al. Colorectal cancer screening: clinical guidelines and rationale. Gastroenterology. 1997;112(2):594-642.
6. Lieberman DA, Weiss DG. One-time screening for colorectal cancer with combined fecal occult-blood testing and examination of the distal colon. N Engl J Med. 2001;345(8):555-60.
7. Cole SR, Young GP, Esterman A, Cadd B, Morcom J. A randomised trial of the impact of new faecal haemoglobin test technologies on population participation in screening for colorectal cancer. J Med Screen. 2003;10(3):117-22.
8. Mandel JS, Church TR, Bond JH, Ederer F, Geisser MS, Mongin SJ, et al. The effect of fecal occult-blood screening on the incidence of colorectal cancer. N Engl J Med. 2000;343(22):1603-7.
9. Toyota M, Ohe-Toyota M, Ahuja N, Issa JP. Distinct genetic profiles in colorectal tumors with or without the CpG island methylator phenotype. Proc Natl Acad Sci U S A. 2000;97(2):710-5.
10. Yamashita K, Dai T, Dai Y, Yamamoto F, Perucho M. Genetics supersedes epigenetics in colon cancer phenotype. Cancer Cell. 2003;4(2):121-31.
11. Toyota M, Ahuja N, Ohe-Toyota M, Herman JG, Baylin SB, Issa JP. CpG island methylator phenotype in colorectal cancer. Proc Natl Acad Sci U S A. 1999;96(15):8681-6.
12. Tsao J-L, Yatabe Y, Salovaara R, Järvinen HJ, Mecklin J-P, Aaltonen LA, et al. Genetic reconstruction of individual colorectal tumor histories. Proceedings of the National Academy of Sciences. 2000;97(3):1236-41.
13. Pearlman R, Frankel WL, Swanson B, Zhao W, Yilmaz A, Miller K, et al. Prevalence and Spectrum of Germline Cancer Susceptibility Gene Mutations Among Patients With Early-Onset Colorectal Cancer. JAMA Oncol. 2017;3(4):464-71.
14. Ichii S, Horii A, Nakatsuru S, Furuyama J, Utsunomiya J, Nakamura Y. Inactivation of both APC alleles in an early stage of colon adenomas in a patient with familial adenomatous polyposis (FAP). Human Molecular Genetics. 1992;1(6):387-90.
15. Croner RS, Brueckl WM, Reingruber B, Hohenberger W, Guenther K. Age and manifestation related symptoms in familial adenomatous polyposis. BMC Cancer. 2005;5:24.
16. Reitmair AH, Cai JC, Bjerknes M, Redston M, Cheng H, Pind MT, et al. MSH2 deficiency contributes to accelerated APC-mediated intestinal tumorigenesis. Cancer Res. 1996;56(13):2922-6.
17. Le DT, Uram JN, Wang H, Bartlett BR, Kemberling H, Eyring AD, et al. PD-1 Blockade in Tumors with Mismatch-Repair Deficiency. N Engl J Med. 2015;372(26):2509-20.
18. Khalid-de Bakker CA, Jonkers DM, Hameeteman W, de Ridder RJ, Masclee AA, Stockbrügger RW. Opportunistic Screening of Hospital Staff Using Primary Colonoscopy:

Participation, Discomfort and Willingness to Repeat the Procedure. Digestion. 2011;84(4):281-8.
19. Alouani E, Mercier M, Flecchia C, Auclin E, Hollebecque A, Mazard T, et al. Efficacy of immunotherapy in mismatch repair-deficient advanced colorectal cancer in routine clinical practice. An AGEO study. ESMO Open. 2023;8(3):101574.
20. Bartlett DL, Berlin J, Lauwers GY, Messersmith WA, Petrelli NJ, Venook AP. Chemotherapy and Regional Therapy of Hepatic Colorectal Metastases: Expert Consensus Statement. Annals of Surgical Oncology. 2006;13(10):1284-92.
21. Ellis LM, Curley SA, Grothey A. Surgical resection after downsizing of colorectal liver metastasis in the era of bevacizumab. J Clin Oncol. 2005;23(22):4853-5.
22. Saltz LB, Lenz HJ, Kindler HL, Hochster HS, Wadler S, Hoff PM, et al. Randomized phase II trial of cetuximab, bevacizumab, and irinotecan compared with cetuximab and bevacizumab alone in irinotecan-refractory colorectal cancer: the BOND-2 study. J Clin Oncol. 2007;25(29):4557-61.
23. Moertel CG, Fleming TR, Macdonald JS, Haller DG, Laurie JA, Tangen CM, et al. Fluorouracil plus levamisole as effective adjuvant therapy after resection of stage III colon carcinoma: a final report. Ann Intern Med. 1995;122(5):321-6.
24. Douillard JY, Cunningham D, Roth AD, Navarro M, James RD, Karasek P, et al. Irinotecan combined with fluorouracil compared with fluorouracil alone as first-line treatment for metastatic colorectal cancer: a multicentre randomised trial. Lancet. 2000;355(9209):1041-7.
25. Goldberg RM, Sargent DJ, Morton RF, Fuchs CS, Ramanathan RK, Williamson SK, et al. A randomized controlled trial of fluorouracil plus leucovorin, irinotecan, and oxaliplatin combinations in patients with previously untreated metastatic colorectal cancer. J Clin Oncol. 2004;22(1):23-30.
26. Chalabi M, Fanchi LF, Dijkstra KK, Van den Berg JG, Aalbers AG, Sikorska K, et al. Neoadjuvant immunotherapy leads to pathological responses in MMR-proficient and MMR-deficient early-stage colon cancers. Nature Medicine. 2020;26(4):566-76.
27. André T, Shiu K-K, Kim TW, Jensen BV, Jensen LH, Punt C, et al. Pembrolizumab in Microsatellite-Instability–High Advanced Colorectal Cancer. New England Journal of Medicine. 2020;383(23):2207-18.
28. Overman MJ, McDermott R, Leach JL, Lonardi S, Lenz HJ, Morse MA, et al. Nivolumab in patients with metastatic DNA mismatch repair-deficient or microsatellite instability-high colorectal cancer (CheckMate 142): an open-label, multicentre, phase 2 study. Lancet Oncol. 2017;18(9):1182-91.
29. Lu Z, Zhao ZX, Cheng P, Huang F, Guan X, Zhang MG, et al. B7-H3 immune checkpoint expression is a poor prognostic factor in colorectal carcinoma. Mod Pathol. 2020;33(11):2330-40.
30. Chapoval AI, Ni J, Lau JS, Wilcox RA, Flies DB, Liu D, et al. B7-H3: a costimulatory molecule for T cell activation and IFN-gamma production. Nat Immunol. 2001;2(3):269-74.
31. Lu H, Shi T, Wang M, Li X, Gu Y, Zhang X, et al. B7-H3 inhibits the IFN-γ-dependent cytotoxicity of Vγ9Vδ2 T cells against colon cancer cells. Oncoimmunology. 2020;9(1):1748991.
32. Steinberger P, Majdic O, Derdak SV, Pfistershammer K, Kirchberger S, Klauser C, et al. Molecular characterization of human 4Ig-B7-H3, a member of the B7 family with four Ig-like domains. J Immunol. 2004;172(4):2352-9.

33. Chen LC, Yang PC, Chen CY, Chiang SF, Chen TW, Chen WT, et al. Dual Inhibition of B7-H3 and EGFR Overcomes Acquired Chemoresistance in Colon Adenocarcinoma. J Cancer. 2024;15(6):1750-61.
34. Lee H, Kim JH, Yang SY, Kong J, Oh M, Jeong DH, et al. Peripheral blood gene expression of B7 and CD28 family members associated with tumor progression and microscopic lymphovascular invasion in colon cancer patients. J Cancer Res Clin Oncol. 2010;136(9):1445-52.
35. Kovaleva OV, Gratchev AN, Sokolov NY, Maslennikov VV, Kuzmin YB, Gershtein ES, et al. Soluble B7-H3 in Colorectal Cancer. Bull Exp Biol Med. 2023;176(1):87-90.
36. Lim S, Liu H, Madeira da Silva L, Arora R, Liu Z, Phillips JB, et al. Immunoregulatory Protein B7-H3 Reprograms Glucose Metabolism in Cancer Cells by ROS-Mediated Stabilization of HIF1α. Cancer Res. 2016;76(8):2231-42.
37. Wang R, Ma Y, Zhan S, Zhang G, Cao L, Zhang X, et al. B7-H3 promotes colorectal cancer angiogenesis through activating the NF-κB pathway to induce VEGFA expression. Cell Death Dis. 2020;11(1):55.
38. Jiang B, Zhang T, Liu F, Sun Z, Shi H, Hua D, et al. The co-stimulatory molecule B7-H3 promotes the epithelial-mesenchymal transition in colorectal cancer. Oncotarget. 2016;7(22):31755-71.
39. Liu F, Zhang T, Zou S, Jiang B, Hua D. B7-H3 promotes cell migration and invasion through the Jak2/Stat3/MMP9 signaling pathway in colorectal cancer. Mol Med Rep. 2015;12(4):5455-60.
40. Zhang Z-y, Xu J-h, Zhang J-l, Lin Y-x, Ou-Yang J. CD276 enhances sunitinib resistance in clear cell renal cell carcinoma by promoting DNA damage repair and activation of FAK-MAPK signaling pathway. BMC Cancer. 2024;24(1):650.
41. Peuker K, Strigli A, Tauriello DVF, Hendricks A, von Schonfels W, Burmeister G, et al. Microbiota-dependent activation of the myeloid calcineurin-NFAT pathway inhibits B7H3- and B7H4-dependent anti-tumor immunity in colorectal cancer. Immunity. 2022;55(4):701-17 e7.
42. Meng F, Yang M, Chen Y, Chen W, Wang W. miR-34a induces immunosuppression in colorectal carcinoma through modulating a SIRT1/NF-kappaB/B7-H3/TNF-alpha axis. Cancer Immunol Immunother. 2021;70(8):2247-59.
43. Hashiguchi M, Kobori H, Ritprajak P, Kamimura Y, Kozono H, Azuma M. Triggering receptor expressed on myeloid cell-like transcript 2 (TLT-2) is a counter-receptor for B7-H3 and enhances T cell responses. Proc Natl Acad Sci U S A. 2008;105(30):10495-500.
44. Leitner J, Klauser C, Pickl WF, Stockl J, Majdic O, Bardet AF, et al. B7-H3 is a potent inhibitor of human T-cell activation: No evidence for B7-H3 and TREML2 interaction. Eur J Immunol. 2009;39(7):1754-64.
45. Husain B, Ramani SR, Chiang E, Lehoux I, Paduchuri S, Arena TA, et al. A Platform for Extracellular Interactome Discovery Identifies Novel Functional Binding Partners for the Immune Receptors B7-H3/CD276 and PVR/CD155. Mol Cell Proteomics. 2019;18(11):2310-23.
46. Luo L, Chapoval AI, Flies DB, Zhu G, Hirano F, Wang S, et al. B7-H3 enhances tumor immunity in vivo by costimulating rapid clonal expansion of antigen-specific CD8+ cytolytic T cells. J Immunol. 2004;173(9):5445-50.
47. Yamato I, Sho M, Nomi T, Akahori T, Shimada K, Hotta K, et al. Clinical importance of B7-H3 expression in human pancreatic cancer. Br J Cancer. 2009;101(10):1709-16.

48. Lee YH, Martin-Orozco N, Zheng P, Li J, Zhang P, Tan H, et al. Inhibition of the B7-H3 immune checkpoint limits tumor growth by enhancing cytotoxic lymphocyte function. Cell Res. 2017;27(8):1034-45.
49. Suh WK, Gajewska BU, Okada H, Gronski MA, Bertram EM, Dawicki W, et al. The B7 family member B7-H3 preferentially down-regulates T helper type 1-mediated immune responses. Nat Immunol. 2003;4(9):899-906.
50. Durlanik S, Fundel-Clemens K, Viollet C, Huber HJ, Lenter M, Kitt K, et al. CD276 is an important player in macrophage recruitment into the tumor and an upstream regulator for PAI-1. Sci Rep. 2021;11(1):14849.
51. Sun L, Wang Q, Chen B, Zhao Y, Shen B, Wang H, et al. Gastric cancer mesenchymal stem cells derived IL-8 induces PD-L1 expression in gastric cancer cells via STAT3/mTOR-c-Myc signal axis. Cell Death Dis. 2018;9(9):928.
52. Gao Q, Cui L, Huang C, Chen Z, Wang X, Wen S, et al. Gastric cancer-derived mesenchymal stem cells promote gastric cancer cell lines migration by modulating CD276 expression. Exp Cell Res. 2023;422(1):113414.
53. Gao Q, Huang C, Liu T, Yang F, Chen Z, Sun L, et al. Gastric cancer mesenchymal stem cells promote tumor glycolysis and chemoresistance by regulating B7H3 in gastric cancer cells. J Cell Biochem. 2024;125(3):e30521.
54. Zhang P, Chen Z, Ning K, Jin J, Han X. Inhibition of B7-H3 reverses oxaliplatin resistance in human colorectal cancer cells. Biochem Biophys Res Commun. 2017;490(3):1132-8.
55. Hu C, Wang S, Wang J, Ruan X, Wu L, Zhang Z, et al. B7-H3 enhances colorectal cancer progression by regulating HB-EGF via HIF-1alpha. J Gastrointest Oncol. 2024;15(3):1035-49.
56. Ke TW, Chen CY, Chen WT, Tsai YY, Chiang SF, Huang CH, et al. Targeting B7-H3 enhances the efficacy of neoantigen-based cancer vaccine in combination with radiotherapy. NPJ Vaccines. 2025;10(1):80.
57. Loo D, Alderson RF, Chen FZ, Huang L, Zhang W, Gorlatov S, et al. Development of an Fc-enhanced anti-B7-H3 monoclonal antibody with potent antitumor activity. Clin Cancer Res. 2012;18(14):3834-45.
58. Wang C, Li Y, Jia L, Kim JK, Li J, Deng P, et al. CD276 expression enables squamous cell carcinoma stem cells to evade immune surveillance. Cell Stem Cell. 2021;28(9):1597-613 e7.
59. Seaman S, Zhu Z, Saha S, Zhang XM, Yang MY, Hilton MB, et al. Eradication of Tumors through Simultaneous Ablation of CD276/B7-H3-Positive Tumor Cells and Tumor Vasculature. Cancer Cell. 2017;31(4):501-15.e8.
60. Zhang J, Zhou ZZ, Chen K, Kim S, Cho IS, Varadkar T, et al. A CD276-Targeted Antibody-Drug Conjugate to Treat Non-Small Lung Cancer (NSCLC). Cells. 2023;12(19).
61. Du H, Hirabayashi K, Ahn S, Kren NP, Montgomery SA, Wang X, et al. Antitumor Responses in the Absence of Toxicity in Solid Tumors by Targeting B7-H3 via Chimeric Antigen Receptor T Cells. Cancer Cell. 2019;35(2):221-37.e8.
62. Wang M, Zhang Z, Chen M, Lv Y, Tian S, Meng F, et al. FDW028, a novel FUT8 inhibitor, impels lysosomal proteolysis of B7-H3 via chaperone-mediated autophagy pathway and exhibits potent efficacy against metastatic colorectal cancer. Cell Death Dis. 2023;14(8):495.
63. Huang M, Luo J, Ji X, Hu M, Xue Y, Liu Q. Deficiency of tumor-expressed B7-H3 augments anti-tumor efficacy of anti-PD-L1 monotherapy rather than the combined chemoimmunotherapy in ovarian cancer. Pharmacol Res. 2022;186:106512.

64. Cao W, Zhang X, Chen J, Sun L, He H, Yu F. Codelivery of apigenin, FdUMP and CD276 antibody synergistic inhibit colorectal cancer by ferroptosis-apoptosis-pyroptosis and CD276 blockade. Asian J Pharm Sci. 2025;20(2):101016.
65. Pinho SS, Reis CA. Glycosylation in cancer: mechanisms and clinical implications. Nat Rev Cancer. 2015;15(9):540-55.
66. Varki A, Sharon N. Historical Background and Overview. In: Varki A, Cummings RD, Esko JD, Freeze HH, Stanley P, Bertozzi CR, et al., editors. Essentials of Glycobiology. Cold Spring Harbor (NY): Cold Spring Harbor Laboratory Press
Copyright © 2009, The Consortium of Glycobiology Editors, La Jolla, California.; 2009.
67. Hanson SR, Culyba EK, Hsu TL, Wong CH, Kelly JW, Powers ET. The core trisaccharide of an N-linked glycoprotein intrinsically accelerates folding and enhances stability. Proc Natl Acad Sci U S A. 2009;106(9):3131-6.
68. Kung LA, Tao SC, Qian J, Smith MG, Snyder M, Zhu H. Global analysis of the glycoproteome in Saccharomyces cerevisiae reveals new roles for protein glycosylation in eukaryotes. Mol Syst Biol. 2009;5:308.
69. Ferreira JA, Magalhães A, Gomes J, Peixoto A, Gaiteiro C, Fernandes E, et al. Protein glycosylation in gastric and colorectal cancers: Toward cancer detection and targeted therapeutics. Cancer Letters. 2017;387:32-45.
70. Hu C, Zhang S, Duan F, Huang X, Huang J, Zhu Z, et al. Sialylated IgG expressed in triple-negative breast cancer cells promotes cancer progression by promoting glycolysis. Breast Cancer Res. 2025;27(1):96.
71. Balog CI, Stavenhagen K, Fung WL, Koeleman CA, McDonnell LA, Verhoeven A, et al. N-glycosylation of colorectal cancer tissues: a liquid chromatography and mass spectrometry-based investigation. Mol Cell Proteomics. 2012;11(9):571-85.
72. Jiang Y, Liu Z, Xu F, Dong X, Cheng Y, Hu Y, et al. Aberrant O-glycosylation contributes to tumorigenesis in human colorectal cancer. J Cell Mol Med. 2018;22(10):4875-85.
73. Chen YW, Tekle C, Fodstad O. The immunoregulatory protein human B7H3 is a tumor-associated antigen that regulates tumor cell migration and invasion. Curr Cancer Drug Targets. 2008;8(5):404-13.
74. Liu G, Chen L, Zhao J, Jiang Y, Guo Y, Mao X, et al. Deciphering the Metabolic Impact and Clinical Relevance of N-Glycosylation in Colorectal Cancer through Comprehensive Glycoproteomic Profiling. Adv Sci (Weinh). 2025;12(21):e2415645.
75. Funayama R, Wang Y, Hosogane M, Kao W-C, Toyama S, Ohira M, et al. Alternative Splicing of FBLN2 Generates a Prometastatic Extracellular Matrix in Gastrointestinal Cancers by Determining N-Glycosylation of Fibulin 2. Genes to Cells. 2025;30(3):e70027.
76. Krug J, Rodrian G, Petter K, Yang H, Khoziainova S, Guo W, et al. N-glycosylation Regulates Intrinsic IFN-gamma Resistance in Colorectal Cancer: Implications for Immunotherapy. Gastroenterology. 2023;164(3):392-406 e5.
77. Wang Y, Liu N, Zou Y, Jie J, Liu Z, Zou X. A robust label-free workflow for the immunoglobulin G subclass site-specific N-glycopeptides and the glycosylation of IgG 2 correlated with colorectal cancer. Talanta. 2025;296:128326.
78. He L, Guo Z, Wang W, Tian S, Lin R. FUT2 inhibits the EMT and metastasis of colorectal cancer by increasing LRP1 fucosylation. Cell Commun Signal. 2023;21(1):63.
79. Muinelo-Romay L, Gil-Martín E, Fernández-Briera A. α(1,2)fucosylation in human colorectal carcinoma. Oncol Lett. 2010;1(2):361-6.

80. Phueaouan T, Chaiyawat P, Netsirisawan P, Chokchaichamnankit D, Punyarit P, Srisomsap C, et al. Aberrant O-GlcNAc-modified proteins expressed in primary colorectal cancer. Oncol Rep. 2013;30(6):2929-36.
81. Brockhausen I, Wandall HH, Hagen KGT, Stanley P. O-GalNAc Glycans. In: Varki A, Cummings RD, Esko JD, Stanley P, Hart GW, Aebi M, et al., editors. Essentials of Glycobiology. Cold Spring Harbor (NY): Cold Spring Harbor Laboratory Press
Copyright © 2022 The Consortium of Glycobiology Editors, La Jolla, California; published by Cold Spring Harbor Laboratory Press; doi:10.1101/glycobiology.4e.10. All rights reserved.; 2022. p. 117-28.
82. Barrow H, Tam B, Duckworth CA, Rhodes JM, Yu LG. Suppression of core 1 Gal-transferase is associated with reduction of TF and reciprocal increase of Tn, sialyl-Tn and Core 3 glycans in human colon cancer cells. PLoS One. 2013;8(3):e59792.
83. Giuffrè G, Vitarelli E, Tuccari G, Ponz de Leon M, Barresi G. Detection of Tn, sialosyl-Tn and T antigens in hereditary nonpolyposis colorectal cancer. Virchows Arch. 1996;429(6):345-52.
84. Yang JM, Byrd JC, Siddiki BB, Chung YS, Okuno M, Sowa M, et al. Alterations of O-glycan biosynthesis in human colon cancer tissues. Glycobiology. 1994;4(6):873-84.
85. Hung JS, Huang J, Lin YC, Huang MJ, Lee PH, Lai HS, et al. C1GALT1 overexpression promotes the invasive behavior of colon cancer cells through modifying O-glycosylation of FGFR2. Oncotarget. 2014;5(8):2096-106.
86. Radhakrishnan P, Dabelsteen S, Madsen FB, Francavilla C, Kopp KL, Steentoft C, et al. Immature truncated O-glycophenotype of cancer directly induces oncogenic features. Proc Natl Acad Sci U S A. 2014;111(39):E4066-75.
87. Iwai T, Kudo T, Kawamoto R, Kubota T, Togayachi A, Hiruma T, et al. Core 3 synthase is down-regulated in colon carcinoma and profoundly suppresses the metastatic potential of carcinoma cells. Proceedings of the National Academy of Sciences. 2005;102(12):4572-7.
88. Huang MC, Chen HY, Huang HC, Huang J, Liang JT, Shen TL, et al. C2GnT-M is downregulated in colorectal cancer and its re-expression causes growth inhibition of colon cancer cells. Oncogene. 2006;25(23):3267-76.
89. Liu Z, Liu J, Dong X, Hu X, Jiang Y, Li L, et al. Tn antigen promotes human colorectal cancer metastasis via H-Ras mediated epithelial-mesenchymal transition activation. J Cell Mol Med. 2019;23(3):2083-92.
90. Itzkowitz SH, Bloom EJ, Kokal WA, Modin G, Hakomori S, Kim YS. Sialosyl-Tn. A novel mucin antigen associated with prognosis in colorectal cancer patients. Cancer. 1990;66(9):1960-6.
91. Hsu HP, Lai MD, Lee JC, Yen MC, Weng TY, Chen WC, et al. Mucin 2 silencing promotes colon cancer metastasis through interleukin-6 signaling. Sci Rep. 2017;7(1):5823.
92. Zhang K, Sikut R, Hansson GC. A MUC1 mucin secreted from a colon carcinoma cell line inhibits target cell lysis by natural killer cells. Cell Immunol. 1997;176(2):158-65.
93. Wu YM, Liu CH, Huang MJ, Lai HS, Lee PH, Hu RH, et al. C1GALT1 enhances proliferation of hepatocellular carcinoma cells via modulating MET glycosylation and dimerization. Cancer Res. 2013;73(17):5580-90.
94. Gu Y, Ye Q, Huang X, Cao Y, Chaiswing L, She QB. Glycosaminoglycan modification of NRP1 exon 4-skipping variant drives colorectal cancer metastasis via endosomal-exosomal trafficking. Cancer Lett. 2025;620:217683.
95. Wan Y, Adair K, Herrmann A, Shan X, Xia L, Duckworth CA, et al. C1GalT1 expression reciprocally controls tumour cell-cell and tumour-macrophage interactions mediated by

galectin-3 and MGL with double impact on cancer development and progression. Cell Death Dis. 2023;14(8):547.
96. Saeland E, van Kooyk Y. Highly glycosylated tumour antigens: interactions with the immune system. Biochem Soc Trans. 2011;39(1):388-92.
97. Barrow H, Guo X, Wandall HH, Pedersen JW, Fu B, Zhao Q, et al. Serum galectin-2, -4, and -8 are greatly increased in colon and breast cancer patients and promote cancer cell adhesion to blood vascular endothelium. Clin Cancer Res. 2011;17(22):7035-46.
98. Yue S, Wang X, Wang L, Li J, Zhou Y, Chen Y, et al. MOTAI: A Novel Method for the Study of O-GalNAcylation and Complex O-Glycosylation in Cancer. Anal Chem. 2024;96(28):11137-45.
99. Loison I, Pioger A, Paget S, Metatla I, Mariette C, Piessen G, et al. O-GlcNAcylation inhibition redirects the response of colon cancer cells to chemotherapy from senescence to apoptosis. Cell Death & Disease. 2024;15(10):762.
100. Neves M, Azevedo R, Lima L, Oliveira MI, Peixoto A, Ferreira D, et al. Exploring sialyl-Tn expression in microfluidic-isolated circulating tumour cells: A novel biomarker and an analytical tool for precision oncology applications. N Biotechnol. 2019;49:77-87.
101. Heimburg-Molinaro J, Almogren A, Morey S, Glinskii OV, Roy R, Wilding GE, et al. Development, characterization, and immunotherapeutic use of peptide mimics of the Thomsen-Friedenreich carbohydrate antigen. Neoplasia. 2009;11(8):780-92.
102. O'Boyle KP, Zamore R, Adluri S, Cohen A, Kemeny N, Welt S, et al. Immunization of colorectal cancer patients with modified ovine submaxillary gland mucin and adjuvants induces IgM and IgG antibodies to sialylated Tn. Cancer Res. 1992;52(20):5663-7.
103. Ju T, Lanneau GS, Gautam T, Wang Y, Xia B, Stowell SR, et al. Human tumor antigens Tn and sialyl Tn arise from mutations in Cosmc. Cancer Res. 2008;68(6):1636-46.
104. An G, Wei B, Xia B, McDaniel JM, Ju T, Cummings RD, et al. Increased susceptibility to colitis and colorectal tumors in mice lacking core 3-derived O-glycans. J Exp Med. 2007;204(6):1417-29.
105. Freitas R, Miranda A, Ferreira D, Relvas-Santos M, Castro F, Ferreira E, et al. A multivalent CD44 glycoconjugate vaccine candidate for cancer immunotherapy. J Control Release. 2024;367:540-56.
106. Huang Y, Zhang HL, Li ZL, Du T, Chen YH, Wang Y, et al. FUT8-mediated aberrant N-glycosylation of B7H3 suppresses the immune response in triple-negative breast cancer. Nat Commun. 2021;12(1):2672.
107. Huang Y, Zhong W-Q, Yang X-Y, Shan J-L, Zhou L, Li Z-L, et al. Targeting site-specific N-glycosylated B7H3 induces potent antitumor immunity. Nature Communications. 2025;16(1).
108. Chen J-T, Chen C-H, Ku K-L, Hsiao M, Chiang C-P, Hsu T-L, et al. Glycoprotein B7-H3 overexpression and aberrant glycosylation in oral cancer and immune response. Proceedings of the National Academy of Sciences. 2015;112(42):13057-62.
109. Gao Y, Shen L, Dong T, Yang X, Cui H, Guo Y, et al. An N-glycoproteomic site-mapping analysis reveals glycoprotein alterations in esophageal squamous cell carcinoma. J Transl Med. 2022;20(1):285.
110. Yamato M, Hasegawa J, Maejima T, Hattori C, Kumagai K, Watanabe A, et al. DS-7300a, a DNA Topoisomerase I Inhibitor, DXd-Based Antibody-Drug Conjugate Targeting B7-H3, Exerts Potent Antitumor Activities in Preclinical Models. Mol Cancer Ther. 2022;21(4):635-46.

111. Shannon P, Markiel A, Ozier O, Baliga NS, Wang JT, Ramage D, et al. Cytoscape: a software environment for integrated models of biomolecular interaction networks. Genome Res. 2003;13(11):2498-504.
112. Bindea G, Mlecnik B, Hackl H, Charoentong P, Tosolini M, Kirilovsky A, et al. ClueGO: a Cytoscape plug-in to decipher functionally grouped gene ontology and pathway annotation networks. Bioinformatics. 2009;25(8):1091-3.
113. Tyanova S, Temu T, Cox J. The MaxQuant computational platform for mass spectrometry-based shotgun proteomics. Nature Protocols. 2016;11(12):2301-19.
114. Leeming MG, O'Callaghan S, Licata L, Iannuccelli M, Lo Surdo P, Micarelli E, et al. Phosphomatics: interactive interrogation of substrate-kinase networks in global phosphoproteomics datasets. Bioinformatics. 2021;37(11):1635-6.
115. Wang HB, Yao H, Li CS, Liang LX, Zhang Y, Chen YX, et al. Rise of PD-L1 expression during metastasis of colorectal cancer: Implications for immunotherapy. J Dig Dis. 2017;18(10):574-81.
116. Walter P, Ibrahimi I, Blobel G. Translocation of proteins across the endoplasmic reticulum. I. Signal recognition protein (SRP) binds to in-vitro-assembled polysomes synthesizing secretory protein. J Cell Biol. 1981;91(2 Pt 1):545-50.
117. Huranová M, Ivani I, Benda A, Poser I, Brody Y, Hof M, et al. The differential interaction of snRNPs with pre-mRNA reveals splicing kinetics in living cells. Journal of Cell Biology. 2010;191(1):75-86.
118. Luukkonen BGM, Séraphin B. A conditional U5 snRNA mutation affecting pre-mRNA splicing and nuclear pre-mRNA retention identifies SSD1/SRK1 as a general splicing mutant suppressor. Nucleic Acids Research. 1999;27(17):3455-65.
119. Zhai W, Comai L. Repression of RNA polymerase I transcription by the tumor suppressor p53. Mol Cell Biol. 2000;20(16):5930-8.
120. Hong H, Benveniste EN. The Immune Regulatory Role of Protein Kinase CK2 and Its Implications for Treatment of Cancer. Biomedicines. 2021;9(12).
121. Bhattacharjee RN, Banks GC, Trotter KW, Lee HL, Archer TK. Histone H1 phosphorylation by Cdk2 selectively modulates mouse mammary tumor virus transcription through chromatin remodeling. Mol Cell Biol. 2001;21(16):5417-25.
122. Fazil M, Prasannan P, Wong BHS, Kottaiswamy A, Salim N, Sze SK, et al. GSK3β Interacts With CRMP2 and Notch1 and Controls T-Cell Motility. Front Immunol. 2021;12:680071.
123. Casado P, Rodriguez-Prados JC, Cosulich SC, Guichard S, Vanhaesebroeck B, Joel S, et al. Kinase-substrate enrichment analysis provides insights into the heterogeneity of signaling pathway activation in leukemia cells. Sci Signal. 2013;6(268):rs6.
124. Strum SW, Gyenis L, Litchfield DW. CSNK2 in cancer: pathophysiology and translational applications. British Journal of Cancer. 2022;126(7):994-1003.
125. Liu Z, Ajit K, Wu Y, Zhu W-G, Gullerova M. The GATAD2B-NuRD complex drives DNA:RNA hybrid-dependent chromatin boundary formation upon DNA damage. The EMBO Journal. 2024;43(12):2453-85.
126. Sharifi Tabar M, Giardina C, Feng Y, Francis H, Moghaddas Sani H, Low JKK, et al. Unique protein interaction networks define the chromatin remodelling module of the NuRD complex. The FEBS Journal. 2022;289(1):199-214.
127. Simboeck E, Sawicka A, Zupkovitz G, Senese S, Winter S, Dequiedt F, et al. A Phosphorylation Switch Regulates the Transcriptional Activation of Cell Cycle Regulator p21 by Histone Deacetylase Inhibitors *. Journal of Biological Chemistry. 2010;285(52):41062-73.

128. Adenuga D, Rahman I. Protein kinase CK2-mediated phosphorylation of HDAC2 regulates co-repressor formation, deacetylase activity and acetylation of HDAC2 by cigarette smoke and aldehydes. Archives of Biochemistry and Biophysics. 2010;498(1):62-73.
129. O'Shaughnessy A, Hendrich B. CHD4 in the DNA-damage response and cell cycle progression: not so NuRDy now. Biochemical Society Transactions. 2013;41(3):777-82.
130. Markwell SM, Ammer AG, Interval ET, Allen JL, Papenberg BW, Hames RA, et al. Cortactin Phosphorylation by Casein Kinase 2 Regulates Actin-Related Protein 2/3 Complex Activity, Invadopodia Function, and Tumor Cell Invasion. Molecular Cancer Research. 2019;17(4):987-1001.
131. Rizki A, Mott JD, Bissell MJ. Polo-like Kinase 1 Is Involved in Invasion through Extracellular Matrix. Cancer Research. 2007;67(23):11106-10.
132. Cipponi A, Goode DL, Bedo J, McCabe MJ, Pajic M, Croucher DR, et al. MTOR signaling orchestrates stress-induced mutagenesis, facilitating adaptive evolution in cancer. Science. 2020;368(6495):1127-31.
133. Bahrami-B F, Ataie-Kachoie P, Pourgholami MH, Morris DL. p70 Ribosomal protein S6 kinase (Rps6kb1): an update. Journal of Clinical Pathology. 2014;67(12):1019.
134. Yoshida T, Kim JH, Carver K, Su Y, Weremowicz S, Mulvey L, et al. CLK2 Is an Oncogenic Kinase and Splicing Regulator in Breast Cancer. Cancer Research. 2015;75(7):1516-26.

Annex I

The research presented in this thesis provides fundamental data that contributes to a broader scientific article currently submitted to the journal Advanced Science at 3rd August 2025 (https://doi.org/10.1101/2025.08.01.668091). The complete manuscript, which incorporates these results as part of a larger study, is included in the annex.

CD276 Immature Glycosylation Drives Colorectal Cancer Aggressiveness and T-cell Mediated Immune Escape

Janine Soares[1,2,3], Dylan Ferreira[1,2], Martina Gonçalves[1], Andreia Miranda[1,2,4], Marta Relvas-Santos[1,2,4,5], Andreia Brandão[1], Paula Paulo[1], Sofia Cotton[1], Rui Freitas[1,2,4], Mariana Magalhães[1,6], Eduardo Ferreira[1,2,4], Beatriz Marinho-Santos[1,2], Luís Pedro Afonso[7], André M N Silva[2,5], Carlos Palmeira[1,8,9], Francisco Amado[3], Andreia Peixoto[1,4], Lúcio Lara Santos[1,2,9,10], José Alexandre Ferreira[1,2*]

[1]Research Center of IPO-Porto (CI-IPOP) / RISE@CI-IPOP (Health Research Network), Portuguese Oncology Institute of Porto (IPO-Porto) / Porto Comprehensive Cancer Center (P.ccc) Raquel Seruca, Porto, Portugal; [2]School of Medicine and Biomedical Sciences (ICBAS), University of Porto, Porto, Portugal; [3]LAQV-REQUIMTE & Department of Chemistry, University of Aveiro, Campus Universitário de Santiago, Aveiro, Portugal; [4]i3S – Instituto de Investigação e Inovação em Saúde, Universidade do Porto, Porto, Portugal; [5]LAQV-REQUIMTE, Department of Chemistry and Biochemistry, Faculty of Sciences, University of Porto, Porto, Portugal; [6]MSc Biochemistry in Health, Biomolecules na Chemical Sciences, ESS, Polytechnic of Porto, R. Dr. António Bernardino de Almeida, 400, 4200 - 072, Porto, Portugal; [7]Pathology Department, Portuguese Oncology Institute of Porto, Porto, Portugal; [7]Immunology Department, Portuguese Oncology Institute of Porto, Porto, Portugal; [9]School of Medicine and Biomedical Sciences of University Fernando Pessoa, Porto, Portugal; [10]Department of Surgical Oncology, Portuguese Oncology Institute of Porto, Porto, Portugal.

Corresponding author:

José Alexandre Ferreira
Experimental Pathology and Therapeutics Group,
Research Centre, Portuguese Oncology Institute of Porto,
R. Dr. António Bernardino de Almeida 4200-072 Porto,
Portugal; Tel. +351 225084000 (ext. 5111).
Email: jose.a.ferreira@ipoporto.min-saude.pt.

Keywords: colorectal cancer; cancer metastasis; glycoproteomics; CD276; immune suppression

Table of Contents: Colorectal cancer (CRC) progression is closely linked to immune evasion, yet the molecular mechanisms underlying this process remain poorly understood. This study identifies CD276 (B7-H3) as a glycosylation-driven regulator of CRC aggressiveness and demonstrates how *O*-glycosylation remodeling promotes tumour immune escape. These findings establish CD276 as a potential therapeutic target and highlight the role of glycoproteoform-specific immune modulation in cancer progression.

Abstract

Colorectal cancer (CRC) progression is fueled by immune evasion, yet the underlying molecular mechanisms remain to be fully characterized. CD276 (B7-H3), an immune checkpoint glycoprotein frequently overexpressed in aggressive tumours, is extensively modified by glycosylation, a process known to regulate protein stability, localization, and immune interactions. However, its glycosylation-dependent functions in CRC remain unclear. Here, we show that poor-prognosis CRC tumours exhibit dysregulated glycogene expression, leading to an immature *O*-glycosylation phenotype that enhances malignancy. Using *C1GALT1*-knockout CRC cells, which recapitulate the cancer glycocalyx, we demonstrate that this glycosylation shift promotes proliferation and invasion. We further identify CD276 as a metastasis-associated glycoprotein whose function is shaped by *O*-glycan modifications. Mechanistically, immature *O*-glycosylation of CD276 enhances invasion, suppresses T-cell activation, and induces an immunosuppressive cytokine milieu, reinforcing its role in tumour immune escape. These findings establish CD276 as a glycosylation-dependent

immune checkpoint and a promising therapeutic target to overcome immune evasion in CRC.

Introduction

Colorectal cancer (CRC) remains one of the most lethal malignancies worldwide, with poor survival rates for patients with metastatic disease [1]. While immune checkpoint inhibitors (ICIs) have transformed cancer therapy, their efficacy in CRC is largely restricted to tumours with microsatellite instability (MSI) and high tumour mutational burden (TMB) [2]. Most CRC cases, particularly those with microsatellite stability (MSS), remain resistant [3], highlighting a critical gap in understanding alternative immune evasion mechanisms that drive tumour progression.

Among the emerging immune modulators in cancer, CD276 (B7-H3) has gained attention as a non-canonical immune checkpoint molecule with a pivotal role in tumour progression. CD276 is a type I transmembrane glycoprotein belonging to the B7 family of co-stimulatory and co-inhibitory immune regulators, yet its physiological immune function remains controversial [4]. Unlike classical immune checkpoints such as PD-L1 and CTLA-4, CD276 lacks a well-defined receptor and can exert both immunosuppressive and pro-tumorigenic functions depending on the tumour context [4b, 5]. Nonetheless, CD276 overexpression has been reported across multiple malignancies, including lung [6], breast [7], prostate [8], and colorectal cancers [9], where it correlates with poor prognosis, increased metastatic potential, and therapy resistance. Beyond immune regulation, CD276 has been implicated in epithelial-mesenchymal transition (EMT) [10], resistance to apoptosis [11], and angiogenesis [12], yet the molecular mechanisms governing its function remain incompletely understood, particularly at the post-translational level.

Glycosylation plays a crucial role in regulating immune checkpoint function and response to immunotherapy, including CD276 [13]. Recent evidence indicates that core fucose *N*-glycosylation, mediated by FUT8, stabilizes CD276,

modulates its surface expression, and suppresses T-cell activation and proliferation in triple-negative breast cancer [13a]. Inhibiting core fucosylation has emerged as a promising strategy to enhance anti-tumour immune responses, underscoring the significance of glycosylation as a therapeutic target. However, the role of *O*-glycosylation, an essential post-translational modification in immune regulation and tumour progression [14], remains poorly defined in CD276 function. In CRC, extensive remodeling of the cancer glycocalyx leads to an immature *O*-glycosylation phenotype, primarily due to Cosmc (encoded by *C1GALT1C1*) dysregulation [15]. Cosmc is essential for the function of Core 1 β1,3-galactosyltransferase (encoded by *C1GALT1*), the key enzyme responsible for *O*-glycan elongation via Core 1 synthesis. Loss of Cosmc activity results in the accumulation of Tn antigen, a hallmark of aberrant *O*-glycosylation [16]. These alterations are predominantly driven by *C1GALT1C1* promoter hypermethylation and, in some cases, loss-of-function mutations [17]. This dysregulation has been strongly linked to cancer invasion mainly by disrupting normal *O*-glycosylation of cell surface proteins, leading to impaired cell-cell adhesion, enhanced migration, and metastasis [18], while also promoting immune evasion via macrophage-binding lectins on innate immune cells [19]. While the role of C1GALT1C1 in CRC is well established, the direct contribution of C1GALT1 itself in tumour progression remains poorly understood [15a]. More broadly, despite growing evidence of *O*-glycosylation's impact on cancer biology and immune modulation, how it shapes CD276 function, particularly in the context of immune interactions and tumour progression, remains largely unknown.

In this study, leveraging a systematic analysis of the cancer glycome, we identify CD276 as a metastasis-associated glycoprotein extensively modified by *O*-glycosylation in CRC. We demonstrate that tumours with poor prognostic features exhibit aberrant glycogene expression, leading to an immature *O*-glycosylation phenotype that enhances malignancy. Using *C1GALT1*-knockout CRC cells, which recapitulate the cancer-associated glycocalyx, we reveal that *O*-glycan remodelling amplifies CD276-driven tumour invasion and impairs T-cell activation. These findings establish CD276 as a glycosylation-dependent immune checkpoint and highlight its potential as a therapeutic target to overcome immune evasion in CRC.

Results

In this study, we started by investigating the role of immature protein *O*-glycosylation in aggressive CRC. We first analyzed glycogene expression patterns in patient samples and then profiled glycan composition in CRC tissues across differentiation states. Finally, we focused on CD276, a metastasis-associated immune checkpoint glycoprotein, to examine how *O*-glycan remodeling influences tumour cell behavior and immune suppression.

Transcriptomic shifts in O-glycosylation pathways define CRC aggressiveness

We began by addressing the expression of key glycogenes encoding glycosyltransferases involved in the initial steps of protein *O*-glycosylation. Analysis of TCGA dataset, comprising over 600 CRC cases across all disease stages and normal mucosa samples, revealed significant alterations in glycosylation pathways associated with tumour progression and aggressiveness. Most notably, *B3GNT6*, which initiates core 3 *O*-glycan biosynthesis, was markedly downregulated in CRC (**Figure 1A**), suggesting a reduction in core 3-type *O*-glycans in malignant tissues. In parallel, *ST6GALNAC1-4*, which mediate *O*-6 GalNAc sialylation, were consistently decreased in cancer tissues compared to healthy mucosa. In contrast, there was significant upregulation of *C1GALT1* and its chaperone *C1GALT1C1*, which extend glycans beyond the Tn antigen into core 1 structures. ST3GAL3, a sialyltransferase promoting sialyl-T antigen formation, was also upregulated. These findings indicate a biosynthetic shift favoring core 1 over core 3 *O*-glycans in CRC (as highlighted by the schematic *O*-glycosylation pathway representation in **Figure S1**, Supporting Information). Importantly, low *B3GNT6* expression was strongly associated with poor clinical outcomes, with patients with *B3GNT6*Low tumours showing significantly worse overall survival (p = 0.0002; HR = 2.32, p < 0.001; **Figure 1B**). To further investigate glycophenotypic patterns, we stratified tumours based on *B3GNT6* expression in combination with either *C1GALT1* or *C1GALT1C1*. Tumours with a *B3GNT6*Low/*C1GALT1*Low or *B3GNT6*Low/*C1GALT1C1*Low profile, likely reflecting an immature glycosylation state, were associated with the poorest prognosis (*B3GNT6*Low/*C1GALT1*Low: HR = 2.18, p < 0.02; *B3GNT6*Low/*C1GALT1C1*Low: HR = 2.79, p < 0.001; **Figure 1C**). Together, these findings suggest that CRC progression is linked to simple glycophenotypes,

marked by the accumulation of Tn and potentially sTn antigens, which correlate with more aggressive disease and poorer clinical outcomes.

Differentiation-linked glycome profiles reveal simple glycophenotypes in advanced CRC

To explore whether these transcriptional alterations translate into distinct glycan phenotypes, we next profiled the tissue glycome in healthy mucosa and advanced CRC (stage ≥3), focusing on how tumour differentiation shapes *O*-glycosylation patterns. The tumours were further characterized based on their differentiation status, a feature often linked to consensus molecular subtypes (CMS) [20]. Accordingly, we categorized tumours into two groups: i) Differentiated epithelial tumours, characterized by high CDX2 and low FRMD6 and HTR2B expression levels (**Figure S2a**), typically corresponding to CMS2 and CMS3 subtypes; and ii) Undifferentiated mesenchymal tumours, defined by low CDX2 and high FRMD6 and HTR2B levels, generally associated with CMS1 or CMS4 [21].

No differences in survival were observed between these groups (**Figure S2a**), likely reflecting the uniformly advanced stage of disease in the cohort. In healthy mucosa, the glycome was primarily composed of core 3 structures (N2, N2S1; **Figure 1D**, **Figure S3, Table S1 and Table S2**), predominantly decorated with *O-6-GalNAc*-linked sialic acids (**Figure S3**). The sTn antigen (N1S1) was also present at lower levels, consistent with previous reports [22]. These features align with the higher expression of *B3GNT6* and *ST6GALNAc* sialyltransferase genes in healthy colon tissue (**Figure 1A**). By contrast, tumour samples showed significantly lower levels of core 3 glycans and were predominantly enriched in sialyl-T antigens (H1N1S1), with lower levels of di-sialyl-T antigens (H1, N2S2; **Figure 1D**). Most tumours expressed Tn (N1) and/or sTn (N1S1), while a smaller subset, particularly among mesenchymal-like tumours, also exhibited extended core 2 *O*-glycans, including H2N2, H2N2F1, H1N2F1F2, H1N2S1, H2N2S2, H2N2S1, H1N2F1, and H2N2F1S2. Nevertheless, a striking difference emerged between epithelial-like and mesenchymal-like tumours. Epithelial-like tumours exhibited higher levels of core 3 and sTn and *de novo* expression of Tn antigens, consistent with a shift toward simpler glycophenotypes (**Figure 1D**). In contrast, mesenchymal-like tumours were enriched in mono- and di-sialylated T antigens,

with low relative expression of other glycan structures. Remarkably, all tumours with distant metastases, regardless of differentiation status, exhibited multiple sialylated core 2-related structures (H1N2S1, H2N2S2, H2N2S1, H2N2F1S2; **Figure 1D**). No additional associations were observed between tumour stage, grade, patient survival, and glycome composition (data not shown). Complementary immunohistochemistry confirmed the presence of Tn and sTn antigens in 90% of primary tumours, lymph node metastases, and distant metastases (**Table S3**), in agreement with MS analysis. Interestingly, while the relative abundance of these glycans varied between epithelial- and mesenchymal-like tumours, overall expression levels of Tn and sTn remained consistent across differentiation states (**Figure 1D**). Notably, their expression showed no association with histopathological variables (**Table S3**).

In summary, these findings highlight distinct glycome profiles between tumour differentiation states in aggressive colorectal cancer. Immature glycosylation patterns were prevalent across advanced tumours, including lymph node and distant metastases. Epithelial-like lesions displayed an intermediate glycophenotype, situated between healthy colonic mucosa and mesenchymal-like tumours. This profile was marked by a partial loss of core 3 structures, reduced glycan complexity, and increased expression of Tn and sTn antigens. In contrast, mesenchymal tumours were more enriched in sialylated core 1 and extended core 2 glycans. Despite these subtype-specific differences, simple glycophenotypes, particularly Tn and sTn, were widely present across tumour types, with their relative abundance shaped by differentiation status. These findings align with transcriptomics data, confirming that downregulation of core 3–associated enzymes, with reduced expression of *C1GALT1* and its chaperone *C1GALT1C1*, is consistent with the emergence of simple glycophenotypes, whose abundance is shaped by tumour differentiation and associated with disease progression.

Simple glycophenotypes enhance CRC cell invasiveness

To explore the functional role of simple glycophenotypes, we first profiled the *O*-glycome of a panel of CRC cell lines representative of epithelial-like (HCA7, SW480) and mesenchymal-like (SW620, HCT116, RKO, LS174T) phenotypes (**Figure S4 and Table S4**). These profiles closely mirrored human tumours, with

epithelial-like cells predominantly expressing core 3 glycans with little to no sialylated T antigens, which contrast with findings *in vivo*, while mesenchymal-like lines were enriched in core 1 structures. Notably, Tn and sTn antigens were absent in epithelial-like cells, suggesting their expression in tumours may be influenced by the tumour microenvironment.

To experimentally induce simple glycophenotypes, we knocked out *C1GALT1* using CRISPR-Cas9 in both SW480 (epithelial-like, derived from a primary tumour) and SW620 (mesenchymal-like, from a lymph node metastasis of the same patient) cell lines (**Figure S5**). Despite their differing baseline glycomes, *C1GALT1* knockout completely suppressed core 1 structures in both cell lines and led to robust overexpression of Tn and sTn antigens (**Figure 1E, Figure S6**). Additionally, both cell lines presented a marked decrease in core 3 glycans. These changes were accompanied by reduced expression of *B3GNT6* (**Figure S5c**), suggesting a degree of co-regulation between core 1 and core 3 glycosyltransferases, in mimicry of the *C1GALT1*Low/*B3GNT6*Low phenotype associated with poor prognosis in patient samples (**Figure 1B-C**). Both SW480 and SW620 *C1GALT1* knockout cells exhibited enhanced invasive capacity of Matrigel *in vitro* compared to controls (**Figure 1G**). Interestingly, proliferation was unaffected in SW620 cells but significantly increased in SW480 *C1GALT1* knockouts (**Figure 1F**), indicating cell line–specific responses to glycome remodeling. Collectively, these findings demonstrate that acquisition of simple glycophenotypes, marked by the loss of core 1 and core 3 glycans and accumulation of Tn/sTn antigens, enhances the invasive potential of CRC cells. This glycome remodeling mirrors the poor-prognosis transcriptional signatures identified in patient tumours and highlights a functional role for immature *O*-glycans in promoting CRC aggressiveness.

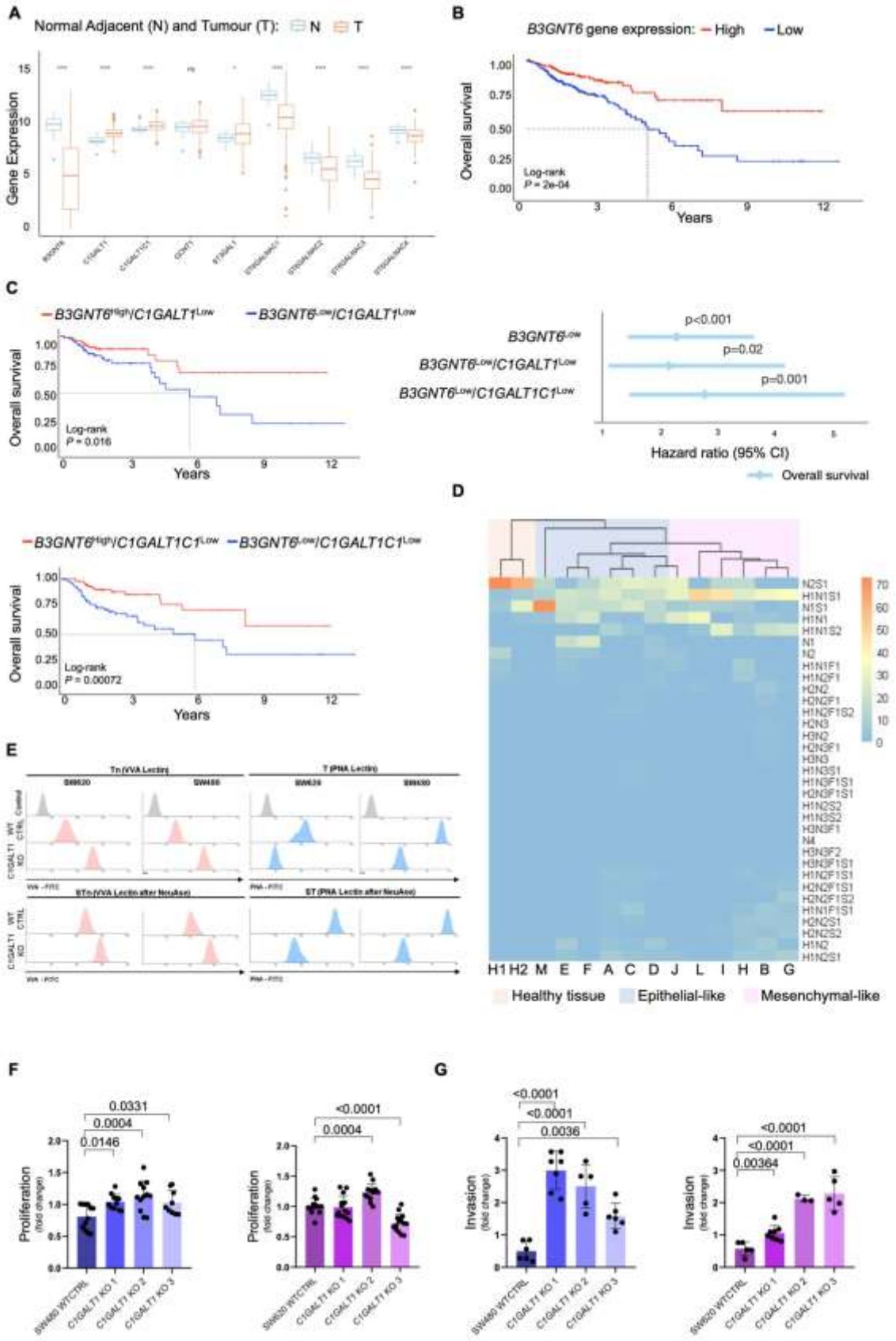

Figure 1. Downregulation of *B3GNT6* and *C1GALT1* promotes immature *O*-glycosylation, defines poor-prognosis CRC subtypes, and enhances tumour cell aggressiveness. A. Key

O-glycosylation enzymes are downregulated in colorectal tumours. Transcriptomic analysis of the TCGA-COADREAD dataset (480 tumour and 41 adjacent normal tissues) revealed significant downregulation of *C1GALT1*, *C1GALT1C1*, and *B3GNT6* in tumour samples compared to normal tissue (Wilcoxon test, $p < 0.05$), indicating impairment in core 1 and core 3 *O*-glycan synthesis. **B. *B3GNT6* expression is associated with patient prognosis.** Kaplan–Meier survival analysis showed that lower *B3GNT6* expression is significantly associated with decreased overall survival in CRC patients (log-rank $p < 0.05$). **C. Combined downregulation of *B3GNT6* and *C1GALT1* or *C1GALT1C1* identifies high-risk subgroups.** Patients with low *B3GNT6* and either *C1GALT1* or *C1GALT1C1* expression had significantly worse survival (log-rank $p < 0.05$), reinforcing the prognostic relevance of immature *O*-glycosylation profiles. **D. Glycomic profiling distinguishes tumour differentiation states, metastatic potential, and deviation from normal glycosylation.** Mass spectrometry-based glycomic analysis revealed that healthy colon mucosa (H1, H2) predominantly expresses sialylated core 3 *O*-glycans. In contrast, epithelial-like tumours are enriched in Tn/STn antigens, while mesenchymal-like tumours present mono- or di-sialylated core 1 structures. Metastatic tumours exhibit elongated core 2 *O*-glycans irrespective of differentiation state, illustrating the progressive shift from mature to truncated *O*-glycan profiles across CRC progression. **E. *C1GALT1* knockout induces immature *O*-glycans in CRC cells, mimicking tumour-associated glycophenotypes.** Flow cytometry analysis of SW480 and SW620 *C1GALT1*-KO cells (n=3 independent replicates per condition) revealed reduced PNA binding, both with and without neuraminidase treatment, indicating loss of core 1 and sialylated core 1 glycans, consistent with impaired *O*-glycan elongation. Concurrently, increased VVA binding was observed, revealing accumulation of Tn antigens. After neuraminidase treatment, a further increase in VVA signal confirmed the presence of sTn, demonstrating that many Tn structures are capped by sialic acids. Together, these results validate the induction of a truncated and sialylated *O*-glycophenotype in *C1GALT1*-deficient cells, which closely mimics glycosylation features of colorectal tumours. **F. Immature glycosylation enhances tumour cell proliferation.** *C1GALT1*-KO SW480 and SW620 cells exhibited significantly increased proliferation compared to wild-type controls, with ~25% increase observed across independent clones (n = 15 wells per condition, from 3 independent experiments; one-way ANOVA with Tukey post-hoc; $p < 0.05$). **G. Immature glycosylation increases tumour cell invasiveness.** Matrigel invasion assays revealed a 4- to 5-fold increase in invasiveness in SW480 *C1GALT1*-KO cells (n = 8 wells per condition, from 3 independent experiments) and approximately 3- to 3.5-fold increase in SW620 KO cells (n = 9 wells per condition), compared to wild-type. Invasion values were normalized to proliferation, and differences were statistically significant ($p < 0.05$; one-way ANOVA with Tukey post-hoc test).

CD276 carries immature *O*-glycans in CRC and associates with poor prognosis

We next investigated whether CD276 could act as a carrier of immature *O*-glycans in CRC. Using immunohistochemistry, we confirmed CD276 expression in approximately 80% of primary advanced CRC tumours, as well as in corresponding lymph node and distant metastases. Notably, CD276 co-localized with areas of high Tn and/or sTn expression in all CD276-positive tumours (**Figure 2A**). In healthy colon tissue, although some apparent co-localization was observed, CD276 was primarily expressed in enterocytes, whereas Tn and sTn antigens were restricted to goblet cells and were much less abundant than in tumours (**Figure 2A**). To further assess whether CD276 directly carried these immature glycans, proximity ligation assay (PLA) and immunofluorescence analyses were performed. Both approaches provided positive signals in CRC samples, supporting the notion that CD276 is a major carrier of Tn and sTn antigens in cancer (**Figure 2B-C**). In contrast, no evidence of CD276 carrying abnormal glycosylation was found in healthy colon tissue or in other normal tissues, including stomach, liver, pancreas, appendix, gallbladder, lung, testis, thyroid, kidney, and bladder (**Figure 2G**), suggesting a cancer-specific nature.

Clinically, CD276-positive tumours were associated with significantly worse prognosis compared to CD276-negative lesions ($p = 0.0025$; **Figure 2F**). Furthermore, aberrantly glycosylated CD276 was enriched in right-sided colon tumours ($p < 0.05$; **Figure 2D**), a subgroup known for its more aggressive clinical behavior. However, no differences were observed in the frequency of CD276 expression, nor the prevalence of its abnormally glycosylated forms, between epithelial-like and mesenchymal-like tumours (data not shown).

Having established CD276 as a potential cancer-specific carrier of immature *O*-glycans, we next explored its gene expression profile. TCGA analysis revealed that CD276 was significantly upregulated in CRC compared to adjacent normal mucosa (**Figure 2H**). Moreover, CD276 expression showed a trend toward higher levels in more advanced tumour stages ($p = 0.07$ for stage III/IV; **Figure 2I**), reinforcing the link between CD276 and poor prognosis.

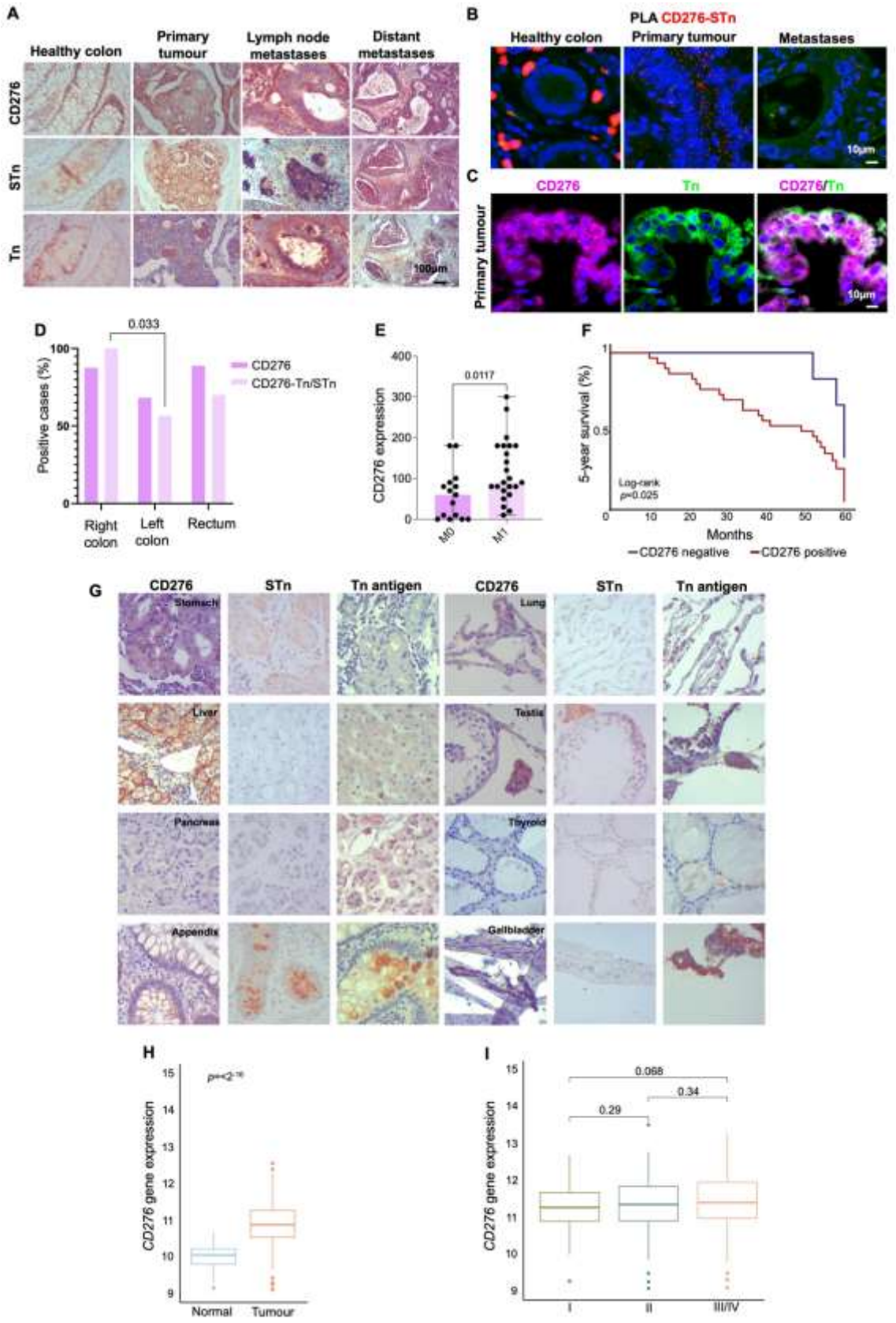

Figure 2. CD276 is a marker of poor prognosis in colorectal cancer and displays cancer-specific aberrant *O*-glycosylation. A. CD276 colocalizes with Tn and sTn antigens in CRC and metastases. Immunohistochemistry reveals diffuse CD276 expression throughout tumour

regions, both in the cytoplasm and at the cell membrane, overlapping with Tn and sTn antigen distribution. Unlike sTn, CD276 is also detected in the extracellular matrix surrounding tumour areas. Tn expression appears in scattered niches without a consistent pattern. In contrast, the healthy colon shows only weak cytoplasmic staining for CD276, Tn, and sTn, with no evidence of colocalization. **B. *In situ* proximity ligation confirms (PLA) CD276-STn glycoproteoforms in CRC and metastases.** PLA reveals strong spatial proximity (< 30 nm; red puncta) between CD276 and sTn in tumour cells from both primary tumours and metastases, but not in healthy colon, highlighting the cancer-specific nature of this aberrant glycoform. **C. Double immunofluorescence reveals CD276-Tn glycoproteoforms in CRC and metastases.** In CD276-enriched tumours and matched metastases, CD276 (magenta) and Tn (green) co-localize at both the membrane and cytoplasm of the same cells, confirming CD276 as a direct carrier of immature O-glycans. **D. CD276 and its aberrantly glycosylated forms are enriched in right-sided colorectal tumours** CD276 and CD276-Tn/sTn glycoform prevalence across tumour locations revealed anatomical distinctions in both expression and glycosylation. In the right colon, 100% of tumours were CD276-positive and all exhibited aberrant glycosylation with Tn and/or sTn antigens. In contrast, only ~60% of left-sided tumours expressed CD276, with significantly fewer showing aberrant glycosylation ($p = 0.020$, Fisher's exact test vs right colon). Although CD276 expression in the rectum was comparable to the right colon, the frequency of CD276-Tn/sTn glycoforms was significantly lower ($p = 0.036$), highlighting regional variation in CD276 glycosylation within the colon. Together, these findings suggest that aberrantly glycosylated CD276 is a defining feature of right-sided CRC. **E. CD276 expression is elevated in metastatic CRC.** IHC quantification shows significantly higher CD276 scores in M1 (metastatic) versus M0 (non-metastatic) tumours ($p = 0.0117$, unpaired t-test). **F. CD276 expression is associated with poor prognosis.** Kaplan–Meier survival analysis reveals significantly worse 5-year survival in patients with CD276-positive tumours compared to CD276-negative cases ($p = 0.025$, log-rank test). **G. Aberrant CD276 glycoforms are cancer specific.** Immunohistochemistry analysis of healthy tissues reveals limited CD276 expression, primarily cytoplasmic in select epithelial cells (e.g. enterocytes, hepatocytes, Leydig cells), and no co-localization with Tn or sTn antigens except occasional overlap in Leydig cells. In contrast to tumours, sTn and Tn were either absent or restricted to secretory or immune compartments, supporting the tumour-specific nature of CD276-Tn/sTn glycoforms. **H. *CD276* is significantly upregulated in CRC compared to matched normal tissue.** TCGA analysis of tumour samples and adjacent normal tissues shows robust overexpression of CD276 in tumours ($p < 0.0001$, Wilcoxon test), confirming its cancer-associated expression profile. **I. *CD276* expression increases with tumour stage.** TCGA data reveal a progressive increase in CD276 expression from stage I to stage IV, with a trend toward higher expression in advanced stages ($p = 0.068$, one-way ANOVA).

CD276 exhibits distinct glycocodes across colorectal cancer differentiation states

To further dissect the glycocode of CD276, we interrogated a well-characterized proteomics dataset from the PRIDE repository, comprising 95 CRC patients, stratified by tumour stage, location, and differentiation status according to CMS. Although the dataset was not specifically optimized for glycoprotein detection, it provided valuable insights into CD276 glycosylation patterns across CRC subtypes. Over 80% of these tumours were positive for CD276, with widespread expression across all stages of the disease (**Figure 3A**). All tumours in stages III and IV exhibited CD276 positivity (**Figure 3A**). Notably, the proportion of abnormally glycosylated CD276 (Tn/sTn glycoforms) was significantly higher in stage II–IV tumours compared to stage I (40–60% vs. 5%; **Figure 3A**). Furthermore, right-sided colon tumours showed a higher frequency of abnormally glycosylated CD276 compared to left-sided lesions (**Figure 3B**), consistent with earlier observations in the patient cohort. Rectal tumours also displayed high CD276 expression (**Figure 3B**), although differences in glycosylation were less pronounced. When stratified by tumour differentiation states, mesenchymal-like tumours (CMS1/4) exhibited significantly higher CD276 protein expression compared to epithelial-like tumours (CMS2/3) ($p < 0.0001$; **Figure 3C**). However, no significant differences were observed in the expression of abnormally glycosylated CD276 forms between epithelial- and mesenchymal-like subtypes (**Figure 3D, Figure S7**). Furthermore, in-depth tandem mass spectrometry analysis revealed distinct patterns of glycosite occupancy across the CD276 protein depending on tumour differentiation state, regardless of tumour location or stage (**Figure 3E**). Specifically, a higher density of glycosylation sites was detected within the extracellular region of CD276 in epithelial-like tumours, particularly concentrated on glycopeptides bridging the immunoglobulin variable (IgV) and constant (IgC) domains (**Figure 3E**). Interestingly, *O*-glycosylation site prediction using NetOGlyc identified only three putative sites in CD276, including T244, which was also confirmed in our analysis. Our MS-based profiling, however, revealed a substantially broader and differentiation-specific glycosite landscape, highlighting the limitations of predictive algorithms and the added value of experimental mapping (**Figure 3E**). These differentiation-linked glycosylation patterns could modulate molecular

interactions and represent exploitable targets for precision oncology. Together, the results indicate that tumour differentiation state, rather than anatomical location or metastatic potential, is the primary determinant of CD276 glycosylation patterning, underscoring the dominant role of cellular phenotype in shaping cancer-associated glycan remodeling.

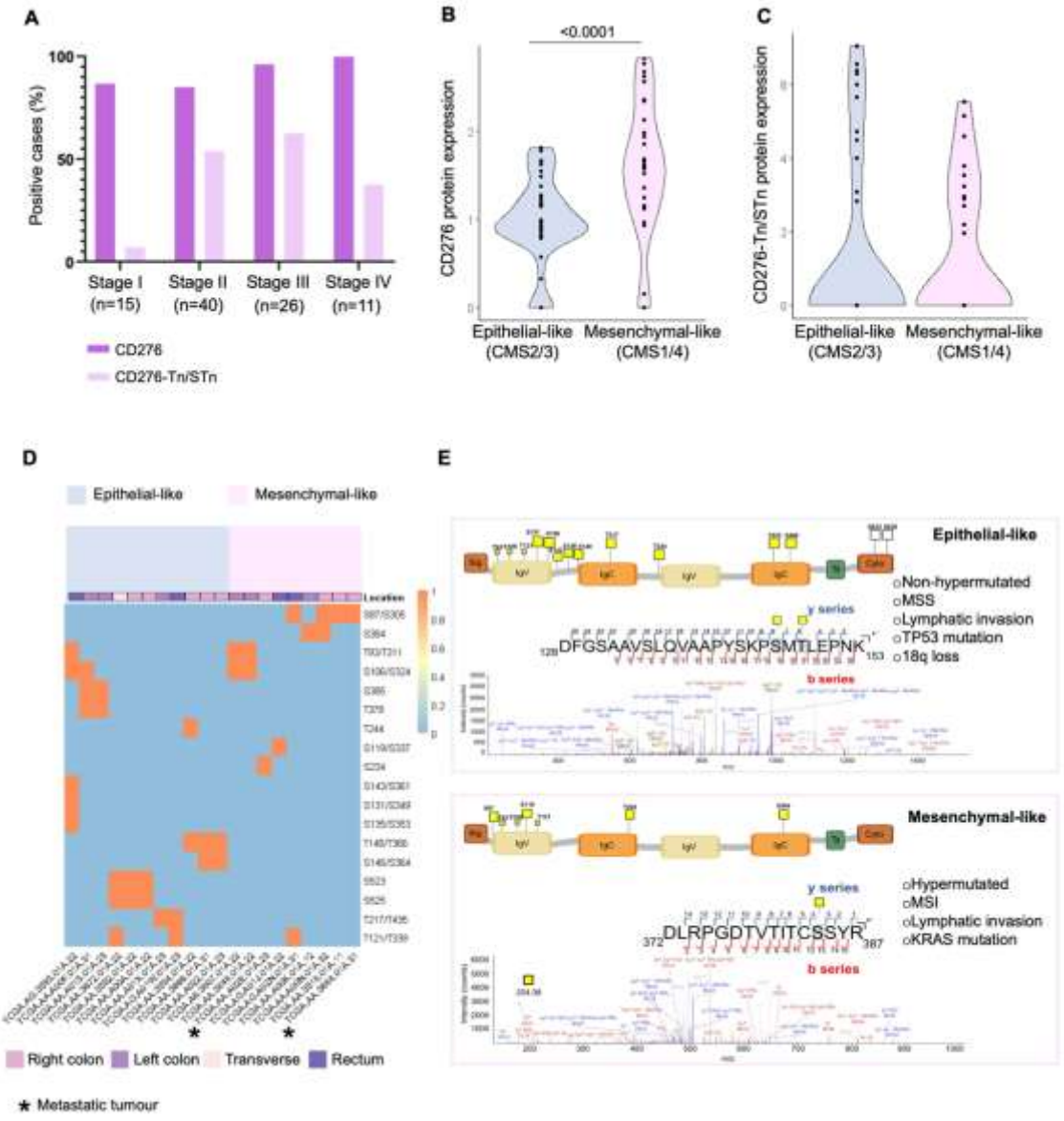

Figure 3. CD276 is widely expressed across CRC stages and displays distinct glycosylation patterns according to tumour differentiation. A. CD276 is broadly expressed across colorectal cancer stages, while immature CD276 glycoforms (Tn/sTn-modified) are enriched in advanced tumors. The plot concerning TCGA-based proteomics data shows the percentage of positive cases for total CD276 and CD276 glycosylated with Tn/sTn antigens across CRC stages I–IV. Aberrant CD276 glycoforms were significantly more frequent in stages

II–IV compared to stage I (Fisher's exact test, $p = 0.0026$). **B. CD276 expression is associated with tumour differentiation state.** Mesenchymal-like tumours (CMS1/4) exhibited significantly higher CD276 protein expression than epithelial-like tumours (CMS2/3) ($p < 0.0001$, Wilcoxon test). **C. Glycosylated CD276 is not significantly associated with tumour subtype.** No difference in CD276-Tn/sTn glycoform expression was observed between epithelial-like and mesenchymal-like tumours. **D. CD276 glycosylation site occupancy differs between epithelial-like and mesenchymal-like colorectal cancers. E. CD276 glycosylation site occupancy differs between epithelial-like and mesenchymal-like colorectal cancers.** Tandem mass spectrometry revealed distinct *O*-glycosylation profiles along the CD276 extracellular domain. The heatmap (left) displays the distribution of identified glycosylation sites across tumor samples stratified by transcriptomic subtype (CMS2/3: epithelial-like; CMS1/4: mesenchymal-like). Each row corresponds to a specific glycosylation site (by amino acid position), with colored blocks indicating detection in individual tumors. Epithelial-like tumors exhibited denser and more widely distributed glycosylation, particularly clustered within the IgV and IgC domains, while mesenchymal-like tumors showed fewer and more membrane-proximal modifications, suggesting subtype-specific glycan regulation. These patterns are further illustrated in the schematic diagrams (right), which highlight representative subtype-specific glycopeptides. Larger GalNAc symbols denote glycosylation sites unique to each subtype, while smaller symbols indicate shared sites. CID-MS/MS spectra confirm glycopeptide identity and modification of site localization. These glycosylation profiles align with known molecular features: epithelial-like tumors were enriched for *TP53* mutations, MSS, and 18q loss, whereas mesenchymal-like tumors were associated with *KRAS* mutations, MSI, and a hypermutated phenotype.

CD276 overexpression is driven by immature glycosylation

We next investigated CD276 glycoproteoforms in both wild-type and *C1GALT1* knockout CRC cell models. Immunoblotting using an antibody directed against the membrane portion of CD276 revealed an increase in the 100 kDa band following *C1GALT1* knockout in both SW480 and SW620 cells (**Figure 4A, Figure S8**). A similar pattern was observed using an antibody targeting the cytoplasmic domain (**Figure 4B, Figure S8**). The 100 kDa species is consistent with the full-length CD276 isoform containing two IgV–IgC domain pairs, with the increased apparent molecular weight reflecting extensive glycosylation. These findings indicate that *C1GALT1* knockouts consistently lead to the accumulation of a densely glycosylated CD276 form, independent of the antibody epitope targeted. Additional lower molecular weight bands were detected with the cytoplasmic domain targeting antibody (**Figure 4B**), potentially representing

alternative isoforms; however, these bands did not show consistent glycosylation patterns. To further validate the presence of immature *O*-glycans, CD276 was immunoprecipitated from wild-type and *C1GALT1* knockout cells. Isotype control immunoprecipitations showed no detectable bands, confirming the specificity of CD276 pulldown. In both models, the predominant 100 kDa band was enriched and exhibited strong reactivity with the VVA lectin, confirming the accumulation of Tn antigen on CD276 following glycosylation extension disruption (**Figure 4C, Figure S8**). To investigate whether *C1GALT1* knockout, and the consequent loss of core 1 and more extended *O*-glycans, also affected CD276 protein stability, cells were treated with cycloheximide to block new protein synthesis, and CD276 degradation was monitored over time. Across three independent replicates per cell line, CD276 levels consistently declined in control cells, as expected following inhibition of protein synthesis. In contrast, *C1GALT1* knockout cells exhibited higher CD276 levels over time, with several replicates showing sustained or even increasing signal intensity, indicative of enhanced protein stability (**Figure 4D and Figure S9**). While the degree and kinetics of stabilization varied between replicates and between cell lines, the overall trend was reproducible: CD276 decayed more slowly in KO cells than in their respective controls. This phenotype was particularly pronounced in SW480 cells but also evident in SW620 cells despite more variable temporal dynamics. These findings support the notion that loss of core 1 O-glycosylation impairs CD276 turnover, stabilizing the protein post-translationally.

Finally, we addressed CD276 transcript levels, which were significantly increased in *C1GALT1* knockout cells compared to wild-type controls in both cell lines (**Figure 4E**). Analysis of patient TCGA datasets further revealed a significant inverse correlation between *CD276* expression and both *C1GALT1* and *C1GALT1C1* expression (**Figure 4F**), reinforcing the possible transcriptional co-regulation mechanisms linking immature *O*-glycosylation to CD276 upregulation suggested by glycoengineered cell lines. Similar observations were made for *GCNT1*, involved in core 2 branching, reinforcing a link with immature glycosylation. In addition, CD276 associated with increased expression of *ST3GAL1*, *ST6GALNAC2*, and *ST6GALNAC3*, suggesting a shift toward enhanced sialylation of immature O-glycans, particularly Tn and core 1 structures. These observations point to broader, previously unrecognized

regulatory networks linking *O*-glycosylation remodeling and CD276 expression in CRC, warranting further investigation.

Collectively, these findings demonstrate that immature *O*-glycosylation driven by *C1GALT1* loss promotes CD276 overexpression through combined effects on protein stability and gene transcription, highlighting a mechanistic link between glycome remodeling and immune checkpoint regulation in colorectal cancer.

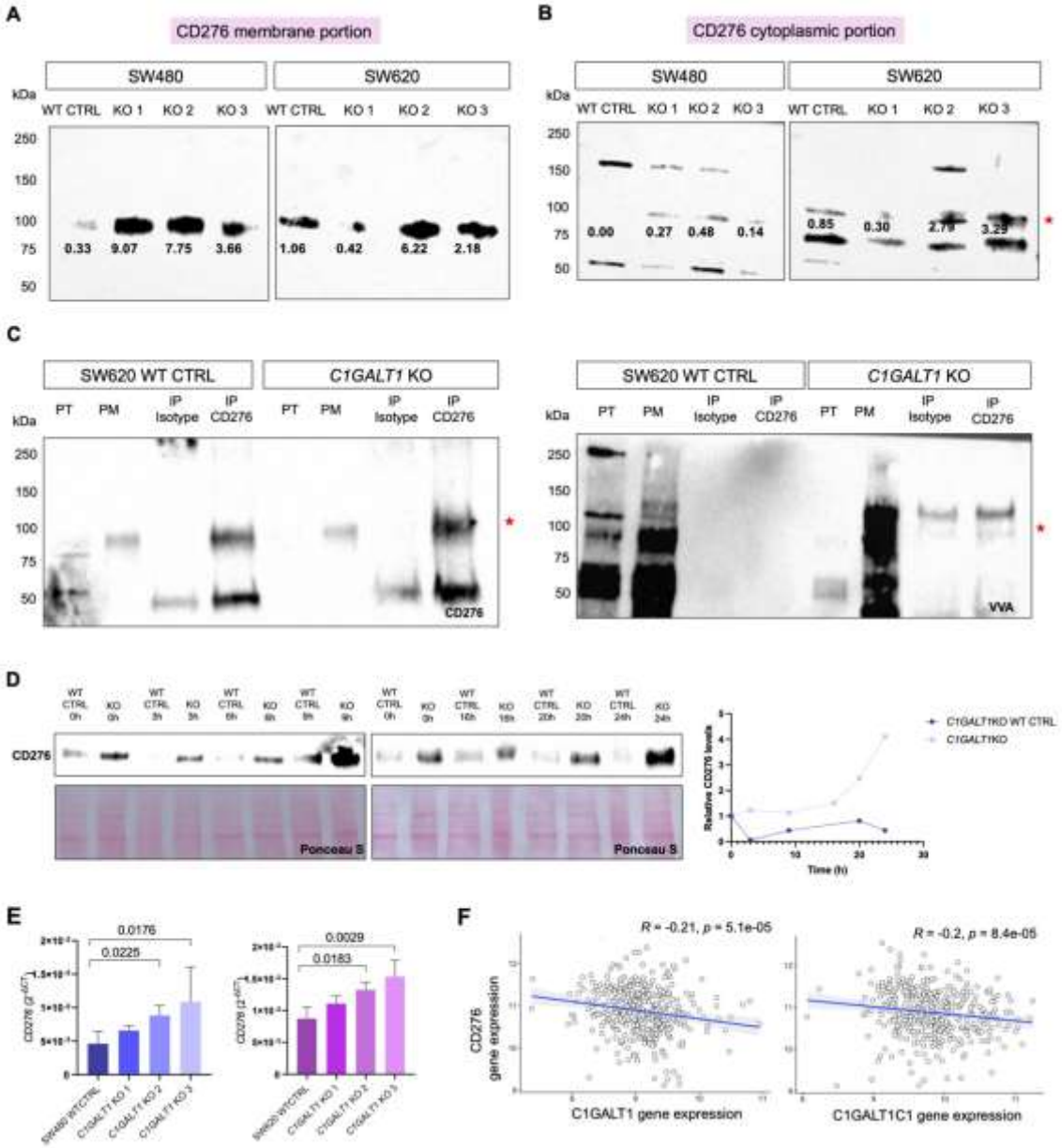

Figure 4. Loss of *C1GALT1* expression increases CD276 expression and results in accumulation of immature Tn-modified glycoforms. A–B) Loss of *C1GALT1* leads to an increase in CD276 protein levels in CRC cells. Western blot analysis was performed on total

protein lysates (T) and plasma membrane fractions (PM) from SW480 and SW620 wild-type (WT) and *C1GALT1* knockout (KO) cells using antibodies against either the extracellular (**A**) or cytoplasmic (**B**) domains of CD276. KO cells showed increased CD276 protein expression compared to WT. A prominent 100 kDa band (red asterisk), corresponding to a CD276 glycoproteoform, was observed in *C1GALT1* KO cells. **C. Immunoprecipitation of CD276 confirms increased protein levels and enrichment of a 100 kDa glycoform in *C1GALT1* KO cells.** CD276 was immunoprecipitated from plasma membrane fractions of WT and KO cells. Western blotting detected a clear ~100 kDa band in *C1GALT1* KO samples, which was absent in isotype controls and enhanced relative to WT. This result confirms successful IP and increased expression of CD276 glycoproteoforms in KO cells. VVA lectin blotting was also performed to assess Tn antigen on CD276, confirming the presence of immature glycoforms in CD236 IPs. Ponceau S staining was used to verify equal protein loading. **D. Cycloheximide treatment reveals enhanced CD276 protein stability in *C1GALT1* knockout cells.** SW620 WT CTRL and *C1GALT1* KO cells were treated with cycloheximide for the indicated durations, and CD276 levels were assessed by immunoblotting. Ponceau S staining served as a loading control. Quantification (right panel) shows a marked accumulation of CD276 over time in *C1GALT1* KO cells compared to WT, supporting increased protein stability in cells carrying immature glycosylation. **E. Loss of *C1GALT1* leads to transcriptional upregulation of *CD276*.** In both cell lines, CD276 gene expression was significantly elevated in *C1GALT1* KO clones compared to WT controls. Each bar represents a biologically independent C1GALT1 KO clone, and results are shown as the mean of technical triplicates. Statistical significance was determined using one-way ANOVA followed by Tukey's multiple comparison test. **F. Reduced expression of core 1 O-glycosylation enzymes is associated with increased CD276 expression in CRC.** TCGA transcriptomic analysis revealed that *CD276* gene expression inversely correlates with that of *C1GALT1* ($R = -0.21$, $p = 5.1 \times 10^{-5}$) and *C1GALT1C1* ($R = -0.20$, $p = 8.4 \times 10^{-5}$). These results support a negative association between core 1 *O*-glycan biosynthesis and CD276 expression in CRC, consistent with increased CD276 levels and immature glycosylation under reduced *C1GALT1* expression.

Aberrantly glycosylated CD276 drives cancer cell aggressiveness

We further explored the functional implications of CD276 and its aberrant glycosylation in CRC cells. CD276 was transiently knocked down using two siRNAs (si1 and si2) in SW480 and SW620 wild-type cells, as well as in their corresponding *C1GALT1* knockout models. Effects on proliferation and invasion were then assessed (**Figure 5A-C**). Efficient knockdown was confirmed by a strong reduction in *CD276* mRNA levels and a near-complete loss of CD276 protein within 72 hours, which was sustained for at least 5 days (**Figure 5A, Figure S9**). In SW480 cells, proliferation remained largely unaffected across all

conditions, with a modest reduction observed in *CD276* si1-treated *C1GALT1* KO cells (p = 0.0053). This partial effect, not recapitulated with si2, suggests that CD276 plays a limited role in regulating proliferation in this model, even in the presence of immature glycosylation. In contrast, proliferation in the metastatic SW620 model was significantly reduced following CD276 knockdown in glycoengineered cells (p = 0.0016 and p = 0.0135 for si1 and si2, respectively). CD276 knockdown in wild-type SW620 cells had no measurable effect on proliferation. These findings indicate that aberrant *O*-glycosylation enhances CD276's capacity to support proliferative signaling in a cell line–specific manner, and that this effect is more prominent in the metastatic, mesenchymal-like setting. In addition, in both SW480 and SW620 *C1GALT1* knockout cells, CD276 knockdown significantly reduced invasion (all $p < 0.01$), highlighting the role of aberrantly glycosylated CD276 in sustaining invasive behavior. Notably, in SW620 cells, *C1GALT1* knockout alone increased invasion, consistent with earlier findings (**Figure 1**), and this effect was reversed by CD276 silencing, reinforcing its functional contribution in the context of immature *O*-glycosylation. Collectively, these results demonstrate that CD276 contributes to both proliferation and invasion in a glycosylation- and cell context–dependent manner, with its tumour-promoting effects most evident in the metastatic SW620 model. These findings establish a functional link between aberrant *O*-glycosylation and CD276-driven aggressiveness, supporting the use of SW620 cells as a robust platform for in-depth mechanistic studies, including phosphoproteomic and immune-modulatory analyses.

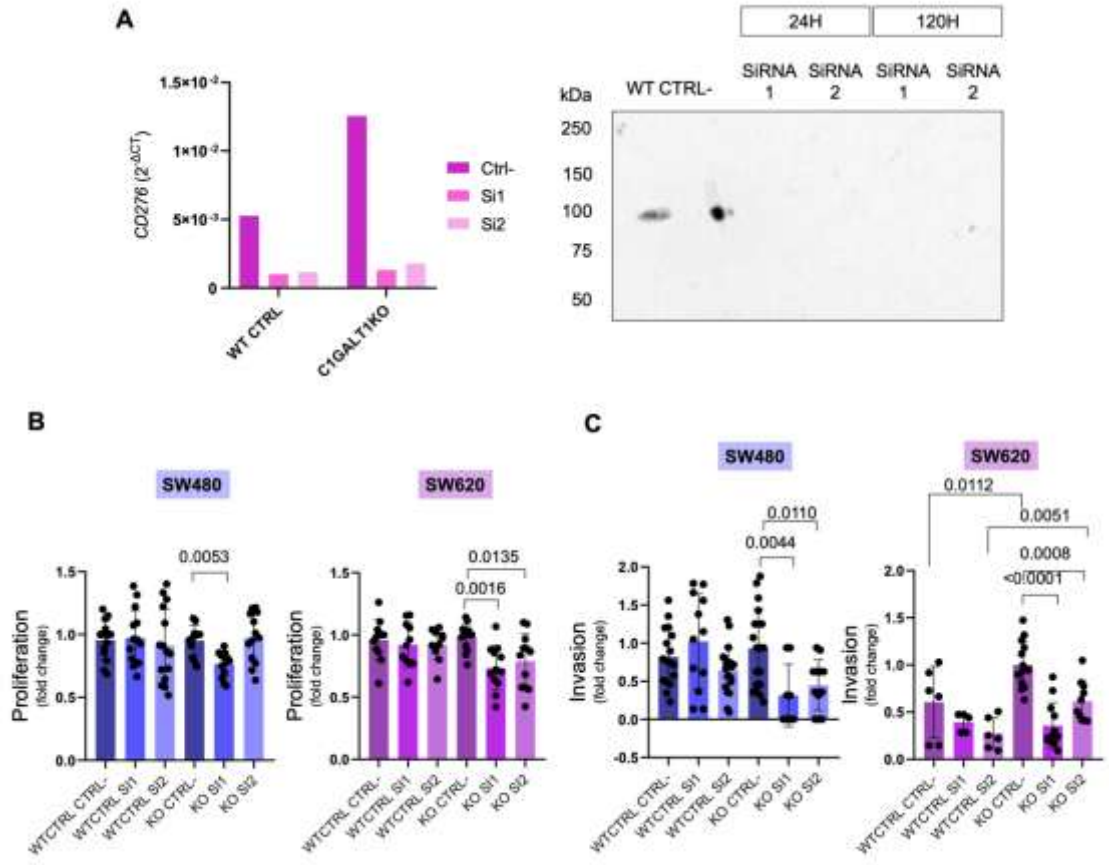

Figure 5. A *CD276* silencing using siRNA effectively reduces gene and protein expression in both wild-type and *C1GALT1* KO CRC cells. qPCR shows ~85% knockdown of *CD276* transcripts with two independent siRNAs (Si1 and Si2) in both cell models compared to non-targeting control (Ctrl-). Western blot analysis confirms complete abrogation of CD276 protein expression up to 5 days post-transfection. **B Aberrantly glycosylated CD276 supports CRC cell proliferation in a cell line–specific manner.** In SW480 cells, *CD276* silencing did not significantly affect proliferation in either wild-type or *C1GALT1* KO backgrounds, with exception for si1. In contrast, in SW620 cells, *CD276* silencing significantly reduced proliferation in *C1GALT1* KO cells, with both siRNAs (si1 and si2) showing consistent effects ($p = 0.0135$ and $p = 0.0016$, respectively; one-way ANOVA, Tukey's post hoc test). Data represents the mean fold change relative to control from three independent experiments. These findings suggest that abnormally glycosylated CD276 enhance proliferation specifically in highly aggressive SW620 cells. **C Aberrantly glycosylated CD276 promotes CRC cell invasion in both SW480 and SW620 models.** In wild-type SW480 and SW620 cells with normal glycosylation, *CD276* silencing had no significant effect on invasion. In contrast, in *C1GALT1* KO cells - characterized by expression of Tn and STn antigens and lack of core 1 *O*-glycans - *CD276* silencing with both siRNAs (Si1 and Si2) led to a consistent and statistically significant reduction in invasion in both cell lines (SW480: $p = 0.0044$ for Si2, $p = 0.0110$ for Si1; SW620: $p = 0.0051$ for Si1, $p = 0.0008$ for Si2, Si2 vs WT Ctrl- $p < 0.0001$; one-way ANOVA, Tukey's post hoc test). Data represents fold change relative to control and are derived from three independent experiments. These results indicate that the pro-invasive role of CD276 is dependent on its aberrant glycosylation.

Aberrantly glycosylated CD276 drives pro-invasive signaling

To dissect the mechanistic consequences of aberrantly glycosylated CD276 in colorectal cancer, we performed quantitative phosphoproteomic profiling of SW620 *C1GALT1* knockout cells with or without CD276 knockdown. Principal component analysis revealed distinct phospho-signaling profiles between CD276-silenced and control glycoengineered cells (**Figure 6A**). Kinase–substrate enrichment analysis showed significantly reduced activity (negative z-scores) for ATR, ATM, AKT1, and CHEK1, which are key regulators of DNA damage response, checkpoint control, and pro-survival signaling (**Figure 6B**) [23]. Inhibition of ATR, ATM, and CHEK1 may compromise DNA repair and genotoxic stress responses, while reduced AKT1 activity is likely to impair cytoskeletal dynamics and cell adhesion [24]. These results suggest that CD276 sustains kinase-driven programs supporting migration, survival, and immune evasion. Interestingly, CDK2 activity showed a modest increase after CD276 knockdown, potentially reflecting compensatory activation of cell cycle progression. Pathway enrichment analysis confirmed CD276's role in regulating phosphorylation-dependent networks involved in spliceosome assembly, chromatin remodeling, cell cycle progression, and cytoskeletal organization (**Figure 6C**). Collectively, CD276 knockdown led to a coordinated downregulation of kinase activity and downstream signaling modules governing DNA repair, adhesion, and transcriptional regulation, which may reduce tumor cell adaptability and resilience. These molecular alterations were evident in substrate-centered network maps (**Figure 6D**) and align with the phenotypic consequences observed in CD276 loss-of-function models (**Figure 5**), including reduced proliferation, impaired migration, and weakened immune evasion.

Network-based mapping of phosphosite changes further reinforced these findings, revealing prominent dephosphorylation of nuclear and chromatin-associated regulators following CD276 knockdown. This included core components of the NuRD complex such as CHD4 (S308, S310), HDAC2 (S394), and MTA1 (S522) (**Figure 6D)**. Downregulation of CHD4 phosphorylation is consistent with a shift towards a quiescent chromatin state and reduced proliferative capacity [25]. Also, HDAC2-S394 hypo-phosphorylation is associated with impaired deacetylase activity and induction of growth-inhibitory

genes such as *CDKN1A/p21* [26], while MTA1-S522 loss has been linked to reduced cellular adaptability to stress [27]. CD276 knockdown also led to widespread dephosphorylation of cytoskeletal effectors controlling intercellular junctions and migratory behavior. This included CTTN, MYH10, and LMO7, key regulators of lamellipodia dynamics and microtubule remodeling [28]. Their decreased phosphorylation supports a loss of invasive plasticity upon CD276 depletion (**Figure 6D**). We further observed phosphosite losses for RB1 and JUN (S63), both known to be critical for cell cycle progression and apoptosis resistance [29]. Conversely, MAPK3 (ERK1) phosphorylation was sustained or elevated, likely reflecting compensatory ErbB signaling in response to CD276 silencing. However, the net signaling effect favored cell cycle arrest and reduced invasion.

Collectively, these findings support a role for immature CD276 glycosylation in sustaining kinase-driven signaling programs that promote proliferation, cytoskeletal plasticity, and resistance to apoptosis. Accordingly, its silencing triggered a coordinated shutdown of these pathways, leading to reduced cell cycle activity, reinforcement of junctional architecture, and chromatin stabilization. By contrast, control cells expressing immaturely glycosylated CD276 retain phosphoproteomic signatures of checkpoint adaptation, alternative splicing, and EMT-like transitions, underscoring CD276's role as a regulator of invasive reprogramming in colorectal cancer.

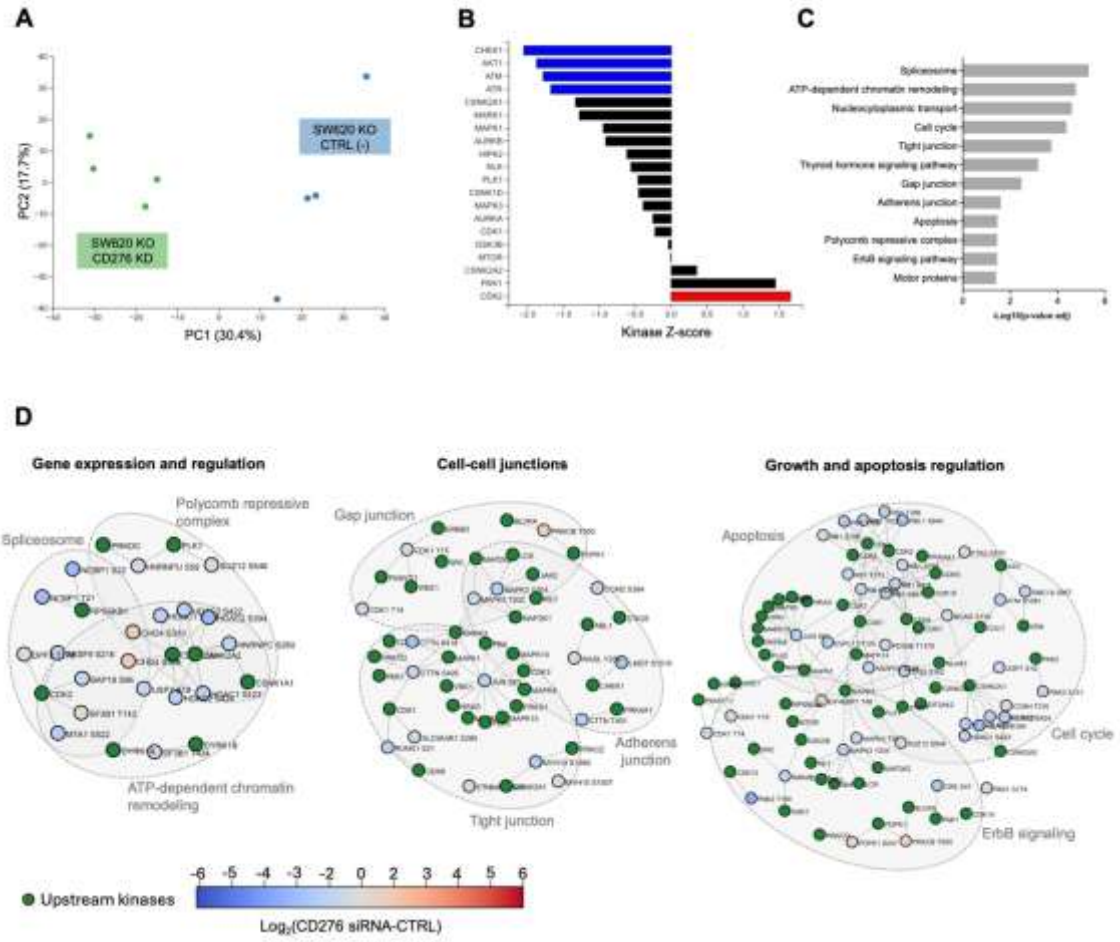

Figure 6. **Aberrantly glycosylated CD276 sustains phospho-signaling programs that promote proliferation, cytoskeletal remodeling, and immune evasion in SW620 cells.** Phosphoproteomic profiling was performed on glycoengineered SW620 CRC cells expressing Tn-modified CD276, with or without *CD276* knockdown. CD276 glycosylation was previously associated with increased proliferation and invasion; here, mass spectrometry and Phosphomatics-based analysis reveal that these phenotypes are underpinned by distinct phospho-regulatory networks. **A. Immature glycosylated CD276 supports a distinct phospho-signaling landscape.** Principal component analysis (PCA) of phosphopeptide intensities revealed a clear separation between *CD276*-silenced and control cells, indicating widespread remodeling. **B. Abnormally CD276 glycosylation promotes kinase signaling programs linked to proliferation and cytoskeletal organization.** Kinase-substrate enrichment analysis (KSEA) revealed reduced activity of kinases such as CHEK1, AKT1, ATM and ATR upon *CD276* knockdown, indicating that these proliferative and motility-associated kinases are supported by immature CD276 glycosylation. In contrast, kinases involved in checkpoint control and stress responses, including CDK2, were activated following *CD276* silencing, consistent with induction of growth restraint and DNA damage surveillance mechanisms. **C. Abnormal CD276 glycosylation maintains signaling across pathways involved in chromatin remodeling, cytoskeletal integrity, and cell survival.** Pathway enrichment analysis of differentially

phosphorylated proteins revealed that *CD276* knockdown suppresses phospho-regulated processes such as spliceosome and chromatin remodeling complexes (e.g., NuRD), tight junction organization, nucleocytoplasmic transport, and apoptotic resistance. These programs collectively support enhanced plasticity, proliferation, and invasive behavior observed in SW620 *C1GALT1* KO cells. **D. Abnormal CD276 glycosylation maintains phosphorylation of regulatory hubs that drive proliferation, invasion, chromatin remodeling, and immune modulation.** Phosphomatics network analysis identified distinct phospho-signaling modules dependent on glycosylated CD276, which were disrupted upon its silencing. These include: i) Chromatin regulators (HDAC1/2, CHD4, CSNK2A2), promoting transcriptional reprogramming and epigenetic adaptability; ii) Cytoskeletal and junction-associated proteins (CTTN, MAPKs), supporting cell motility and invasiveness; iii) Growth and survival kinases (RB1, MAPK3), reflecting pathways that enable tumor persistence and proliferation. Together, these data demonstrate that aberrant CD276 *O*-glycosylation drives SW620 pro-oncogenic phosphorylation programs that coordinate enhanced proliferation, invasion, and immune suppression.

Aberrantly Glycosylated CD276 Promotes Immune Evasion in CRC

To investigate whether the glycosylation status of CD276 modulates its immune regulatory functions, we first conducted *in vitro* experiments by co-culturing pre-activated, CFSE-labelled human T cells with SW620 wild-type and *C1GALT1* knockout cells, with or without CD276 knockdown. Flow cytometry analyses revealed that T cells co-cultured with *C1GALT1* KO cells exhibited significantly reduced proliferation, as indicated by higher CFSE mean fluorescence intensity in both $CD4^+$ and $CD8^+$ subsets (**Figure 7A**). This was accompanied by a marked reduction in early (CD69) and late (CD25) activation markers across both $CD4^+$ and $CD8^+$ T cell subsets (**Figure 7B-C, Figure S11**). Notably, these immunosuppressive effects were reversed upon CD276 knockdown in the *C1GALT1* KO background, strongly implicating aberrantly glycosylated CD276 as a key mediator of T cell inhibition.

Furthermore, T cells co-cultured with *C1GALT1* KO cells exhibited a cytokine profile skewed toward an immunosuppressive and regulatory phenotype, with significantly elevated levels of IL-10 and IL-8, and a corresponding decrease in IFN-γ (**Figure 7C and Figure S12**). Given that IL-8 and IL-10 are not canonical T cell cytokines, their elevation in the co-cultures may also originate from the cancer cells and reflect a contact-dependent response to T cell engagement, modulated by the CD276 glycosylation status. Broad-spectrum cytokine profiling further revealed a constant trend reduction of pro-

inflammatory mediators secretion, including TNF-α, IL-17A, and IL-12p70, accompanied by increased levels of type 2 and tolerogenic cytokines such as IL-13 and IL-5 (**Figure S12**), suggesting a shift away from Th1/effector polarization toward an immune-modulatory state. Importantly, these cytokine alterations were largely reversed upon CD276 knockdown in the *C1GALT1* KO background, restoring IFN-γ production and attenuating IL-10 and IL-8 secretion (**Figure 7C**). Together, these findings support a model in which immature CD276 glycosylation promotes immune escape by shaping a non-permissive cytokine environment. Although T cells remain physically engaged in the co-culture, their activation is blunted and they fail to acquire effector functions in response to this glycophenotype. This aligns with previous reports showing that cancer cells can respond to T cell-derived inflammatory cues, such as TNF-α via NF-κB, by increasing IL-8 production, a chemokine known to recruit MDSCs and TAMs, promote angiogenesis, and reinforce immune exclusion [30]. In parallel, IL-10 suppresses T cell function and promotes peripheral tolerance [31], while diminished IFN-γ reflects impaired effector polarization of $CD4^+$ T cells and reduced cytotoxic capacity of CD8+ T cells [32]. In summary, our data define a glycosylation-dependent mechanism of immune modulation, whereby the acquisition of immature glycosylation by CD276 in cancer cells contributes to the establishment of a suppressive cytokine milieu and an immune-excluded, tumor-permissive niche.

We then interrogated TCGA CRC datasets to find support for these findings in clinical samples. Correlation and clustering analyses revealed that low expression of the glycosyltransferases *C1GALT1* and *C1GALT1C1* correlated with increased expression of key immune checkpoints and T cell exhaustion markers, including PD-1 (PDCD1) and TIM-3 (HAVCR2) (**Figure 7D**) [33]. In contrast, *B3GNT6* expression showed weaker and less consistent correlations with immune-related genes, suggesting a more limited role in modulating immune escape. CD276 expression itself was positively correlated with multiple immune checkpoints such as *PDCD1*, *CD274*, and *HAVCR2*, and inversely correlated with *C1GALT1* and *C1GALT1C1* (**Figure 7D**), as previously described. To explore this further, we stratified tumors based on *CD276* and *C1GALT1* expression levels to mirror the *in vitro* phenotype for CD276 with immature glycosylation. Tumors with high *CD276* and low *C1GALT1* expressions

(*CD276*High/*C1GALT1*Low) exhibited significantly elevated levels of exhaustion markers including *TIGIT*, *LAG3*, *HAVCR2*, and *PDCD1*, when compared to *CD276*Low/*C1GALT1*Low tumors (**Figure 7E, Panel I**). A similar pattern emerged when stratifying by *C1GALT1C1* expression (*CD276*High/*C1GALT1C1*Low vs. *CD276*Low/*C1GALT1C1*Low; **Figure 7E, Panel II**), reinforcing that deficiencies in core 1 *O*-glycosylation whether *via* C1GALT1 or its chaperone potentiate CD276-associated immune evasion. Cytokine gene expression analysis further supported the presence of a reprogrammed immune environment. *IL10* and *IL8* levels were significantly elevated, while *IL12A* was reduced in both *CD276*High/*C1GALT1*Low and *CD276*High/*C1GALT1C1*Low tumors, mirroring cytokine shifts observed *in vitro*. Interestingly, *IFNG* expression was only elevated in *CD276*High/*C1GALT1*Low tumors, suggesting that T cells may become initially activated but subsequently driven toward exhaustion due to sustained immune checkpoint signaling, which warrants future demonstration. By contrast, when *CD276* expression remained high but *C1GALT1* or *C1GALT1C1* expressions were restored, most immune-related genes were no longer differentially expressed, except for IL8 and IL12A (**Figure 7E, Panel III**). Together with *in vitro* data, these transcriptomic associations suggest that aberrant *O*-glycosylation enhances the immunomodulatory capacity of CD276 and contributes to the establishment of an immunosuppressive program in CRC.

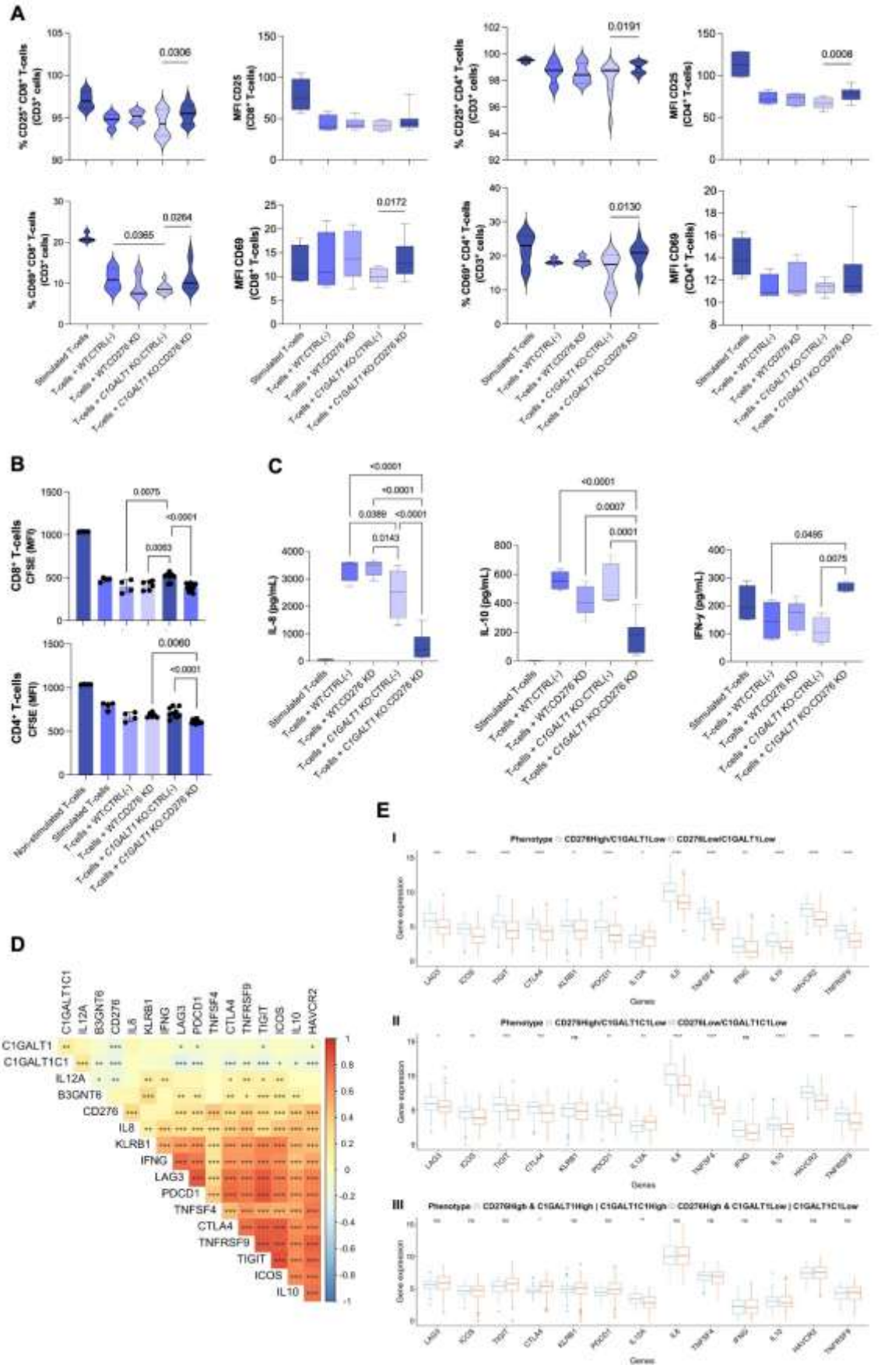

Figure 7. Aberrant CD276 glycosylation suppresses T cell function and shapes an immunosuppressive tumor microenvironment. A–C) Aberrant CD276 glycosylation

dampens T cell activation, proliferation, and functional cytokine output. *In vitro* co-culture assays and cytokine profiling were conducted using SW620 colorectal cancer cells glycoengineered with *C1GALT1* KO (resulting in immature CD276-Tn glycoforms) and wild-type controls, with or without *CD276* knockdown. These cell models were co-cultured with pre-activated human T cells to evaluate functional immune responses. Across three independent replicates, T cell activation, proliferation, and cytokine secretion were significantly influenced by the glycosylation status of CD276. Statistical comparisons were performed using one-way ANOVA followed by Tukey's multiple comparisons test. **A. Aberrant CD276 glycosylation dampens T cell activation.** Flow cytometry revealed a significant reduction in $CD25^+$ cells within both $CD4^+$ and $CD8^+$ T cell subsets after 5 days of co-culture with *C1GALT1* KO cells. Mean fluorescence intensity (MFI) of CD25 was also lower in these T cells, indicating a subdued activation profile. CD276 knockdown in the KO background restored CD25 expression (both percentage and MFI), implicating glycosylated CD276 in the suppressive phenotype. While the percentage of $CD69^+$ cells was not significantly altered, CD69 MFI was reduced in T cells exposed to CD276-expressing KO cells, further supporting impaired activation. Importantly, CD25 and CD69 levels in WT and *C1GALT1* KO CD276 knockdown co-cultures were similar, underscoring the dominant role of CD276 in modulating activation. **B. Abnormal CD276 glycosylation inhibits T cell proliferation.** CFSE dilution assays showed higher fluorescence retention in both $CD4^+$ and $CD8^+$ T cells co-cultured with *C1GALT1* KO cells, indicating reduced proliferation. Silencing CD276 rescued CFSE dilution, confirming that the glycosylated form of CD276 actively suppresses T cell proliferative responses. **C. Abnormal CD276 glycosylation reprograms cytokine secretion toward an immunosuppressive profile.** Supernatants from co-cultures with *C1GALT1* KO cells displayed elevated IL-8 and IL-10 and reduced IFN- γ levels, supporting a shift toward immune suppression. These cytokine alterations were reversed by *CD276* knockdown. **D. Expression correlations suggest an association between CD276, core 1 *O*-glycosylation genes, and immune regulatory markers in patient samples.** A correlogram of TCGA CRC samples revealed strong positive correlations between CD276 and immune checkpoint molecules associated with T cell exhaustion, including PDCD1 (PD-1) and HAVCR2 (TIM-3). Additionally, *CD276* expression was inversely correlated with *C1GALT1* and *C1GALT1C1*, further reinforcing that impaired core 1 O-glycosylation may be linked to enhanced CD276 expression and transcriptional profiles consistent with immune evasion. **E. Tumours co-expressing high *CD276* and low levels of core 1 *O*-glycosylation enzymes exhibit transcriptional profiles indicative of T cell dysfunction and immune suppression.** Analysis of TCGA CRC samples revealed that tumours with high *CD276* and low *C1GALT1* expression (**Panel I**) displayed marked reductions in genes associated with T cell exhaustion and elevated immunosuppressive cytokines *IL10* and *IL8*, closely mirroring the phenotypes observed in *in vitro* co-culture assays. These tumours serve as a surrogate of altered CD276 glycosylation, where impaired core 1 *O*-glycan biosynthesis leads to stabilization/increase of immature CD276 glycoforms with immunosuppressive properties. **Panel II** reinforces this observation, showing that tumours with *CD276*High/*C1GALT1C1*Low expression recapitulate the immunosuppressive

phenotype. **Panel III** extends this observation by stratifying tumours co-expressing *CD276*High with low expression of both *C1GALT1* and its chaperone *C1GALT1C1* (with high probability of expressing high levels of immature glycosylation), confirming a broader immunosuppressive transcriptional program that includes increased expression of exhaustion marker such as *CTLA4* and reduced pro-inflammatory cytokine IL12A.

Discussion

The glycome is pivotal in cancer progression and dissemination, offering significant potential for the precise detection, targeting, and elimination of cancer cells. Despite recent advances in understanding CRC glycome alterations by high-throughput mass spectrometry, a considerable gap in grasping the underlying functional and clinical implications of these alterations remains [22, 34]. This study addresses these gaps through an in-depth exploration of *O*-glycosylation and its impact in colorectal cancer.

We confirm previous findings linking premature termination in *O*-glycan elongation to cancer aggressiveness [35]. We began by identifying glycogene deregulation in colorectal tumours compared to normal tissue, with *B3GNT6* downregulation emerging as a poor prognosis marker in CRC. This was frequently accompanied by concomitant *C1GALT1* and/or *C1GALT1C1* downregulation, which had a significant impact on the decreased overall survival of CRC patients. Advancing beyond current knowledge, we demonstrate that these events coincide with the loss of normal colonic glycosylation, predominantly characterized by *O*-6 sialylated core 3 structures, likely supported by elevated *B3GNT6* and *ST6GALNACs* expression. Moreover, we found that advanced epithelial-like and mesenchymal-like CRC showed unique glycocode profiles. Epithelial-like tumours displayed an intermediate glycome between normal colon tissue and mesenchymal-like cancers. In these cases, the loss of core 3-related structures was not compensated by the capacity to shift the glycophenotype toward core 1 and core 2-related structures, resulting in an enrichment for short Tn and sTn antigens. Mesenchymal-like tumours, while also exhibiting high levels of Tn and sTn antigens, were predominantly enriched for sialylated T antigens. Interestingly, tumours of both differentiation states that showed signs of distant metastases also displayed extended core 2 structures, including glycans compatible with the presence of sLe antigens. These antigens are known to facilitate cancer cell intravasation into the bloodstream and colonization of distant

locations by mediating adhesion to endothelial cells via E-selectin [36]. These findings reinforce previous reports and underscore the heterogeneous and dynamic nature of the CRC glycome, where distinct subpopulations may coexist to drive aggressive traits [34b, 37]. We further broadened our understanding of the events potentially dictating immature glycosylation at the surface of CRC cells. Here, we show that in more aggressive tumours associated with an unfavorable prognosis, the concurrent downregulation of *B3GNT6* and *C1GALT1* play a decisive role in driving immature glycosylation, which had previously been largely attributed to *C1GALT1C1* loss-of-function mutations [38]. Utilizing *C1GALT1* knockout cell lines with distinct molecular backgrounds, we confirmed that immature glycosylation drives enhanced invasion and, in a context-dependent manner, increases proliferation. This reinforces previous findings regarding *C1GALT1C1* and decisively links the acquisition of immature glycophenotypes through different mechanisms to cancer aggressiveness [39].

We finally identified CD276 as a carrier of immature *O*-glycans in CRC. Also known as B7-H3, CD276 belongs to the B7 family of immune checkpoint molecules and can either enhance or suppress immune responses depending on context [40]. Namely, it has been shown to interact with cognate receptors on immune cells, particularly T cells, regulating their activation and function [40]. CD276 is overexpressed in several malignancies, including CRC [9], where its expression correlates with poor prognosis. Our findings go beyond the state-of-the-art by demonstrating that immature *O*-glycosylation also regulates CD276 stability, enhances its expression, and shapes its immunomodulatory role in CRC. This underscores that CD276 regulation in cancer is not solely governed by *N*-glycans but is also critically shaped by the *O*-glycome, revealing new layers of regulatory control and therapeutic potential. Specifically, we show that aberrantly *O*-glycosylated CD276 is abundant in primary CRC tumours and metastases but absent from healthy colon tissue, suggesting a cancer-specific modification. Moreover, expression of CD276 carrying immature *O*-glycans was enriched in right-sided tumours, which are commonly associated with more aggressive clinical behavior, and was linked to significantly worse patient survival. Proteomic and glycoproteomic analyses further revealed that, while CD276 is broadly expressed across tumour stages and differentiation states, the density and distribution of its glycosylation sites vary with tumour differentiation,

highlighting potential implications for tumour behavior and therapeutic design. We also show that loss or downregulation of *C1GALT1* promotes immature *O*-glycosylation on CD276, leading to increased protein stability and elevated expression. Although our data support a posttranslational stabilization mechanism, the basis for the observed transcriptional upregulation of CD276 remains unclear. One plausible explanation is that defective *O*-glycosylation perturbs cellular homeostasis, activating compensatory stress response pathways. Previous studies have shown that glycosylation defects can induce endoplasmic reticulum stress or Golgi dysfunction, triggering transcriptional programs that upregulate membrane protein expression [41]. CD276 may therefore be indirectly upregulated as part of a broader adaptive response, which warrants further exploration.

Additionally, emerging evidence suggests that glycosylation status can modulate epigenetic and transcriptional regulators. Altered glycosylation has been shown to affect the stability and function of key transcription factors such as SP1 and STAT3, both implicated in immune checkpoint regulation [42]. It is conceivable that similar mechanisms contribute to increased CD276 transcription in CRC. Although the precise pathways remain to be defined, our findings lay the groundwork for future investigations into how glycome remodeling interfaces with CD276 transcriptional control in cancer.

Functionally, we demonstrated that immature glycosylation supports CD276-mediated invasion through phospho-signaling rewiring, enhanced cell proliferation, and suppressed T cell activation. *In vitro*, *CD276* knockdown in glycoengineered cells reduced both invasive capacity and proliferation, particularly in metastatic models. Quantitative phosphoproteomic analysis revealed that aberrantly glycosylated CD276 sustains pro-invasive and pro-proliferative signaling through kinases such as CSNK2A2, AKT1, and CDK2, and modulates chromatin and cytoskeletal regulators, including HDAC2, CHD4, and cortactin [23, 43]. These findings define a cell-intrinsic function of CD276, wherein its abnormal glycosylation promotes tumour aggressiveness through activation of oncogenic signaling cascades.

Aberrant CD276 glycosylation also reprogrammed cytokine profiles, promoting IL-10 and IL-8 production while decreasing pro-inflammatory IFN-γ secretion. These changes suggest that aberrantly glycosylated CD276 not only

impairs T cell activation but also actively reconditions the tumour microenvironment to favor immune evasion [30-31, 44].

Together, these results position glycosylated CD276 as a multifunctional effector, orchestrating both tumour-intrinsic signaling and immune suppression. Importantly, TCGA data corroborated these findings at the clinical level, showing that tumours with high *CD276* and low *C1GALT1* expression exhibited reduced expression of T cell activation and cytotoxicity markers, and higher levels of immunosuppressive cytokines such as IL10, reinforcing the translational relevance of our findings. This intersection of intracellular and immunomodulatory effects likely provides a strong selective advantage to cancer cells, enabling both aggressive growth and immune escape.

In conclusion, our findings establish a mechanistic and functional framework linking glycosylation-driven CD276 remodeling to tumour aggressiveness and immune escape in colorectal cancer. Collectively, we position CD276 *O*-glycosylation remodeling as a novel driver of immune checkpoint activity and tumour aggressiveness in CRC. Future studies should focus on providing definitive demonstrations of the role of abnormally glycosylated CD276 as an immune checkpoint in CRC by exploiting *in vivo* models. Investigation into the impact of other CRC glycans, including extended core 2 structures associated with distant metastasis [22], on CD276 functions is also warranted. Moreover, gaining a deeper understanding of CD276 impact on other immune cells and its role in disease pathology will be key for designing appropriate countermeasures. Ultimately, this work provides foundational insights for the rational design of therapeutic strategies that selectively target aberrantly glycosylated CD276 in cancer. Together, our findings unveil a previously unrecognized link between cancer-associated glycome remodeling and immune evasion in colorectal cancer. By suggesting CD276 as a glycosylation-dependent immune checkpoint, this study opens new avenues for innovative therapeutic strategies aimed at selectively targeting tumour-specific glycoforms. Future efforts to decode the broader "glycocode" of the tumour microenvironment, including the identification of receptors and lectin networks that interpret this altered glycosylation landscape. This will be critical to unlocking next-generation immunotherapies and advancing precision oncology.

Materials and Methods

Clinical Tissue Samples and Ethical Compliance

A retrospective cohort of 40 formalin-fixed paraffin-embedded (FFPE) CRC tissue samples was selected from the institutional pathology biobank of the Portuguese Institute of Oncology of Porto (IPOPorto). Samples were collected from patients who underwent surgical resection for colorectal (adeno)carcinomas between 2005 and 2012. The cohort included 18 female and 22 male patients, aged 28 to 76 years (mean ± SD: 61 ± 11 years). Whenever present, adjacent histologically normal mucosa was also included for comparative analysis. In addition to CRC samples, a reference panel of healthy tissues, including liver, stomach, pancreas, appendix, lung, testis, thyroid, and gallbladder, was analyzed. Tumour and healthy tissue sections were further screened for CD276 and aberrant glycosylation markers (Tn and sTn antigens) using multiple immunoassays: immunohistochemistry (IHC), PLA, and dual immunofluorescence staining with lectins and specific antibodies. All procedures were conducted in compliance with institutional ethical guidelines and approved by the IPO-Porto Ethics Committee (project reference: CES 86/017). Written informed consent was obtained from all patients. Clinical and pathological data were retrieved from patient medical records and are summarized in **Table 1.** Antibodies and experimental conditions are detailed in **Table S5.**

Table 1. Clinicopathological data associated with tumour tissues assessed in this study (n = 40).

	***n* (%)**
Stage	
I	1 (2.5)
II	4 (10.0)
III	10 (25.0)
IV	25 (62.5)
Tumour (T)	
T1	1 (2.5)

T2	1 (2.5)
T3	31 (77.5)
T4	6 (15.0)
Missing Information	1 (2.5)
Lymph node metastases (N)	
N0	11 (27.5)
N1	12 (30.0)
N2	14 (35.0)
N3	3 (7.5)
Tumour Location	
Right colon	7 (17.5)
Left colon	23 (57.5)
Rectum	10 (25.0)

Transcriptomic Analysis of the TCGA-COADREAD Cohort

RNA sequencing (RNA-seq) data for colorectal cancer were obtained from The Cancer Genome Atlas (TCGA) COADREAD cohort, comprising 623 tumor tissues and 51 matched normal adjacent tissues. Processed gene expression data (log2(FPKM + 1)) and associated clinical annotations - including age, gender, tumor stage, histological subtype, and overall survival - were downloaded via the UCSC Xena platform (https://xena.ucsc.edu/), which hosts curated TCGA datasets. After excluding samples with incomplete clinical data, a final cohort of 598 tumor samples and 51 normal adjacent tissue samples was included for analysis. Clinical characteristics for the COADREAD patients are summarized in **Table 2.**

Table 2. Clinicopathological characteristics of colorectal cancer cases from TCGA COADREAD dataset used in this study.

	n	n = 598[1]
Age	598	66.34 (12.78)
Gender	598	

Female		280 (47)
Male		318 (53)
Histological type	587	
Colon Adenocarcinoma		376 (64)
Colon Mucinous Adenocarcinoma		62 (11)
Rectal Adenocarcinoma		137 (23)
Rectal Mucinous Adenocarcinoma		12 (2)
Missing data		11
Clinical stage	598	
I		104 (17)
II		227 (38)
III		179 (30)
IV		88 (15)
Vital status	598	
Alive		479 (80)
Dead		119 (20)

Proteomic Reanalysis of TCGA-COADREAD for CD276 Glycosylation

A subset of 95 colorectal cancer (COADREAD) cases from TCGA, analyzed by mass spectrometry and annotated with clinicopathological data in Zhang *et al.* [45], was retrieved from the PRIDE Archive (dataset identifier PXD002080). The proteomics data were reanalyzed to identify and quantify glycoproteins modified with Tn and sialyl-Tn (sTn) antigens. Samples were stratified into epithelial-like and mesenchymal-like subtypes according to the TCGA transcriptomic classification used by Zhang *et al.* [45]. Further classification was based on the presence of unglycosylated CD276 or CD276 glycosylated with Tn/sTn antigens (CD276-Tn/STn). All data processing and visualization were performed in R version 4.2.3 [46]. Data wrangling and statistical plotting were conducted using the tidyverse [47] and ggpubr [48] packages. CD276-Tn/STn–positive samples were manually curated to identify glycosylation sites specific to epithelial- and

mesenchymal-like subtypes. These glycosites were visualized as a heatmap using the pheatmap package, enabling subgroup clustering and the identification of potential molecular patterns.

Cell Lines and Culture Conditions

Human CRC cell lines SW480, SW620, HCT118, RKO, LS174T and HCA7 were obtained from the American Type Culture Collection (ATCC). Cells were cultured in RPMI 1640 GlutaMAX™ medium (Gibco) supplemented with 10% fetal bovine serum (FBS) and 1% penicillin-streptomycin at 37 °C in a humidified incubator with 5% CO_2.

CRISPR-Cas9 glycoengineered cell models

Two guide RNAs targeting the human C1GALT1 gene (sequences: *GTAAAGCAGGGCTACATGAG* and *ACAACACTTTGTTACAACGC*) were cloned into a dual-guide RNA CRISPR-Cas9 expression vector (pRP[2CRISPR]-Puro-hCas; VectorBuilder). Wild-type SW480 and SW620 colorectal cancer cell lines were transfected with CRISPR-Cas9 plasmid (1 µg) using jetPRIME® transfection reagent (Polyplus) according to the manufacturer's protocol. Single-cell clones were isolated by limiting dilution in 96-well plates, and successful *C1GALT1* knockout (KO) clones were identified by Indel Detection by Amplicon Analysis (IDAA) using the ABI PRISM™ 3010 Genetic Analyzer (Thermo Fisher Scientific) and confirmed by Sanger sequencing. Three independent KO clones with distinct out-of-frame indels were selected for further studies. In addition, clones harboring silent mutations were used as phenotypic control cell lines. IDAA results were analyzed using Peak Scanner Software v1.0 (Thermo Fisher Scientific).

siRNA-Mediated CD276 Silencing

CD276 gene silencing was performed in SW480 and SW620 glycoengineered colorectal cancer cell models using reverse transfection with siRNA. Two Silencer® Select siRNAs targeting distinct exons of human CD276 (s37289, exon 10; and s37288, exon 7; Invitrogen) were used to ensure target specificity. A Silencer® Select negative control siRNA (catalog no. 4390843, Invitrogen) was included in all experiments as a non-targeting control, as previously described

[49]. Cells were detached and seeded into 24-well plates at a density of 1×10^5 cells/well prior to transfection. siRNAs and Lipofectamine® RNAiMAX (Invitrogen) were separately diluted in Opti-MEM® Reduced Serum Medium (Gibco), incubated for 5 minutes at room temperature, and combined to form siRNA–lipid complexes. Cells were then incubated with the complexes for 72 hours at 37 °C. Each condition was plated in duplicate wells per experiment, and all experiments were performed in at least three independent biological replicates. To evaluate gene silencing efficiency, *CD276* mRNA expression was quantified by RT-qPCR using the TaqMan® Gene Expression Assay Hs00987207_m1 (Thermo Fisher Scientific). *GAPDH* and *ACTB* were used as endogenous controls. To confirm the specificity and rule out off-target effects, both non-targeting negative control siRNA and mock-transfected cells (no siRNA, Lipofectamine only) were included as negative controls. Effective knockdown was confirmed only when both *CD276*-targeting siRNAs produced consistent reductions in mRNA levels compared to controls. Cell viability and morphology were also monitored microscopically to exclude transfection-related cytotoxicity.

Proliferation assay

Cell proliferation was assessed using the Cell Proliferation ELISA, BrdU (colorimetric) kit (Roche), according to the manufacturer's instructions. Absorbance was measured at 450 nm using a microplate reader.

Invasion Assay

Invasion potential was evaluated using Falcon® Permeable Supports for 24-well plates with 8.0 µm transparent PET membranes (Corning), coated with Matrigel® Basement Membrane Matrix (50 µg/mL, Corning). Inserts were pre-coated and incubated at 37 °C for 1 h prior to cell seeding. Subconfluent cells were detached using trypsin/EDTA (Thermo Fisher Scientific) and seeded in the upper chamber at a density of 5×10^4 cells/mL. After 24 h of incubation at 37 °C, non-invading cells were removed from the upper surface, and the inserts were washed with PBS and fixed in 4% paraformaldehyde (Sigma-Aldrich). Filters were mounted in Vectashield with DAPI (Vector Laboratories) and imaged using a Zeiss Axiovert 200M fluorescence microscope (Carl Zeiss). Each assay was performed in

biological triplicate with five technical replicates per condition. Results were normalized to cell proliferation and expressed as fold change relative to control.

RT-qPCR for CD276 and Glycogene Expression

Total RNA was extracted using TriPure Isolation Reagent (Roche Diagnostics). cDNA synthesis and mRNA quantification were performed as previously described [50]. Quantitative RT-PCR was carried out using TaqMan Gene Expression Assays for CD276 (Hs00987207_m1) and B3GNT6 (Hs00371066_s1) on a 7500 Fast Real-Time PCR System (Applied Biosystems). GAPDH (Hs03929097_g1) and ACTB (Hs99999903_m1) were used as endogenous controls. All samples were analyzed in duplicate and relative gene expression was calculated using the 2^–ΔCt method.

Western Blot for CD276 and Glycan Detection

Total and plasma membrane protein extracts, as well as CD276-immunoprecipitated fractions, were analyzed by Western blotting. Total protein lysates were prepared using a buffer containing Tris-HCl (25 mM, pH 7.4), NaCl (150 mM), $MgCl_2$ (5mM), 1% NP-40, and 5% glycerol, supplemented with Halt™ Protease and Phosphatase Inhibitor Cocktail (Thermo Fisher Scientific). Plasma membrane proteins were isolated by ultracentrifugation, as described by Fernandes et al. [51]. Proteins were resolved by SDS-PAGE (4–20% precast gels, Bio-Rad) and transferred to nitrocellulose membranes (Cytiva). Membranes were probed with anti-CD276 antibodies and biotinylated Vicia villosa agglutinin (VVA) lectin (Vector Laboratories) to detect GalNAc residues associated with the Tn antigen. Lectin binding was visualized using streptavidin-HRP and chemiluminescent detection. Membrane transfer efficiency was verified by Ponceau S staining. Antibodies, lectins, and experimental conditions are detailed in **Table S5**.

CD276 Immunoprecipitation

CD276 was immunoprecipitated from plasma membrane protein extracts using Pierce™ Protein G Agarose beads (Thermo Fisher Scientific). Beads were pre-blocked with 1% BSA (Sigma-Aldrich) for 1 h at 4 °C. Protein extracts were precleared with BSA-blocked beads for 2 h at 4 °C to reduce nonspecific binding.

Supernatants were incubated with CD276 polyclonal antibody (10 µg) at 4 °C for 2 h, followed by overnight incubation with fresh blocked beads. After washing, immune complexes were eluted in SDS loading buffer at 95 °C. Eluted proteins were resolved on 4–20% gradient SDS-PAGE gels (Bio-Rad) and transferred to nitrocellulose membranes (Cytiva). Immunodetection was performed with anti-CD276 antibody and VVA lectin, as detailed in **Table S5.**

Flow Cytometry for CD276 and Glycans Detection

Flow cytometry was used to assess the expression of Tn, sTn, T, and sT antigens, as well as CD276, as previously described by Peixoto et al. [52]. Detailed antibody information and staining conditions are listed in **Table S5**. To validate sialylated glycans specificity, isotype controls and cells treated with 70 mU of α-neuraminidase (*Clostridium perfringens*, Sigma-Aldrich) were used as negative controls. Data were acquired on a Beckman Coulter FC500 flow cytometer and analyzed using CXP software (Beckman Coulter).

Protein Stability Assay Using Cycloheximide Chase

To assess CD276 protein stability, 1 × 10^6 SW480 and SW620 colorectal carcinoma cells were seeded per well in 6-well plates and cultured overnight in complete RPMI 1640 GlutaMAX™ medium (Gibco). Cells were treated with cycloheximide (20 µM, CHX) (Sigma-Aldrich), dissolved in DMSO, to inhibit de novo protein synthesis. Control wells were treated with an equivalent volume of DMSO. Whole-cell protein extracts were collected at 2, 4, 8, 16, 24 hours post-treatment using RIPA buffer (50 mM Tris-HCl, pH 8.0; 150 mM NaCl; 1% NP-40; 0.5% sodium deoxycholate; 0.1% SDS) freshly supplemented with Halt™ Protease and Phosphatase Inhibitor Cocktail (Thermo Fisher Scientific). For each time point, 10 µg of protein were resolved by SDS-PAGE on 4–20% precast gradient gels (Bio-Rad) and transferred onto nitrocellulose membranes (Cytiva). Protein transfer and equal loading were verified by staining with Ponceau S solution (Sigma-Aldrich). Membranes were blocked and immunoblotted using primary antibodies against CD276 and appropriate HRP-conjugated secondary antibodies, as detailed in **Table S5**.

O-Glycomics on Cell Models and Patient Samples

O-glycome characterization of CRC and matched healthy tissues was performed on 10 µm FFPE sections. Sections were deparaffinized by sequential immersion in xylene (2×, 7 min), 100% ethanol (2×, 5 min), 96% ethanol (2×, 5 min), 70% ethanol (1×, 5 min), and water (1×, 5 min). Antigen retrieval was carried out for 20 min at high temperature using citrate-based antigen unmasking solution (1:100 dilution; Vector Laboratories). Samples were then incubated with 150 µL of denaturation buffer (145 µL 8 M guanidine hydrochloride and 5 µL 200 mM dithiothreitol) at 60 °C for 30 min. *N*-glycans were enzymatically released in situ using PNGase F from *Elizabethkingia miricola* (1 U/10 µg protein; Promega, V4831), incubated overnight at 37 °C. *O*-glycans were subsequently released by on-tissue reductive β-elimination (1 M $NaBH_4$ in 50 mM KOH, overnight at 50 °C), and desalted using cation-exchange resin (AG 50W-X8; Bio-Rad). For CRC cell lines, *O*-glycans were profiled using the Cellular *O*-Glycome Reporter/Amplification (CORA) approach [53], following the protocol of Fernandes *et al.* [51]. Released glycans were dried and permethylated by resuspension in 500 µL dimethyl sulfoxide, followed by sodium hydroxide addition and stirring for 30 min. Methylation was carried out by adding 300 µL methyl iodide and incubating for another 30 min. An additional 100 µL methyl iodide was added if needed. Permethylated glycans were extracted by chloroform–water partitioning and dried under vacuum centrifugation. LC-MS/MS analysis was performed using an Ultimate 3000 nano-LC system coupled to a Q Exactive mass spectrometer with an EASY-Spray nano-electrospray source (Thermo Fisher Scientific). Eluent A was 0.2% formic acid in water; eluent B was 0.2% formic acid in acetonitrile. Samples were loaded onto a PepMap C18 trap column (5 µm, Thermo Fisher Scientific) and washed isocratically (90% A, 10% B, 30 µL/min). After 3 min, flow was redirected to the analytical column (PepMap C18, 100 Å, 150 mm × 75 µm, 3 µm particle size) operated at 0.3 µL/min and 35 °C. Glycan separation was achieved with a linear gradient: 10% B at 10 min, 38% B at 20 min, 50% B at 55 min, and 90% B at 65 min. The column was held at 90% B for 10 min before re-equilibration. Mass spectrometry (MS) was performed in positive ion mode with a scan range of m/z 500–4000, 120,000 resolution (Full MS), spray voltage of 1.9 kV, and capillary temperature of 275 °C. Data-dependent MS/MS (Top 15) was acquired at 30,000 resolution using higher-

energy collisional dissociation (HCD, 30% normalized collision energy, 4.0 *m/z* isolation window), with a 5 s dynamic exclusion. Data analysis was performed using Xcalibur v3.0 (Thermo Fisher Scientific), applying Gaussian smoothing, 10 ppm mass tolerance, four decimal mass precision, and default baseline subtraction. Glycan structures were assigned based on retention time, monoisotopic m/z, and MS/MS spectra, and matched against GlycoMod and GlyConnect databases. Quantification was based on the extracted ion chromatogram (EIC) areas for z = 1, 2, and 3, normalized to the total glycan signal. Isomeric and isobaric structures were not differentiated. Glycan representations were created using GlycoWorkBench v2.1.

Phosphoproteomics of Cell Models

Glycoengineered SW620 cells, with or without CD276 knockdown by siRNA, were harvested for whole protein extraction using RIPA buffer supplemented with protease and phosphatase inhibitors (Thermo Fisher Scientific). Protein concentration was determined using a BCA assay (Thermo Fisher Scientific). For each condition, 50 µg of total protein was diluted 1:2 in 50 mM Tris-HCl (pH 8.0; Sigma-Aldrich), followed by reduction with 20 mM dithiothreitol (DTT) at 60 °C for 1 h and alkylation with 40 mM iodoacetamide for 30 min in the dark at room temperature. The reaction was quenched by adding 10 mM DTT. Proteins were digested overnight at 37 °C using trypsin (Promega; 1 µg per 50 µg of protein) in 50 mM ammonium bicarbonate. For phosphoproteomics, an enrichment step for phosphopeptides was performed using TiO_2-based spin columns (Thermo Fisher Scientific) according to the manufacturer's protocol. Phosphopeptide-enriched fractions were desalted using C18 spin columns (Thermo Fisher Scientific), eluted in 70% acetonitrile, dried by vacuum centrifugation, and resuspended in 0.1% formic acid for LC-MS/MS analysis. Samples were analyzed using nanoLC-nESI-MS/MS on a Q Exactive™ mass spectrometer (Thermo Fisher Scientific) coupled to an Ultimate 3000 nano-LC system. Peptide separation was carried out on an EASY-Spray™ C18 column using a linear acetonitrile gradient. Data were acquired in data-dependent acquisition mode, and phosphopeptide spectra were collected using higher-energy collisional dissociation (HCD). Raw data were processed using Proteome Discoverer 1.4 (Thermo Fisher Scientific) with the SequestHT search engine. Protein and phosphopeptide identification was

performed against the SwissProt human proteome database, allowing two missed cleavages, a precursor mass tolerance of 10 ppm, and a fragment mass tolerance of 0.6 Da. Carbamidomethylation of cysteine was set as a fixed modification, while oxidation of methionine (+15.995 Da) and phosphorylation of serine, threonine, and tyrosine (+79.966 Da) were included as variable modifications. Identifications were validated using the Percolator algorithm, with a false discovery rate (FDR) set to 1%. Quantitative analysis of phosphoproteins was based on normalized spectral abundance factor (NSAF) values. Only phosphosites with a ≥2-fold change compared to controls and localization probability ≥0.75 were considered for downstream analysis. Differentially phosphorylated proteins were functionally annotated using KEGG and Reactome pathway enrichment, and kinase-substrate relationships were inferred via Kinase-Substrate Enrichment Analysis (KSEA). Phosphomatics was used for phosphosite mapping, functional annotation, and visualization of kinase-substrate networks.

T-cell Activation and Proliferation Assays

Human peripheral T cells were isolated from buffy coats of healthy donors obtained from the Immunochemotherapy Department of Centro Hospitalar São João (CHSJ), Porto, Portugal. All procedures were conducted with informed consent and approved by the institutional ethics committee (Protocol reference 260/11). T cells were enriched using the RosetteSep™ Human T Cell Enrichment Cocktail (StemCell Technologies), following the manufacturer's protocol. Briefly, buffy coats were centrifuged at 1200 × g for 30 minutes at room temperature (acceleration 5, no brake) to isolate peripheral blood mononuclear cells (PBMCs). PBMCs were incubated with RosetteSep reagent, diluted 1:1 in PBS containing 2% fetal bovine serum (FBS), and layered over Histopaque-1077 (Sigma-Aldrich) for density gradient centrifugation (30 minutes, 1200 × g, RT, no acceleration or brake). The T cell–enriched layer was collected and washed three times with PBS. Isolated T cells were cultured in RPMI 1640 GlutaMAX™ medium supplemented with 10% FBS, 1% penicillin/streptomycin, and 100 U/mL interleukin-2 (PeproTech, 200-02) and activated for 3 days using plate-bound anti-CD3 and anti-CD28 antibodies (**Table S5**). For proliferation tracking, T cells were labeled with CellTrace™ CFSE dye (Thermo Fisher Scientific). Cells were

resuspended in PBS and incubated with CFSE (1 µL dye in 18 µL anhydrous DMSO) for 20 minutes at 37 °C. Labeling was quenched by adding complete medium, and cells were washed and resuspended for co-culture. Labeled T cells were co-cultured with glycoengineered SW620 cells (with or without *CD276* knockdown) at a tumor-to-T cell ratio of 1:5, in 24-well plates for 5 days at 37 °C and 5% CO_2. At the endpoint, conditioned media were collected for cytokine analysis, and cells were harvested by incubation with cold PBS on ice for 20 minutes. After washing, cells were stained with Fixable Viability Stain 780 for 15 minutes at 4 °C in the dark, followed by surface marker staining for CD3, CD4, CD8, CD25, and CD69 (**Table S5**) for 40 minutes at 4 °C. Flow cytometry analysis was performed on a NAVIOS flow cytometer (Beckman Coulter). Data were analyzed using Kaluza C software (v1.2) to assess viability, activation marker expression, mean fluorescence intensity (MFI), and the percentage of positive cells across relevant T cell subsets.

Cytokine Evaluation

Conditioned media from CRC cell–T cell co-cultures were collected after 120 hours of direct contact. IL-1β, IL-2, IL-4, IL-5, IL-6, IL-8, IL-10, IL-12(p70), IL-13, IL-17A, IL-23, IFN-γ, TNF-α, and GM-CSF levels were quantified using a Luminex-based human multiplex cytokine assay, outsourced to EVE Technologies, according to their standard protocols.

Tissue-Level Analysis of CD276 and Glycans by IHC

FFPE sections of colorectal tumors and healthy tissues were analyzed by IHC for CD276, Tn, and sTn antigens, as previously described by Peixoto *et al.* [52]. Antibodies, lectins, and detection reagents used are listed in **Table S5**. CD276 and anti-sTn antibodies were detected using the Novolink™ Polymer Detection System (Leica Biosystems) according to the manufacturer's instructions. For Tn antigen detection, biotinylated VVA was used, followed by streptavidin–horseradish peroxidase (HRP) conjugate (Thermo Fisher Scientific, ready-to-use) and chromogenic development with ImmPACT® DAB Peroxidase Substrate (Vector Laboratories, 1:1000 dilution, 5 minutes at room temperature). Negative controls included tissue sections incubated with isotype-matched control antibodies and processed with omission of the primary antibody or lectin to

assess background and non-specific staining. Sialidase digestion (neuraminidase treatment) was performed on selected sections before sTn staining to confirm the specificity of sialylated glycan detection; loss of signal upon treatment validated sialic acid–dependent binding. Positive controls included colorectal tumor tissues previously confirmed to express CD276, Tn, or sTn, as well as *C1GALT1*-knockout CRC cell–derived cells, known to exhibit high levels of exposed GalNAc residues for VVA specificity confirmation. Staining was semi-quantitatively evaluated based on both staining intensity (graded 0–3) and extent of positive staining across the tissue section (0–100%). A composite immunoreactivity score was derived by combining intensity and extension to reflect overall expression levels. All scoring was independently assessed by to trained observers and validated by an experienced pathologist to ensure consistency and biological relevance. All slides were imaged using a Motic BA310E microscope and analyzed with Motic Images Plus 3.0 software (Motic).

Double Staining Immunofluorescence

A subset of FFPE tissue sections previously confirmed to be positive for Tn and CD276 was selected for double immunofluorescence staining to assess the colocalization of both epitopes. Briefly, tissue sections were deparaffinized, rehydrated, and subjected to heat-induced antigen retrieval using 1 mM EDTA buffer (pH 8.0; VWR). Tn antigens were detected using FITC-labeled VVA at a concentration of 40 µg/mL, incubated for 2 h at room temperature. CD276 was detected using an unlabeled rabbit polyclonal anti-CD276 antibody (Thermo Fisher Scientific; 1:250, 1 h at room temperature), followed by an Alexa Fluor 594–conjugated anti-rabbit secondary antibody (30 min at room temperature, in the dark). Controls were consistent with those used for immunohistochemistry, including isotype-matched antibodies, omission of primary reagents. Additionally, single-staining controls were included to exclude bleed-through or spectral overlap between fluorescence channels and to ensure specific signal attribution for each target. Fluorescence images were acquired using a Leica DMI6000 FFW microscope and analyzed with LAS X software (Leica Microsystems).

Proximity Ligation Assay

The PLA was used to detect instances of close spatial proximity (<30 nm) between CD276 and sTn antigens in colorectal tumor and healthy tissue sections. FFPE tissues previously demonstrating co-localization of CD276 and sTn by immunohistochemistry, including normal colon samples, were selected for analysis. Tissue sections were deparaffinized, rehydrated, and subjected to antigen retrieval in boiling 1 mM EDTA buffer (pH 8.0; VWR) for 20 minutes. Non-specific binding was blocked using Blocking Solution (Sigma-Aldrich) for 1 hour at 37 °C. Primary antibodies against CD276 and sTn (anti-TAG-72) were applied and incubated overnight at 4 °C under the same conditions used for immunohistochemistry. PLA signal ligation and rolling circle amplification were performed using the Duolink® In Situ PLA kit (Sigma-Aldrich) according to the manufacturer's instructions. Sections were then counterstained with DAPI and mounted using an aqueous mounting medium (Bio-Optica). To confirm signal specificity and exclude background noise, multiple controls were included. Tissue sections lacking expression of either CD276 or sTn, as determined by prior immunohistochemistry, were processed in parallel as negative controls. Additional negative controls included sections incubated with only one of the primary antibodies or with both primary antibodies omitted, to assess potential non-specific amplification or probe cross-reactivity. Furthermore, selected sections were pre-treated with α-neuraminidase (sialidase) prior to PLA staining to enzymatically remove sialic acids and confirm the sialylation dependence of the STn signal. Positive controls consisted of colorectal tumor tissues previously validated for co-expression and spatial proximity of CD276 and sTn antigens by immunohistochemistry and immunofluorescence. Fluorescence images were acquired on a Leica DMI6000 FFW microscope and analyzed using LAS X software (Leica Microsystems).

Statistical analysis

All statistical analyses were performed using GraphPad Prism (Dotmatics), SPSS for MacOS (version 27; IBM), and R software (version 4.2.1; R Foundation for Statistical Computing). For *in vitro* and *ex vivo* experiments, including glycogenes and *CD276* gene expression (RT-qPCR), cell invasion and proliferation assays, cytokine production, T-cell proliferation, and immune phenotype characterization, statistical comparisons were conducted using one-way ANOVA followed by

Tukey's post hoc multiple comparisons test. Data normality was assessed using the Shapiro–Wilk test, and when variables deviated from normality, non-parametric alternatives such as the Wilcoxon rank-sum test were applied. Chi-square tests were used to evaluate associations between categorical variables such as tumor stage, anatomical location, CD276 status, and CD276–Tn/sTn expression. Differences in CD276 expression and staining extent between metastatic and non-metastatic samples were assessed using a non-parametric t-test (Mann–Whitney U test). For TCGA-based transcriptomic analyses, including comparisons between epithelial-like and mesenchymal-like CRC subtypes, Wilcoxon rank-sum tests were used to evaluate differences in CD276 and CD276–Tn/STn expression levels. Spearman's rank correlation was used to assess associations between gene expression levels, and correlation matrices were visualized using the "corrplot" R package. To explore the prognostic value of CD276 and glycosyltransferase gene expression, univariate and multivariate Cox proportional hazards regression models were performed. Kaplan–Meier survival curves were generated for overall survival (OS) and progression-free survival (PFS), and differences between survival groups were tested using the log-rank test, as implemented in the "survival" and "survminer" R packages. Optimal expression cut-offs for survival stratification were identified using the surv_cutpoint() function. Unless otherwise stated, statistical significance was considered at $p < 0.05$.

Acknowledgments

The authors wish to acknowledge the Portuguese Foundation for Science and Technology (FCT) for PhD grants SFRH/BD/142479/2018 (JS), 2020.09384.BD (DF); 2022.12980.BD (AM), SFRH/BD/146500/2019 (MRS), 2020.09394.BD (SC), 2020.08708.BD (RF), Eduardo Ferreira (2024.04043.BDANA), Beatriz Santos (2024.00895.BD), Principal researcher contract 2022.08311.CEECIND (JAF), and junior researcher contacts 2021.03835.CEECIND (AB), 2023.06366.CEECIND/CP2864/CT0001 (AP). FCT is co-financed by European Social Fund under Human Potential Operation Programme from National Strategic Reference Framework. The authors also acknowledge funding from the IPO-Porto research center (PEst-OE/SAU/UI0776/201, CI-IPOP-29-2016-2022,

CI-IPOP-58-2016-2022), for CQUM (UID/QUI/00686/2020), and the LAQV research unit (UIDB/50006/2020 | UIDP/50006/2020). This article is also a result of the project NORTE-01-0145-FEDER-000012 and “The Porto Comprehensive Cancer Center Raquel Seruca” with the reference NORTE-01-0145-FEDER-072678 - Consórcio PORTO.CCC—Porto.Comprehensive Cancer Center Raquel Seruca, supported by NORTE 2020, under the PORTUGAL 2020 Partnership Agreement, through the European Regional Development Fund. This work was also financed by FEDER through the COMPETE 2020 - Operational Programme for Competitiveness and Internationalisation (POCI-01-0145-FEDER-007274 for i3S unit). Finally, the authors also acknowledge the ICBAS PhD Program in Biomedical Sciences.

Data Availability Statement

All data generated or analyzed during this study are included in this published article and its supplementary information files.

The datasets generated during and/or analyzed during the current study are available in the [NAME] repository, [PERSISTENT WEB LINK TO DATASETS].

Abbreviations: ATCC: American Type Culture Collection; CHSJ: Centro Hospitalar São João; CMS: Consensus Molecular Subtypes; CORA: Cellular O-Glycome Reporter/Amplification; CRC: Colorectal Cancer; dsT: Disialyl-T; DTT: Dithiothreitol; EMT: Epithelial-Mesenchymal Transition; FBS: Fetal Bovine Serum; FC: Flow Cytometry; FDR: False Discovery Rate; FFPE: Formalin-Fixed Paraffin-Embedded; FMO: Fluorescence Minus One; HCD: Higher-energy Collisional Dissociation; HR: Hazard Ration; ICIs: Immune Checkpoint Inhibitors; IDAA: Indel Detection by Amplicon Analysis; IF: Immunofluorescence; IgC: Immunoglobulin Constant Domain; IgV: Immunoglobulin Variable Domain; IHC: Immunohistochemistry; IP: Immunoprecipitation; IPOPorto: Portuguese Institute of Oncology of Porto; KO: Knockout; KSEA: Kinase-Substrate Enrichment Analysis; MFI: Mean Fluorescence Intensity; MS: Mass Spectrometry; MSI: Microsatellite Instability; MSS: Microsatellite Stability; Neu: Neuraminidase; NSAF: Normalized Spectral Abundance Factor; OS: Overall Survival; PBMCs: Peripheral Blood Mononuclear Cells; PCA: Principal Component Analysis; PFS: Progression-free Survival; PLA: Proximity Ligation Assay; PNA: Peanut

agglutinin; ppGalNAc-Ts: Polypeptide N-acetylgalactosamine Transferases; PRIDE: PRoteomics IDEntifications Database; RNA-seq: RNA Sequencing; RT-qPCR: Quantitative Reverse Transcription Polymerase Chain Reaction; siRNAs: Short Interfering RNA or Silencing RNA; sLe: Sialyl Lewis; SSC-A: Side Scatter Area; sT: Sialyl-T; ST3Gal-Ts: α2,3-sialyltransferases; sTn: Sialyl Tn; TCGA: The Cancer Genome Atlas; TMB: Tumour Mutational Burden; VVA: Vicia Villosa Lectin; WB: Western Blot; WT: Wild Type; α3-Fut-Ts: α3-fucosyltransferases.

References

[1] H. Sung, J. Ferlay, R. L. Siegel, M. Laversanne, I. Soerjomataram, A. Jemal, F. Bray, *CA Cancer J Clin* **2021**, *71*(3), 209, https://doi.org/10.3322/caac.21660.

[2] Y. Li, Y. Ma, Z. Wu, F. Zeng, B. Song, Y. Zhang, J. Li, S. Lui, M. Wu, *Frontiers in Immunology* **2021**, *Volume 12 - 2021*, https://doi.org/10.3389/fimmu.2021.751407.

[3] C. W. Kim, H. J. Chon, C. Kim, *Cancers* **2021**, *13*(19), 4906.

[4] a) W.-T. Zhou, W.-L. Jin, *Frontiers in Immunology* **2021**, *Volume 12 - 2021*, https://doi.org/10.3389/fimmu.2021.701006; b) A. A. Getu, A. Tigabu, M. Zhou, J. Lu, O. Fodstad, M. Tan, *Mol Cancer* **2023**, *22* (1), 43, https://doi.org/10.1186/s12943-023-01751-9.

[5] a) J. R. Castellanos, I. J. Purvis, C. M. Labak, M. R. Guda, A. J. Tsung, K. K. Velpula, S. Asuthkar, *Am J Clin Exp Immunol* **2017**, *6* (4), 66; b) K. A. Hofmeyer, A. Ray, X. Zang, *Proc Natl Acad Sci U S A* **2008**, *105*(30), 10277, https://doi.org/10.1073/pnas.0805458105.

[6] P. Zhang, S. Yu, H. Li, C. Liu, J. Li, W. Lin, A. Gao, L. Wang, W. Gao, Y. Sun, *FEBS Letters* **2015**, *589*(17), 2248, https://doi.org/https://doi.org/10.1016/j.febslet.2015.06.037.

[7] T. Arigami, N. Narita, R. Mizuno, L. Nguyen, X. Ye, A. Chung, A. E. Giuliano, D. S. Hoon, *Ann Surg* **2010**, *252*(6), 1044, https://doi.org/10.1097/SLA.0b013e3181f1939d.

[8] X. Zang, R. H. Thompson, H. A. Al-Ahmadie, A. M. Serio, V. E. Reuter, J. A. Eastham, P. T. Scardino, P. Sharma, J. P. Allison, *Proceedings of the National Academy of Sciences* **2007**, *104*(49), 19458, https://doi.org/doi:10.1073/pnas.0709802104.

[9] V. A. Ingebrigtsen, K. Boye, C. Tekle, J. M. Nesland, K. Flatmark, O. Fodstad, *Int J Cancer* **2012**, *131* (11), 2528, https://doi.org/10.1002/ijc.27566.

[10] F.-b. Kang, L. Wang, H.-c. Jia, D. Li, H.-j. Li, Y.-g. Zhang, D.-x. Sun, *Cancer Cell International* **2015**, *15* (1), 45, https://doi.org/10.1186/s12935-015-0195-z.

[11] Z.-y. Zhang, J.-h. Xu, J.-l. Zhang, Y.-x. Lin, J. Ou-Yang, *BMC Cancer* **2024**, *24* (1), 650, https://doi.org/10.1186/s12885-024-12402-7.

[12] S. Seaman, Z. Zhu, S. Saha, X. M. Zhang, M. Y. Yang, M. B. Hilton, K. Morris, C. Szot, H. Morris, D. A. Swing, L. Tessarollo, S. W. Smith, S. Degrado, D. Borkin, N. Jain, J. Scheiermann, Y. Feng, Y. Wang, J. Li, D. Welsch, G. DeCrescenzo, A. Chaudhary, E. Zudaire, K. D. Klarmann, J. R. Keller, D. S. Dimitrov, B. St. Croix, *Cancer Cell* **2017**, *31* (4), 501, https://doi.org/10.1016/j.ccell.2017.03.005.

[13] a) Y. Huang, H.-L. Zhang, Z.-L. Li, T. Du, Y.-H. Chen, Y. Wang, H.-H. Ni, K.-M. Zhang, J. Mai, B.-X. Hu, J.-H. Huang, L.-H. Zhou, D. Yang, X.-D. Peng, G.-K. Feng, J. Tang, X.-F. Zhu, R. Deng, *Nature Communications* **2021**, *12* (1), 2672, https://doi.org/10.1038/s41467-021-22618-x; b) C. W. Li, S. O. Lim, E. M. Chung, Y. S. Kim, A. H. Park, J. Yao, J. H. Cha, W. Xia, L. C. Chan, T. Kim, S. S. Chang, H. H. Lee, C. K. Chou, Y. L. Liu, H. C. Yeh, E. P. Perillo, A. K. Dunn, C. W. Kuo, K. H. Khoo, J. L. Hsu, Y. Wu, J. M. Hsu, H. Yamaguchi, T. H. Huang, A. A. Sahin, G. N. Hortobagyi, S. S. Yoo, M. C. Hung, *Cancer Cell* **2018**, *33* (2), 187, https://doi.org/10.1016/j.ccell.2018.01.009.

[14] X. Ren, S. Lin, F. Guan, H. Kang, *Int J Biol Sci* **2024**, *20* (7), 2607, https://doi.org/10.7150/ijbs.93806.

[15] a) H. Tian, J.-L. Yu, X. Chu, Q. Guan, J. Liu, Y. Liu, *Frontiers in Oncology* **2024**, *Volume 14 - 2024*, https://doi.org/10.3389/fonc.2024.1389713; b) S. Holst, M. Wuhrer, Y. Rombouts, *Adv Cancer Res* **2015**, *126*, 203, https://doi.org/10.1016/bs.acr.2014.11.004.

[16] T. Gao, T. Du, X. Hu, X. Dong, L. Li, Y. Wang, J. Liu, L. Liu, T. Gu, T. Wen, *Journal of Cellular and Molecular Medicine* **2020**, *24* (1), 362, https://doi.org/https://doi.org/10.1111/jcmm.14740.

[17] a) R. Mi, L. Song, Y. Wang, X. Ding, J. Zeng, S. Lehoux, R. P. Aryal, J. Wang, V. K. Crew, I. van Die, A. B. Chapman, R. D. Cummings, T. Ju, *J Biol Chem* **2012**, *287* (49), 41523, https://doi.org/10.1074/jbc.M112.371989; b) T. Ju, G. S. Lanneau, T. Gautam, Y. Wang, B. Xia, S. R. Stowell, M. T. Willard, W. Wang, J. Y. Xia, R. E. Zuna, Z. Laszik, D. M. Benbrook, M. H. Hanigan, R. D. Cummings, *Cancer Res* **2008**, *68* (6), 1636, https://doi.org/10.1158/0008-5472.CAN-07-2345.

[18] a) J. Liu, F. Xu, J. Li, H. Jiang, *Biosci Rep* **2020**, *40* (6), https://doi.org/10.1042/bsr20191062; b) Y. Wang, T. Ju, X. Ding, B. Xia, W. Wang, L. Xia, M. He, R. D. Cummings, *Proceedings of the National Academy of Sciences* **2010**, *107* (20), 9228, https://doi.org/doi:10.1073/pnas.0914004107; c) T. Du, X. Jia, X. Dong, X. Ru, L. Li, Y. Wang, J. Liu, G. Feng, T. Wen, *Cancer Manag Res* **2020**, *12*, 511, https://doi.org/10.2147/cmar.S234735.

[19] R. Beatson, G. Maurstad, G. Picco, A. Arulappu, J. Coleman, H. H. Wandell, H. Clausen, U. Mandel, J. Taylor-Papadimitriou, M. Sletmoen, J. M. Burchell, *PLoS One* **2015**, *10* (5), e0125994, https://doi.org/10.1371/journal.pone.0125994.

[20] J. Guinney, R. Dienstmann, X. Wang, A. de Reynies, A. Schlicker, C. Soneson, L. Marisa, P. Roepman, G. Nyamundanda, P. Angelino, B. M. Bot, J. S. Morris, I. M. Simon, S. Gerster, E. Fessler, E. M. F. De Sousa, E. Missiaglia, H. Ramay, D. Barras, K. Homicsko, D. Maru, G. C. Manyam, B. Broom, V. Boige, B. Perez-Villamil, T. Laderas, R. Salazar, J. W. Gray, D. Hanahan, J. Tabernero, R. Bernards, S. H. Friend, P. Laurent-Puig, J. P. Medema, A. Sadanandam, L. Wessels, M. Delorenzi, S. Kopetz, L. Vermeulen, S. Tejpar, *Nat Med* **2015**, *21* (11), 1350, https://doi.org/10.1038/nm.3967.

[21] A. Trinh, K. Trumpi, E. M. F. De Sousa, X. Wang, J. H. de Jong, E. Fessler, P. J. Kuppen, M. S. Reimers, M. Swets, M. Koopman, I. D. Nagtegaal, M. Jansen, G. K. Hooijer, G. J. Offerhaus, O. Kranenburg, C. J. Punt, J. P. Medema, F. Markowetz, L. Vermeulen, *Clin Cancer Res* **2017**, *23* (2), 387, https://doi.org/10.1158/1078-0432.CCR-16-0680.

[22] K. Madunić, O. A. Mayboroda, T. Zhang, J. Weber, G. J. Boons, H. Morreau, R. van Vlierberghe, T. van Wezel, G. S. M. Lageveen-Kammeijer, M. Wuhrer, *Theranostics* **2022**, *12* (10), 4498, https://doi.org/10.7150/thno.72818.

[23] a) H. Hong, E. N. Benveniste, *Biomedicines* **2021**, *9* (12), https://doi.org/10.3390/biomedicines9121932; b) R. N. Bhattacharjee, G. C. Banks, K. W. Trotter, H. L. Lee, T. K. Archer, *Mol Cell Biol* **2001**, *21* (16), 5417, https://doi.org/10.1128/mcb.21.16.5417-5425.2001; c) M. Fazil, P. Prasannan, B. H. S. Wong, A. Kottaiswamy, N. Salim, S. K. Sze, N. K. Verma, *Front Immunol* **2021**, *12*, 680071, https://doi.org/10.3389/fimmu.2021.680071.

[24] S. W. Strum, L. Gyenis, D. W. Litchfield, *British Journal of Cancer* **2022**, *126* (7), 994, https://doi.org/10.1038/s41416-021-01616-2.

[25] D. H. Larsen, C. Poinsignon, T. Gudjonsson, C. Dinant, M. R. Payne, F. J. Hari, J. M. Rendtlew Danielsen, P. Menard, J. C. Sand, M. Stucki, C. Lukas, J. Bartek, J. S. Andersen, J. Lukas, *J Cell Biol* **2010**, *190* (5), 731, https://doi.org/10.1083/jcb.200912135.

[26] S. Bahl, E. Seto, *Cell Mol Life Sci* **2021**, *78* (2), 427, https://doi.org/10.1007/s00018-020-03599-4.

[27] R. A. Wang, *Cancer Metastasis Rev* **2014**, *33* (4), 1001, https://doi.org/10.1007/s10555-014-9525-1.

[28] a) A. G. Ammer, S. A. Weed, *Cell Motil Cytoskeleton* **2008**, *65* (9), 687, https://doi.org/10.1002/cm.20296; b) Y. Wang, Q. Yang, Y. Cheng, M. Gao, L. Kuang, C. Wang, *Med Sci Monit* **2018**, *24*, 9110, https://doi.org/10.12659/msm.911523; c) Q. Zeng, T. Jiang, J. Wang, *Oncol Rep* **2024**, *52* (3), https://doi.org/10.3892/or.2024.8776.

[29] a) P. Indovina, F. Pentimalli, N. Casini, I. Vocca, A. Giordano, *Oncotarget* **2015**, *6* (20), 17873, https://doi.org/10.18632/oncotarget.4286; b) R. Wisdom, R. S. Johnson, C. Moore, *Embo j* **1999**, *18* (1), 188, https://doi.org/10.1093/emboj/18.1.188.

[30] C. Alfaro, A. Teijeira, C. Oñate, G. Pérez, M. F. Sanmamed, M. P. Andueza, D. Alignani, S. Labiano, A. Azpilikueta, A. Rodriguez-Paulete, S. Garasa, J. P. Fusco, A. Aznar, S. Inogés, M. De Pizzol, M. Allegretti, J. Medina-Echeverz, P. Berraondo, J. L. Perez-Gracia, I. Melero, *Clinical Cancer Research* **2016**, *22* (15), 3924, https://doi.org/10.1158/1078-0432.Ccr-15-2463.

[31] A. Joss, M. Akdis, A. Faith, K. Blaser, C. A. Akdis, *European Journal of Immunology* **2000**, *30* (6), 1683, https://doi.org/https://doi.org/10.1002/1521-4141(200006)30:6<1683::AID-IMMU1683>3.0.CO;2-A.

[32] D. Jorgovanovic, M. Song, L. Wang, Y. Zhang, *Biomarker Research* **2020**, *8* (1), 49, https://doi.org/10.1186/s40364-020-00228-x.

[33] K. Sakuishi, L. Apetoh, J. M. Sullivan, B. R. Blazar, V. K. Kuchroo, A. C. Anderson, *Journal of Experimental Medicine* **2010**, *207* (10), 2187, https://doi.org/10.1084/jem.20100643.

[34] a) M. Kotsias, K. Madunic, S. Nicolardi, R. P. Kozak, R. A. Gardner, B. C. Jansen, D. I. R. Spencer, M. Wuhrer, *Glycoconj J* **2021**, *38* (6), 747, https://doi.org/10.1007/s10719-021-10003-1; b) K. Madunić, T. Zhang, O. A. Mayboroda, S. Holst, K. Stavenhagen, C. Jin, N. G. Karlsson, G. S. M. Lageveen-Kammeijer, M. Wuhrer, *Cell Mol Life Sci* **2021**, *78* (1), 337, https://doi.org/10.1007/s00018-020-03504-z.

[35] P. Radhakrishnan, S. Dabelsteen, F. B. Madsen, C. Francavilla, K. L. Kopp, C. Steentoft, S. Y. Vakhrushev, J. V. Olsen, L. Hansen, E. P. Bennett, A. Woetmann, G. Yin, L. Chen, H. Song, M. Bak, R. A. Hlady, S. L. Peters, R. Opavsky, C. Thode, K. Qvortrup, K. T. Schjoldager, H. Clausen, M. A. Hollingsworth, H. H. Wandall, *Proc Natl Acad Sci U S A* **2014**, *111* (39), E4066, https://doi.org/10.1073/pnas.1406619111.

[36] C. A. St Hill, *Front Biosci (Landmark Ed)* **2011**, *16* (9), 3233, https://doi.org/10.2741/3909.

[37] X. Sun, T. Ju, R. D. Cummings, *BMC Cancer* **2018**, *18* (1), 827, https://doi.org/10.1186/s12885-018-4708-8.

[38] F. Erger, R. P. Aryal, B. Reusch, Y. Matsumoto, R. Meyer, J. Zeng, C. Knopp, M. Noel, L. Muerner, A. Wenzel, S. Kohl, N. Tschernoster, G. Rappl, I. Rouvet, J. Schröder-Braunstein, F. S. Seibert, H. Thiele, M. G. Häusler, L. T. Weber, M. Büttner-Herold, M. Elbracht, S. F. Cummings, J. Altmüller, S. Habbig, R. D. Cummings, B. B. Beck, *Proceedings of the National Academy of Sciences* **2023**, *120* (22), e2211087120, https://doi.org/doi:10.1073/pnas.2211087120.

[39] T. Xiang, M. Qiao, J. Xie, Z. Li, H. Xie, *Biomolecules* **2022**, *12* (12), https://doi.org/10.3390/biom12121732.

[40] L. Ni, C. Dong, *Molecular Cancer Therapeutics* **2017**, *16* (7), 1203, https://doi.org/10.1158/1535-7163.Mct-16-0761.

[41] a) A. Peixoto, D. Ferreira, A. Miranda, M. Relvas-Santos, R. Freitas, T. S. Veth, A. Brandão, E. Ferreira, P. Paulo, M. Cardoso, C. Gaiteiro, S. Cotton, J. Soares, L. Lima, F. Teixeira, R. Ferreira, C. Palmeira, A. J. R. Heck, M. J. Oliveira, A. M. N. Silva, L. L. Santos, J. A. Ferreira, *iScience* **2025**, *28* (2), 111758, https://doi.org/10.1016/j.isci.2025.111758; b) Y.-X. Xu, L. Liu, C. E. Caffaro, C. B. Hirschberg, *Journal of Biological Chemistry* **2010**, *285* (32), 24600, https://doi.org/10.1074/jbc.M110.134544.

[42] a) I. Han, J. E. Kudlow, *Mol Cell Biol* **1997**, *17* (5), 2550, https://doi.org/10.1128/mcb.17.5.2550; b) Y. Fu, L. Ning, J. Feng, X. Yu, F. Guan, X. Li, *Cellular Signalling* **2022**, *93*, 110277, https://doi.org/https://doi.org/10.1016/j.cellsig.2022.110277.

[43] a) Z. Liu, K. Ajit, Y. Wu, W.-G. Zhu, M. Gullerova, *The EMBO Journal* **2024**, *43* (12), 2453, https://doi.org/https://doi.org/10.1038/s44318-024-00111-7; b) M. Sharifi Tabar, C. Giardina, Y. Feng, H. Francis, H. Moghaddas Sani, J. K. K. Low, J. P. Mackay, C. G. Bailey, J. E. J. Rasko, *The FEBS Journal* **2022**, *289* (1), 199, https://doi.org/https://doi.org/10.1111/febs.16112.

[44] a) K. Fousek, L. A. Horn, C. Palena, *Pharmacol Ther* **2021**, *219*, 107692, https://doi.org/10.1016/j.pharmthera.2020.107692; b) B. M. Carreno, M. Becker-Hapak, A. Huang, M. Chan, A. Alyasiry, W. R. Lie, R. L. Aft, L. A. Cornelius, K. M. Trinkaus, G. P. Linette, *J Clin Invest* **2013**, *123* (8), 3383, https://doi.org/10.1172/jci68395.

[45] B. Zhang, J. Wang, X. Wang, J. Zhu, Q. Liu, Z. Shi, M. C. Chambers, L. J. Zimmerman, K. F. Shaddox, S. Kim, S. R. Davies, S. Wang, P. Wang, C. R. Kinsinger, R. C. Rivers, H. Rodriguez, R. R. Townsend, M. J. Ellis, S. A. Carr, D. L. Tabb, R. J. Coffey, R. J. Slebos, D. C. Liebler, C. Nci, *Nature* **2014**, *513* (7518), 382, https://doi.org/10.1038/nature13438.

[46] R. Team, **2023**.

[47] B. J. Wickham H AM, Chang W, McGowan LD, François R, Grolemund G, Hayes A, Henry L, Hester J,, Kuhn M PT, Miller E, Bache SM, Müller K, Ooms J, Robinson D, Seidel DP, Spinu V, Takahashi K,, Vaughan D WC, Woo K, Yutani H. , *Journal of Open Source Software* **2019**.

[48] K. A, **2023**.

[49] C. Gaiteiro, J. Soares, M. Relvas-Santos, A. Peixoto, D. Ferreira, P. Paulo, A. Brandao, E. Fernandes, R. Azevedo, C. Palmeira, R. Freitas, A. Miranda, H. Osorio, J. Prieto, L. Lima, A. M. N. Silva, L. L. Santos, J. A. Ferreira, *Theranostics* **2022**, *12* (7), 3150, https://doi.org/10.7150/thno.67409.

[50] L. Lima, C. Gaiteiro, A. Peixoto, J. Soares, M. Neves, L. L. Santos, J. A. Ferreira, *PLoS One* **2016**, *11* (11), e0166120, https://doi.org/10.1371/journal.pone.0166120.

[51] E. Fernandes, R. Freitas, D. Ferreira, J. Soares, R. Azevedo, C. Gaiteiro, A. Peixoto, S. Oliveira, S. Cotton, M. Relvas-Santos, L. P. Afonso, C. Palmeira, M. J. Oliveira, R. Ferreira, A. M. N. Silva, L. Lara Santos, J. A. Ferreira, *Cancers (Basel)* **2020**, *12* (4), https://doi.org/10.3390/cancers12040861.

[52] A. Peixoto, D. Ferreira, R. Azevedo, R. Freitas, E. Fernandes, M. Relvas-Santos, C. Gaiteiro, J. Soares, S. Cotton, B. Teixeira, P. Paulo, L. Lima, C. Palmeira, G. Martins, M. J. Oliveira, A. M. N. Silva, L. L. Santos, J. A. Ferreira, *J Exp Clin Cancer Res* **2021**, *40* (1), 191, https://doi.org/10.1186/s13046-021-01988-6.

[53] M. R. Kudelka, A. Antonopoulos, Y. Wang, D. M. Duong, X. Song, N. T. Seyfried, A. Dell, S. M. Haslam, R. D. Cummings, T. Ju, *Nat Methods* **2016**, *13* (1), 81, https://doi.org/10.1038/nmeth.3675.

Author Contributions

Conceptualization: JAF; Methodology: JS, DF, MG, AM, MRS, AB, PP, CP, FA, AP, LLS, JAF; Software: JS, MRS, AB, AMNS, JAF; Validation: JS, DF, MG, AM, MRS, AB, PP, LPA, AMNS, CP, FA, AP, LLS, JAF; Investigation: JS, DF, MG, AM, MRS, AB, PP, SC, RF, MM, EF, BS, JAF; Resources: JS, DF, AM, MRS, AB, LPA, AMNS, CP, FA, AP, LLS, JAF; Data Curation: JS, DF, MG, AM, MRS,

AB, SC, LPA, AMNS, CP, FA, AP, LLS, JAF; Writing- Original Draft: JAF; Writing-Review & Editing: all authors; Visualization: JS, DF, MG, AM, MRS, AB, JAF; Supervision: JAF; Project Administration: JAF; Funding Acquisition: AP, LLS and JAF.

Competing interests

JAF is the founder and CEO of GlycoMatters Biotech. LLS is also one of the founders of the company.

Supporting Information

CD276 Immature Glycosylation Drives Colorectal Cancer Aggressiveness and T-cell Mediated Immune Escape

Janine Soares[1,2,3], Dylan Ferreira[1,2], Martina Gonçalves[1], Andreia Miranda[1,2,4], Marta Relvas-Santos[1,2,4,5], Andreia Brandão[1], Paula Paulo[1], Sofia Cotton[1], Rui Freitas[1,2,4], Mariana Magalhães[1,6], Eduardo Ferreira[1,2,4], Beatriz Santos[1,2], Luís Pedro Afonso[7], André M N Silva[2,5], Carlos Palmeira[1,8,9], Francisco Amado[3], Andreia Peixoto[1,4], Lúcio Lara Santos[1,2,9,10], José Alexandre Ferreira[1,2]

[1]Research Center of IPO-Porto (CI-IPOP) / RISE@CI-IPOP (Health Research Network), Portuguese Oncology Institute of Porto (IPO-Porto) / Porto Comprehensive Cancer Center (P.ccc) Raquel Seruca, Porto, Portugal; [2]School of Medicine and Biomedical Sciences (ICBAS), University of Porto, Porto, Portugal; [3]LAQV-REQUIMTE & Department of Chemistry, University of Aveiro, Campus Universitário de Santiago, Aveiro, Portugal; [4]i3S – Instituto de Investigação e Inovação em Saúde, Universidade do Porto, Porto, Portugal; [5]LAQV-REQUIMTE, Department of Chemistry and Biochemistry, Faculty of Sciences, University of Porto, Porto, Portugal; [6]MSc Biochemistry in Health, Biomolecules na Chemical Sciences, ESS, Polytechnic of Porto, R. Dr. António Bernardino de Almeida, 400, 4200 - 072, Porto, Portugal; [7]Pathology Department, Portuguese Oncology Institute of Porto, Porto, Portugal;

[8]Immunology Department, Portuguese Oncology Institute of Porto, Porto, Portugal; [9]School of Medicine and Biomedical Sciences of University Fernando Pessoa, Porto, Portugal; [10]Department of Surgical Oncology, Portuguese Oncology Institute of Porto, Porto, Portugal.

Corresponding author:

José Alexandre Ferreira

Experimental Pathology and Therapeutics Group,

Research Centre, Portuguese Oncology Institute of Porto,

R. Dr. António Bernardino de Almeida 4200-072 Porto,

Portugal; Tel. +351 225084000 (ext. 5111).

Email: jose.a.ferreira@ipoporto.min-saude.pt.

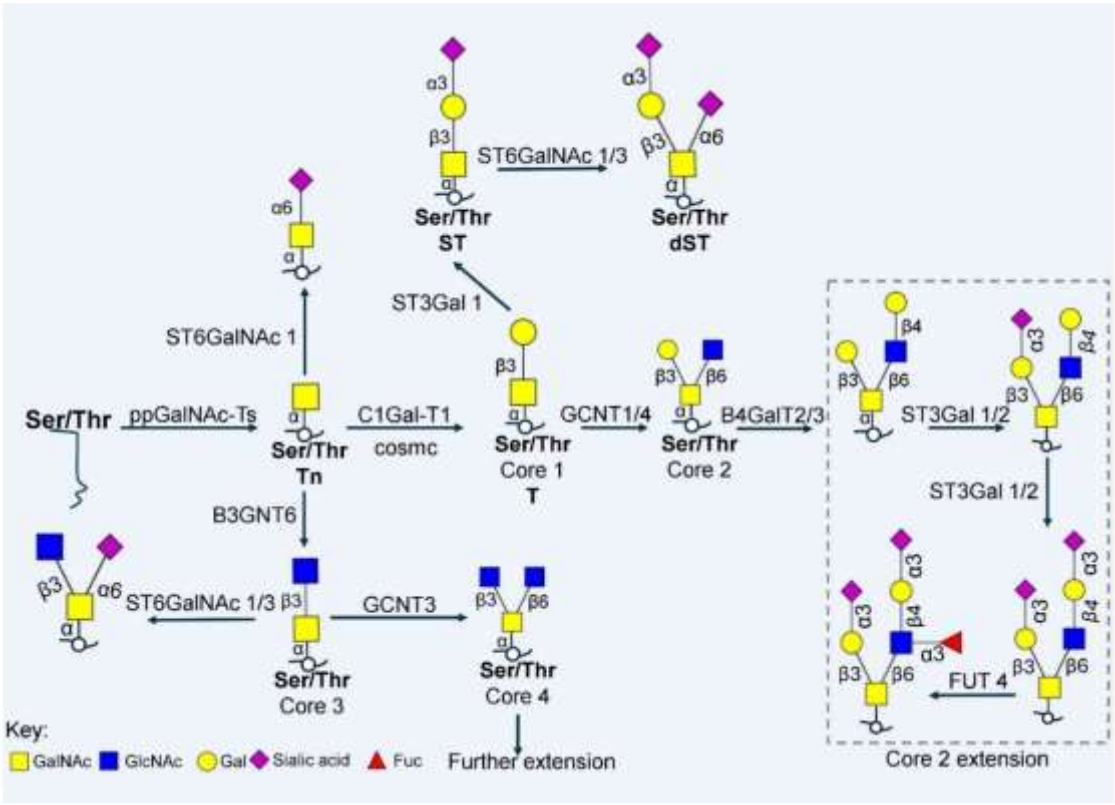

Figure S1. Schematic representation of *O*-glycans biosynthesis. The addition of a GalNAc to a Ser or Thr on a growing peptide chain is prompted by the action of polypeptide N-acetylgalactosamine transferases (ppGalNAc-Ts; a family of 20 enzymes), generating the Tn antigen, which can be extended by the action of C1GalT1 and its chaperone cosmc, forming the Thomsen-Friedenreich or T antigen (core 1). Alternatively, Tn can be sialylated by α2,6-sialyltransferases

(ST6Gal-Ts; a family of 6 enzymes – ST6GalNAc 1, ST6GalNAc 2, ST6GalNAc 3, ST6GalNAc 4, ST6GalNAc 5, ST6GalNAc 6), forming the sialyl-Tn (sTn) and stopping O-glycan extension. Alternatively, Tn can be extended by B3GNT6, forming core 3, which can be further extended into core 4 by GCNT3 or sialyled by ST6GalNAc 1/3. Additionally, T antigen can be sialylated by α2,3-sialyltransferases (ST3Gal-Ts; a family of 6 enzymes - ST3Gal 1, ST3Gal 2, ST3Gal 3, ST3Gal 4, ST3Gal 5, ST3Gal 6), forming the sialyl-T, and further sialylated by ST6GalNAc 1/3, generating di-sialyl-T. T antigen can also be elongated by the action of GCNT1/4, forming core 2. Finally, core 2 can be further extended into complex structures, such as sialyl lewis epitopes, by the action of ST3Gal-Ts and α3-fucosyltransferases (α3-Fut-Ts, a family of 6 enzymes – FUT 3, FUT 4, FUT 5, FUT 6, FUT 7, FUT 9).

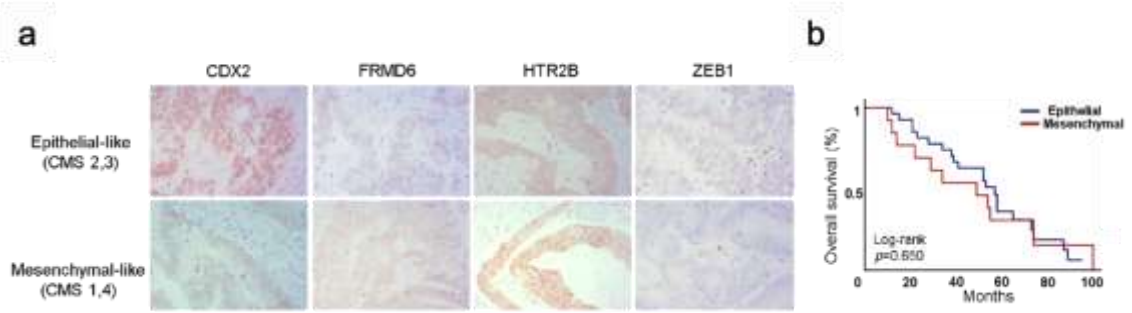

Figure S2. Colorectal cancer differentiation state does not influence prognosis. A. Molecular characterisation of CRC tumours into two differentiation states. Immunohistochemical analysis categorised CRC tumours into Epithelial-like tumours characterised by high expression of CDX2 and low levels of FRMD6 and HTR2B, while mesenchymal-like tumours show low expression of CDX2 and high expression of FRMD6 and HTR2B. ZEB1 is poorly expressed in both subtypes. **B CRC overall survival based on differentiation states.** The Kaplan-Meier analysis does not show a significant association of differentiation states with overall survival.

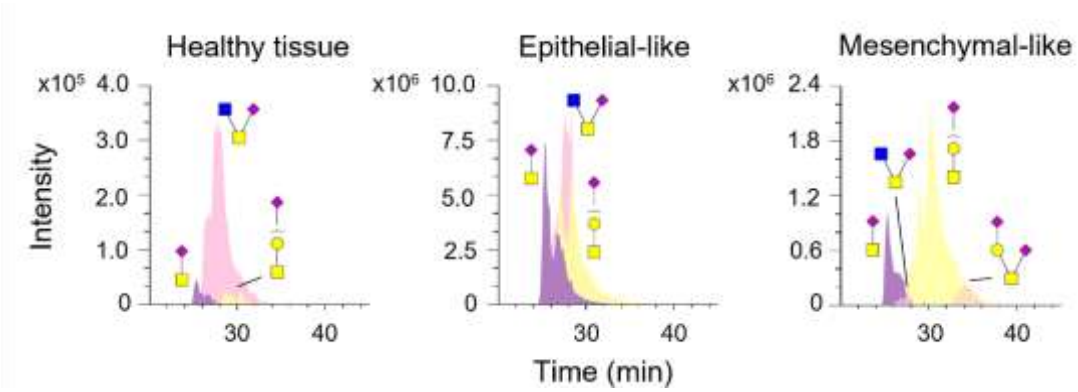

Figure S3. *O*-glycan abundances change between healthy mucosa and colorectal tumours. Healthy tissues are predominantly characterised by a high abundance of sialyl-core 3, while also presenting sTn and (sialyl-)T antigens. Meanwhile, epithelial-like tumours present a higher abundance sTn and (sialyl-)T antigen compared to healthy tissues, although still presenting sialyl-core 3 structures. Finally, mesenchymal-like tumours are mainly characterised by mono- or di-sialylated core 1 structures, while presenting lower sTn and sialylated core-3, compared to epithelial-like tumours and healthy tissues.

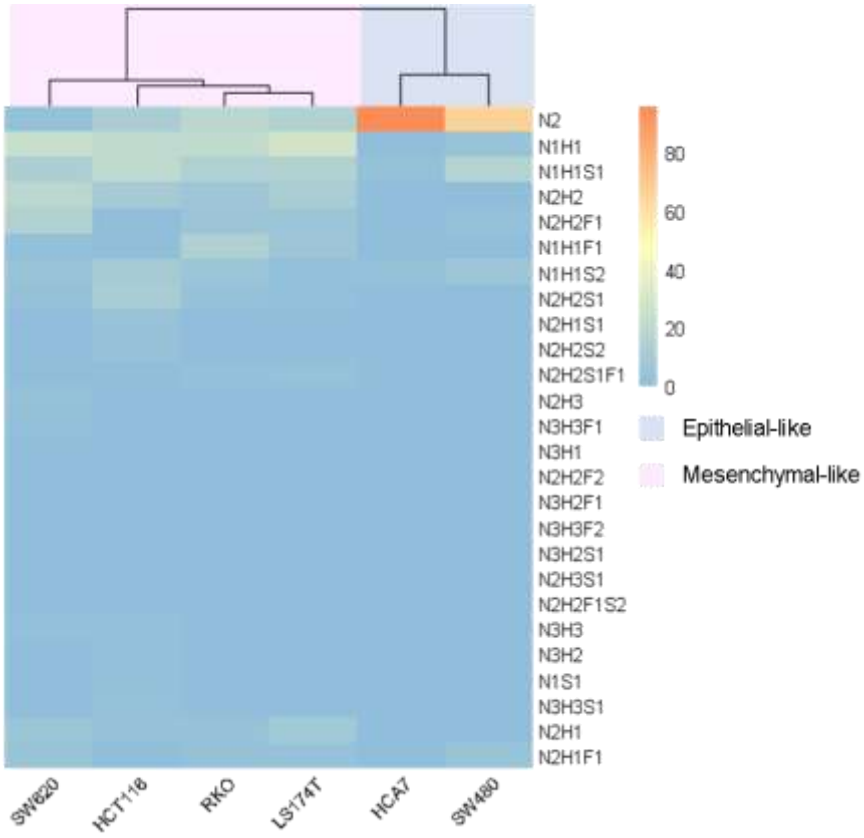

Figure S4. Glycome profiling of colorectal cancer cell lines. Colorectal cancer cell lines mainly show simple short *O*-glycosylation, exhibiting similarities with CRC tumours. According to colorectal tumours similarities, cell lines were clustered into two differentiation states commonly defining CRC, namely epithelial-like and mesenchymal-like phenotypes. HCA7 and SW480 cell lines presented high abundances of core 3 structures, while SW620, HCT116, RKO, and LS174T were mainly characterised by core 1, mono-sialylated core 1and elongated core 2 extensions. Accordingly, HCA7 and SW480 cell lines are epithelial-like, while SW620, HCT116, RKO, and LS174T are more mesenchymal-like cells.

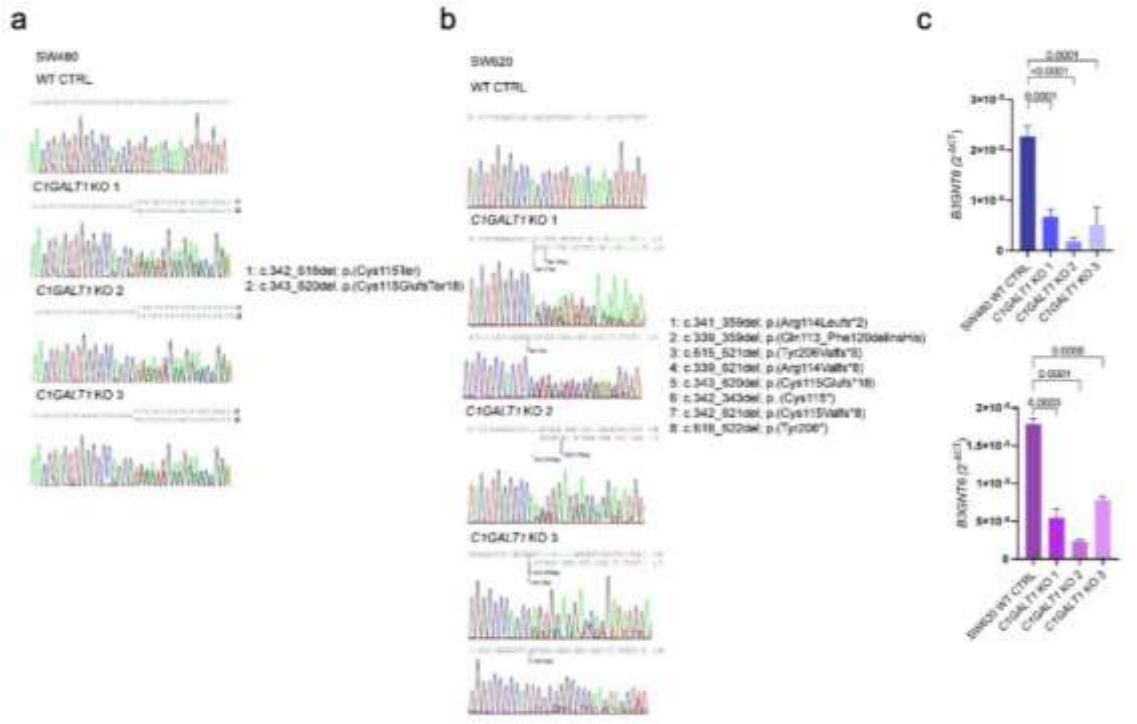

Figure S5. SW480 and SW620 colorectal cancer cell lines were successfully knocked out for the *C1GALT1* gene, subsequently downregulating *B3GNT6*. **A. Sanger sequencing of SW480 *C1GALT1* knockout clones.** Cancer cell line models resembling glycosyltransferases phenotype associated with worse prognosis were generated by Crispr/Cas9 technology. Sanger sequencing showed that SW480 *C1GALT1* KO clones are characterized by two different DNA sequences, with the following observed variants and predicted consequences: 1: c.342_618del; p.(Cys115Ter), leading to a 277bp deletion and introduction of a stop codon at Cys 115; 2: c.343_620del; p.(Cys115Glufs*18), leading to a 278bp deletion and replacement of Cys 115 by Glu, resulting in a frameshift introducing a stop codon 18 a.a ahead. **B. Sanger sequencing of SW620 *C1GALT1* knockout clones.** Sanger sequencing showed that SW620 *C1GALT1* KO clone 1 is characterized by three different DNA sequences, with the following observed variants and predicted consequences: 1: c.341_359del; p.(Arg114Leufs*2), leading to a 21bp deletion and the replacement of Arg 114 by Leu, resulting in a frameshift introducing a stop codon 2 a.a ahead; 2: c.339_359del; p.(Gln113_Phe120delinsHis), leading to a 19bp deletion and replacement of Gln 113 by Phe 120 and insertion of His; 3: c.615_621del; p.(Tyr206Valfs*8), leading to a 7bp deletion and the replacement of Tyr 206 by Val, resulting in a frameshift introducing a stop codon 8 a.a ahead. SW620 *C1GALT1* KO clone 2 is

characterized by two different DNA sequences, with the following observed variants and predicted consequences: 4: c.339_621del; p.(Arg114Valfs*8), leading to a 283bp deletion and the replacement of Arg 114 by Val, resulting in a frameshift introducing a stop codon 8 a.a ahead; 5: c.343_620del; p.(Cys115Glufs*18), leading to a 278bp deletion and replacement of Cys 115 by Glu, resulting in a frameshift introducing a stop codon 18 a.a ahead SW620 *C1GALT1* KO clone 3 is characterized by three different DNA sequences, with the following observed variants and predicted consequences: 6: c.342_343del; p. (Cys115*), leading to a 2bp deletion and introducing a stop codon at Cys 115; 7: c.342_621del; p.(Cys115Valfs*8), leading to a280bp deletion and the replacement of of Cys 115 by Val, resulting in a frameshift introducing a stop codon 8 a.a ahead; 8: c.618_622del; p.(Tyr206*), leading to a 5bp deletion and introducing a stop codon at Tyr 206. **C. B3GNT6 gene expression evaluation in SW480 and SW620 C1GALT1 KO cell models.** B3GNT6 gene expression was significantly decreased in C1GALT1 KO clones for both cell lines when compared to WT controls.

SW480

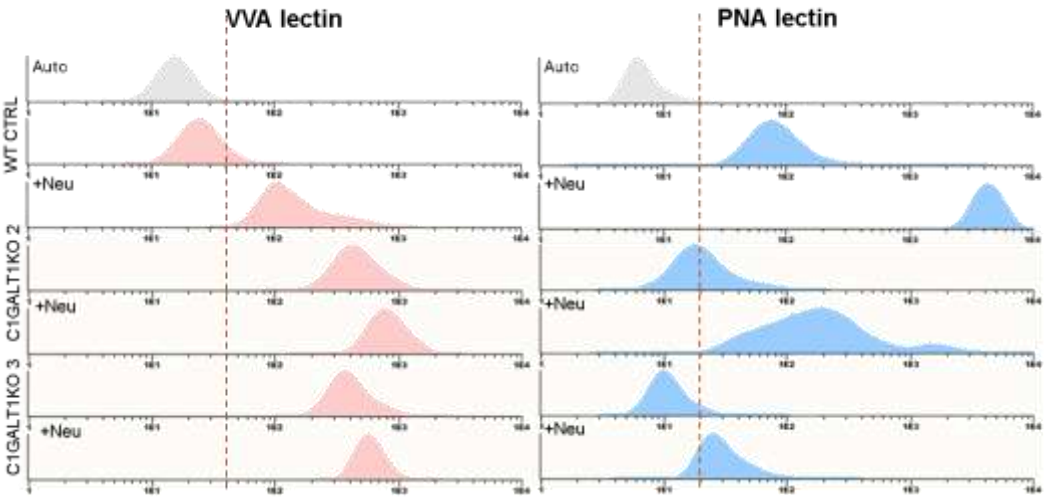
VVA lectin
PNA lectin
Auto
+Neu
WT CTRL
C1GALT1KO 2
C1GALT1KO 3

SW620

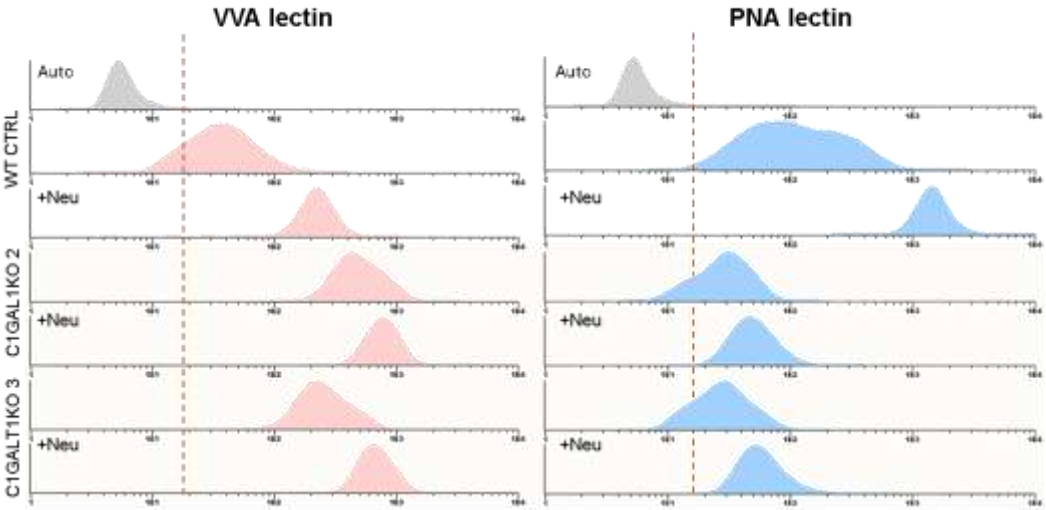
VVA lectin
PNA lectin
Auto
+Neu
WT CTRL
C1GAL1KO 2
C1GALT1KO 3

Figure S6. Flow cytometry analysis of glycoengineered C1GALT1 KO SW480 and SW620 cell lines. Flow cytometry using VVA lectin confirmed the accumulation of the Tn antigen on the cell surface of *C1GALT1* knockout cells (left panels, red), while PNA lectin confirmed the abrogation of O-glycan extension (right panels, blue). To distinguish between sialylated and non-sialylated O-glycans, cells were also treated with neuraminidase (Neu) prior to lectin staining. Neuraminidase treatment enhanced PNA binding, consistent with the presence of sialyl-T antigen (sT) in control cells and its loss in *C1GALT1*-deficient backgrounds. Similarly, VVA binding increased after desialylation, supporting the presence of sTn in the glycoengineered cells. Together, these results confirm the truncation of O-glycans to Tn and sTn structures following *C1GALT1* deletion.

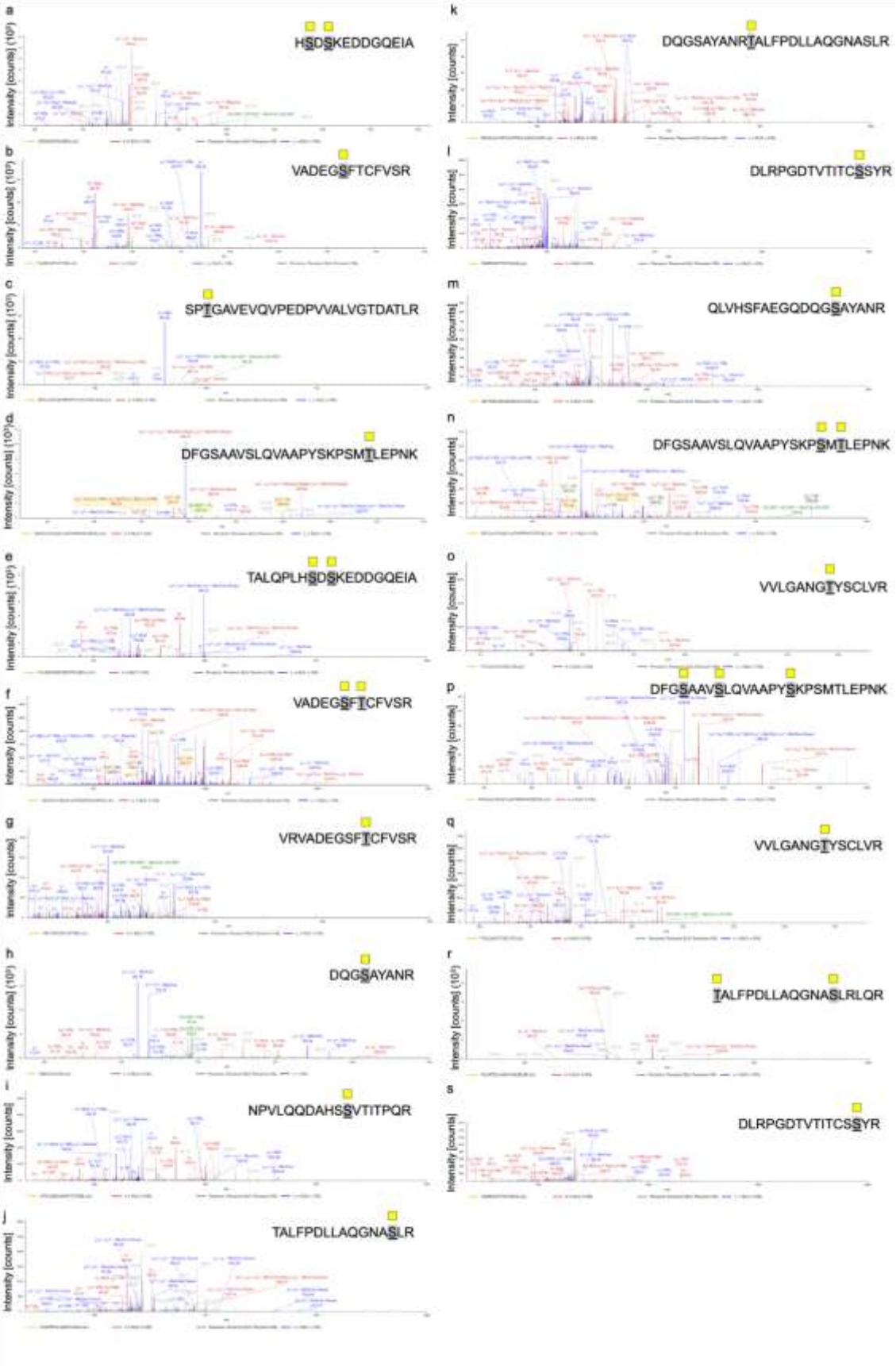
a
HSDSKEDDGQEIA
b
VADEGSFTCFVSR
c
SPTGAVEVQVPEDPVVALVGTDATLR
d
DFGSAAVSLQVAAPYSKPSMTLEPNK
e
TALQPLHSDSKEDDGQEIA
f
VADEGSFTCFVSR
g
VRVADEGSFTCFVSR
h
DQGSAYANR
i
NPVLQQDAHSSVTITPQR
j
TALFPDLLAQGNASLR
k
DQGSAYANRTALFPDLLAQGNASLR
l
DLRPGDTVTITCSSYR
m
QLVHSFAEGQDQGSAYANR
n
DFGSAAVSLQVAAPYSKPSMTLEPNK
o
VVLGANGTYSCLVR
p
DFGSAAVSLQVAAPYSKPSMTLEPNK
q
VVLGANGTYSCLVR
r
TALFPDLLAQGNASLRLQR
s
DLRPGDTVTITCSSYR
Intensity [counts]

Figure S7. Figure S6. CID-MS/MS spectra of CD276 glycopeptides bearing immature O-glycosylation in CRC patient samples. Representative collision-induced dissociation (CID) MS/MS spectra of CD276-derived glycopeptides identified in CRC samples from our proteomics dataset (PRIDE accession: XXXX). The spectra exhibit characteristic oxonium ions, as well as extensive b-, y-, and internal fragment ions typical of CID fragmentation, enabling high sequence coverage while retaining the HexNAc (Tn antigen) on the peptide backbone (yellow square). Due to its small size and relative stability, the Tn antigen is often conserved on b- and y-ions during CID fragmentation, enabling unambiguous localization of O-glycosylation sites for these glycopeptides. Glycopeptides were confidently assigned and manually validated. These data provide direct in vivo evidence that CD276 is a carrier of immature O-glycans in CRC, reinforcing its role as a clinically relevant glycoprotein affected by aberrant glycosylation in the tumor microenvironment.

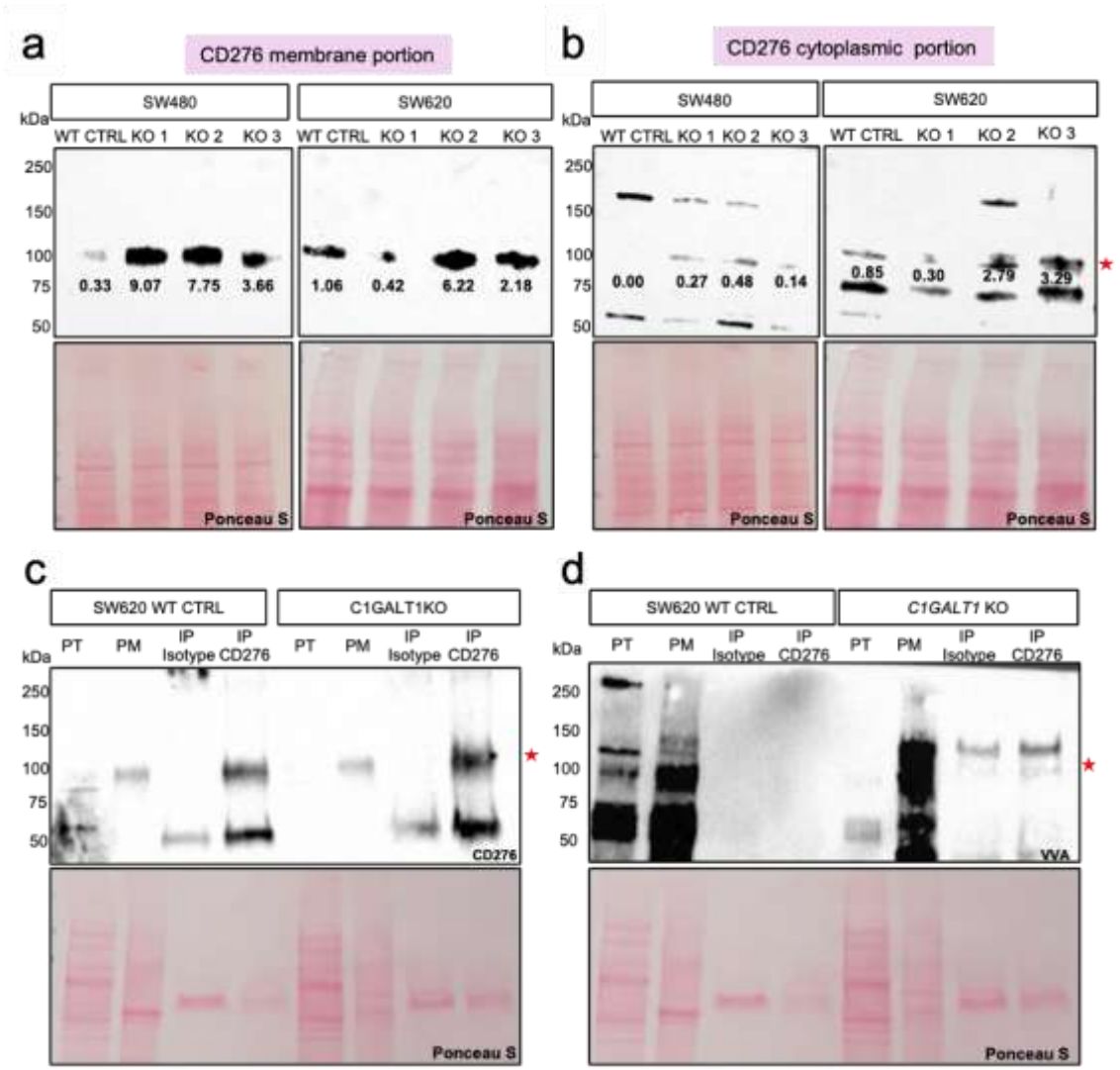

Figure S8. CD276 expression in glycoengineered *C1GALT1* KO SW480 AND SW620 cell lines. Western blot analysis shows increased expression of CD276 in cell models, both in the membrane portion (**a**) and the cytoplasmic portion (**b**). Western blotting of immunoprecipitated CD276 detected a clear ~100 kDa band in *C1GALT1* KO samples, confirming the success of the IP and increased expression of CD276 glycoproteoforms in KO cells (**c**). VVA lectin blotting was also performed to assess Tn antigen on CD276, confirming the presence of immature glycoforms (**d**). Ponceau S staining was used to verify equal protein loading.

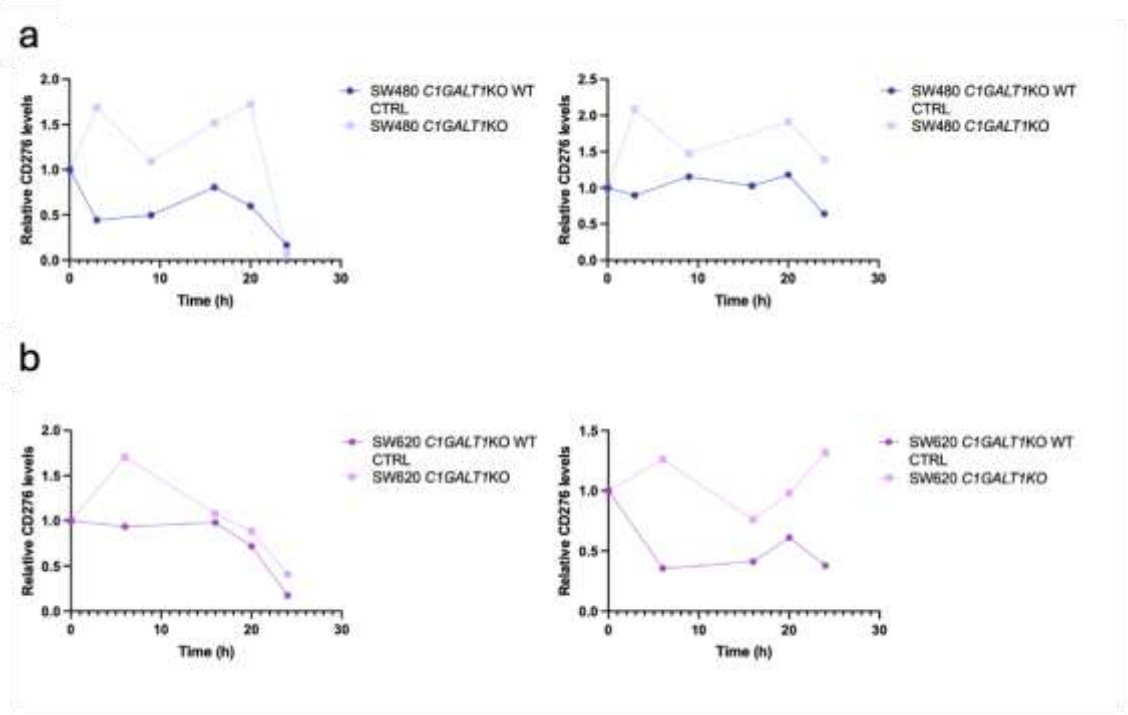

Figure S9. Figure S8. CD276 protein stability in C1GALT1 knockout vs. wild-type CRC cells following cycloheximide treatment. Relative CD276 levels were measured by immunoblot over a 24-hour time course following treatment with cycloheximide (CHX) to block protein synthesis. (a) SW480 and (b) SW620 cells with C1GALT1 knockout (KO) or wild-type (WT) backgrounds were compared. In both cell lines, CD276 levels decline more rapidly in WT cells, while CD276 is relatively stabilized in the C1GALT1 KO context, suggesting that immature O-glycosylation impairs CD276 turnover. These graphs complement the main manuscript data and further support the role of O-glycan truncation in stabilizing CD276 protein.

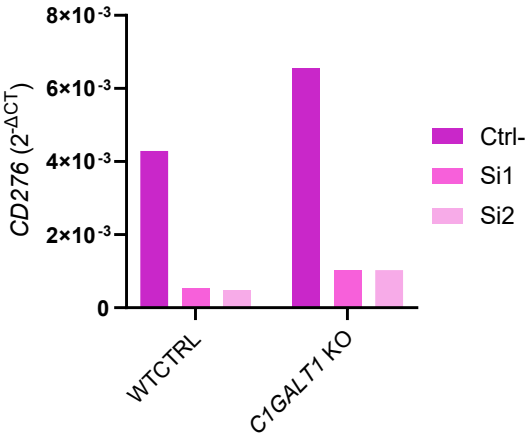

Figure S10. *CD276* silencing using siRNA technology in SW480 C1GALT1 KO models. CD276 siRNA decreased *CD276* gene expression by 88% in comparison to controls.

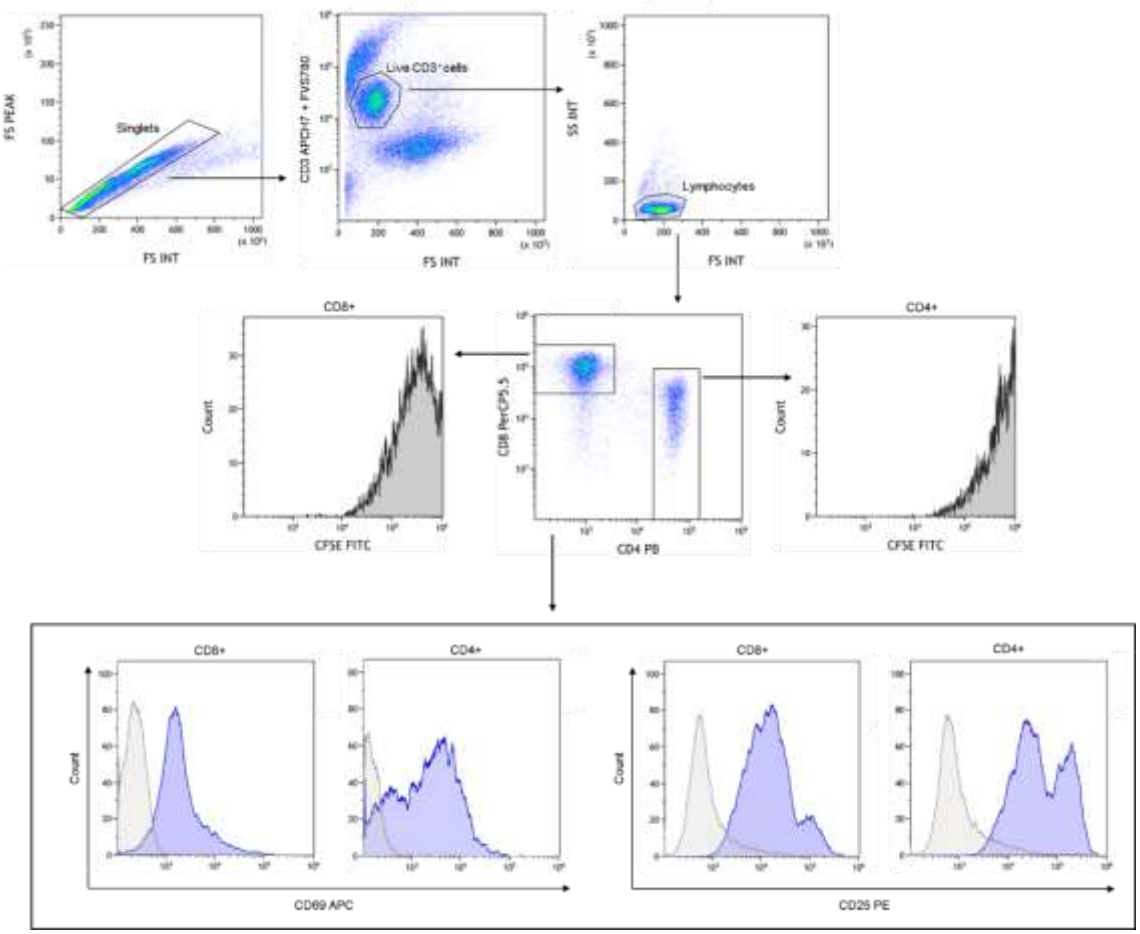

Supporting Figure 11. Flow cytometric gating strategy to evaluate T cell activation and proliferation in co-culture settings with tumour cells. Singlets were selected according to forward scatter-height (FSC-H) versus forward scatter-area (FSC-A). Then, live CD3 positive cells were isolated according to Fixable Viability Stain 780 (FVS780), CD3 expression, size (FSC-A) and granularity characteristics (side scatter-area (SSC-A)). Gated on T cells (CD3+ lymphocytes), CD4+ and CD8+ T cell subsets were identified. For each subset (CD4+ and CD8+), histograms of CFSE expression allowed the evaluation of T cell proliferation by CFSE dilution over each cell division during the 5 days of co-culturing. To investigate the impact of CD276-Tn in T cell activation, early and late activation markers (CD69 and CD25, respectively) were evaluated on CD4+ and CD8+ T cells. Fluorescence minus one (FMO) controls were used to set the gates for CD25 and CD69 positive populations.

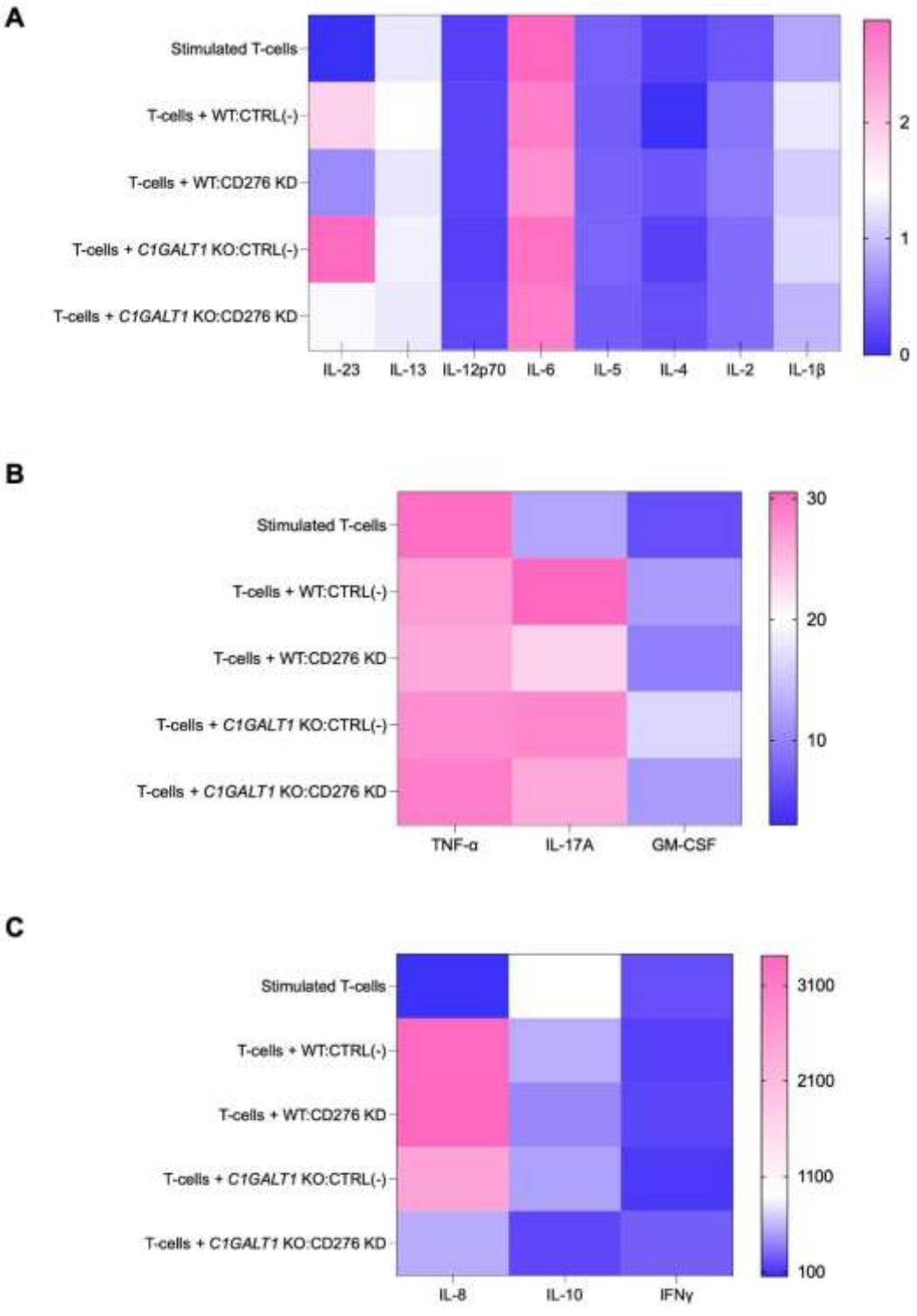

Figure S7. Cytokine secretion profiles of T cells co-cultured with *C1GALT1*-deficient CRC cells, with or without CD276 knockdown. Heatmaps depicting the levels of cytokines secreted by stimulated human T cells co-cultured with either wild-type (WT) or *C1GALT1* knockout (KO) SW620 cells, in the presence

or absence of CD276 knockdown (CD276 KD). **A) Immature O-glycosylation in cancer cells disrupts the cytokine environment that supports T cell activation and polarization.** Analysis of Th2/regulatory cytokines (IL-23, IL-13, IL-12p70, IL-6, IL-5, IL-4, IL-2, IL-1β) reveals that *C1GALT1* KO cells suppress cytokine production relative to WT controls, with partial restoration of secretion upon CD276 knockdown, notably for IL-12p70 and IL-6. **B) The loss of O-glycan extension suppresses pro-inflammatory T cell responses, a defect that is partly reversed by targeting CD276.** Pro-inflammatory cytokines (TNF-α, IL-17A, GM-CSF) are reduced in C1GALT1 KO co-cultures compared to WT, while CD276 knockdown in this background restores TNF-α and GM-CSF levels to those comparable with, or higher than, WT controls. **C) Aberrant glycosylation of CD276 reshapes the cytokine landscape, dampening both innate and adaptive immune outputs.** Cytokines associated with innate and immune regulatory responses (IL-8, IL-10, IFN-γ) show a similar trend, with marked suppression in the *C1GALT1* KO condition and partial or full rescue of IL-8 and IL-10 upon CD276 knockdown. Together, these results suggest that loss of core 1 O-glycosylation in cancer cells broadly suppresses T cell cytokine responses, an effect partially mediated by CD276. Its silencing restores specific immune functions, implicating immaturely glycosylated CD276 as a key modulator of T cell activity.

Table S1. Clinicopathological information of CRC samples used for glycomics analysis.

Sample	Clinical Stage	T	N	M	Molecular classification
H1	-	-	-	-	-
H2	-	-	-	-	-
M	II	T3	N0	M0	Mesenchymal
E	III	T3	N1	M0	Epithelial
F	III	T3	N1	M0	Epithelial
A	IV	T4	N2	M1	Epithelial
C	IV	T4	N2	M1	Epithelial
D	IV	T4	N2	M0	Epithelial
J	III	T3	N2	M0	Mesenchymal
L	III	T3	N2	M0	Mesenchymal
I	IV	T3	N3	M1	Mesenchymal
H	IV	T3	N2	M1	Mesenchymal
B	IV	T3	N1	M1	Epithelial
G	IV	T3	N1	M1	Mesenchymal

Table S2. Mass spectrometry-based characterization of the O-glycome expressed by the analysed colorectal tumours and healthy colon tissues.

Glycans	Permethylated Reduced end	Permethylated Free reducing end	Healthy colon		Colorectal tumours											
					Epithelial						Mesenchymal					
	[M + H]+	$[M + H]^+$	H1	H2	A	B	C	D	E	F	G	H	I	J	L	M
	308,21	292,18	0,00	0,00	0,00	0,00	0,00	3,77	18,69	24,10	0,00	0,00	0,00	0,00	0,00	0,00
	512,31	496,28	0,00	3,36	2,41	4,75	0,95	14,57	17,48	23,08	1,96	4,30	0,00	26,05	32,22	4,08
	553,33	537,30	11,77	0,00	0,00	0,00	0,00	4,55	4,67	3,79	0,00	0,00	0,00	3,48	0,00	0,00
	669,38	653,35	5,13	28,04	18,20	0,00	24,77	15,08	19,12	16,99	2,15	6,75	10,08	7,36	10,56	70,37
	686,40	670,36	3,95	0,00	0,00	0,00	0,00	1,18	3,04	0,00	0,00	7,78	0,00	2,98	0,00	0,05
	757,43	741,40	0,00	0,00	3,53	7,70	1,74	6,27	7,85	0,00	0,00	3,50	0,00	0,00	0,00	0,00
	798,46	782,43	0,00	0,00	0,00	0,00	0,00	0,08	0,00	0,00	0,00	0,00	0,00	0,00	0,00	0,00
	873,48	857,45	3,30	6,95	24,26	32,18	17,76	20,50	21,60	19,48	35,72	26,17	44,85	28,52	50,14	10,57

	914,51	898,48	72,95	60,97	22,93	0,00	28,41	25,76	2,38	12,56	0,80	16,25	15,07	29,42	1,33	14,66
	931,52	915,49	2,90	0,00	0,00	1,31	0,00	2,25	1,25	0,00	0,00	6,43	0,00	0,00	0,00	0,00
	961,53	945,50	0,00	0,00	0,00	5,76	0,74	1,32	0,32	0,00	1,01	0,00	0,00	0,00	1,50	0,00
	1047,57	1031,54	0,00	0,00	1,85	5,49	6,26	0,00	0,00	0,00	3,29	2,05	0,00	0,00	0,00	0,00
	1118,61	1102,58	0,00	0,46	6,88	5,40	3,48	2,36	2,94	0,00	9,87	6,36	0,00	2,19	0,00	0,00
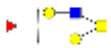	1135,62	1119,59	0,00	0,00	0,00	3,54	0,78	0,42	0,67	0,00	0,00	0,00	0,00	0,00	0,00	0,00
	1165,63	1149,60	0,00	0,00	0,00	1,03	0,00	0,00	0,00	0,00	0,00	0,00	0,00	0,00	0,00	0,00
	1206,66	1190,63	0,00	0,00	0,00	1,47	0,00	0,00	0,00	0,00	0,00	0,00	0,00	0,00	0,00	0,00
	1234,65	1218,62	0,00	0,00	10,84	18,30	4,25	0,20	0,00	0,00	22,30	9,02	28,19	0,00	4,24	0,26
	1292,70	1276,66	0,00	0,22	2,32	0,41	2,44	1,34	0,00	0,00	0,99	2,64	0,00	0,00	0,00	0,00

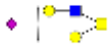	1322,71	1306,68	0,00	0,00	1,11	5,43	1,63	0,14	0,00	0,00	4,48	4,44	0,00	0,00	0,00	0,00
	1363,73	1347,70	0,00	0,00	0,00	0,00	0,75	0,06	0,00	0,00	0,00	0,00	0,00	0,00	0,00	0,00
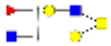	1380,75	1364,72	0,00	0,00	0,00	0,83	0,00	0,00	0,00	0,00	0,00	0,00	0,00	0,00	0,00	0,00
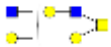	1410,76	1394,73	0,00	0,00	0,00	0,87	0,00	0,00	0,00	0,00	0,00	0,00	0,00	0,00	0,00	0,00
	1479,78	1463,75	0,00	0,00	0,32	0,00	0,12	0,00	0,00	0,00	0,00	0,00	0,00	0,00	0,00	0,00
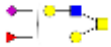	1496,80	1480,76	0,00	0,00	1,01	1,69	1,59	0,15	0,00	0,00	3,34	0,29	0,00	0,00	0,00	0,00
	1537,82	1521,79	0,00	0,00	0,00	0,00	0,80	0,00	0,00	0,00	0,00	0,00	0,00	0,00	0,00	0,00
	1584,85	1568,82	0,00	0,00	0,00	0,27	0,00	0,00	0,00	0,00	0,00	0,00	0,00	0,00	0,00	0,00

	1653,87	1637,84	0,00	0,00	1,35	0,00	1,71	0,00	0,00	0,00	0,10	0,00	0,00	0,00	0,00	0,00
	1683,88	1667,85	0,00	0,00	1,15	3,09	0,47	0,00	0,00	0,00	5,99	4,03	1,45	0,00	0,00	0,00
	1724,91	1708,88	0,00	0,00	0,18	0,00	0,07	0,00	0,00	0,00	0,00	0,00	0,00	0,00	0,00	0,00
	1741,92	1725,89	0,00	0,00	0,00	0,24	0,10	0,00	0,00	0,00	0,40	0,00	0,00	0,00	0,00	0,00
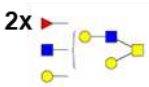	1758,94	1742,91	0,00	0,00	0,00	0,08	0,00	0,00	0,00	0,00	0,00	0,00	0,00	0,00	0,00	0,00
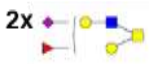	1857,97	1841,94	0,00	0,00	1,67	0,13	1,18	0,00	0,00	0,00	7,60	0,00	0,36	0,00	0,00	0,00
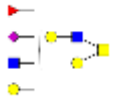	1946,02	1929,99	0,00	0,00	0,00	0,02	0,00	0,00	0,00	0,00	0,00	0,00	0,00	0,00	0,00	0,00

Table S3. Tn/STn immunohistochemical evaluation in CRC tumours

	Tn antigen positive		STn antigen positive	
	n (%)	*p* value	*n* (%)	*p* value
Stage				
I	0 (0.0)	0.187	1 (100.0)	0.881
II	0 (0.0)		4 (100.0)	
III	4 (50.0)		9 (90.0)	
IV	5 (20.0)		22 (88.0)	
Tumour (T)				
T1	0 (0.0)	0.350	0 (0.0)	**0.023**
T2	0 (0.0)		1 (100.0)	
T3	9 (31.0)		28 (90.3)	
T4	0 (0.0)		6 (100.0)	
Lymph node metastasis (N)				
N0	2 (18.2)	0.670	9 (81.8)	0.348
N1	3 (27.3)		10 (83.3)	
N2	4 (30.8)		14 (100.0)	
N3	0 (0.0)		3 (100.0)	
Distant metastasis (M)				
M0	4 (28.6)	0.699	15 (93.8)	0.638
M1	5 (20.8)		21 (87.5)	
Tumour location				
Right colon	2 (28.6)	0.698	7 (100.0)	0.602
Left colon	6 (26.1)		20 (87.0)	
Rectum	1 (12.5)		9 (90.0)	
Cases frequency	9 (24.0)		36 (90.0)	

Table S4. Mass spectrometry-based characterization of the O-glycome expressed by different colorectal cancer cell lines.

Glycans	$[M + H]^+$	Human cells				
		SW620	HCT116	RKO	HCA7	SW480
	572.31	23,90	20,15	21,89	0,00	3,97
	613.33	2,32	11,58	18,71	95,55	66,11
	729.38	0,28	1,42	0,00	0,00	0,00
	746.40	1,20	0,00	14,22	0,00	0,00
	817.43	5,39	3,46	3,53	0,00	0,00
	933.48	12,81	20,50	13,74	2,27	15,50
	991.52	4,51	0,00	2,28	0,00	4,55
	1021.53	18,90	9,67	5,88	0,00	0,00
	1062,56	0,16	0,00	0,00	0,00	0,00
	1178.61	0,66	3,46	0,83	0,00	0,00
	1195.62	15,24	0,00	5,19	0,00	2,55
	1225.63	2,49	0,00	0,72	0,00	0,00
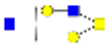	1266,66	0,65	1,15	0,00	0,00	0,00
	1294.65	3,91	9,68	5,47	2,18	5,89
2x 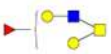	1369.71	0,37	0,00	0,00	0,00	0,46
	1382.71	2,33	10,85	2,93	0,00	0,26

	1440.75	0,74	0,00	0,22	0,00	0,14
	1470.76	1,34	1,86	0,63	0,00	0,00
	1556.80	0,46	0,00	1,86	0,00	0,50
	1586.81	0,00	0,00	0,13	0,00	0,00
	1627.83	0,00	0,49	0,00	0,00	0,00
	1644.85	1,82	0,00	0,52	0,00	0,00
	1743.88	0,08	3,80	0,89	0,00	0,00
2x 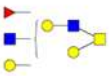	1818.94	0,37	0,00	0,19	0,00	0,06
	1831.93	0,08	1,92	0,10	0,00	0,00
2x 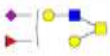	1917.97	0,00	0,00	0,08	0,00	0,00

Table S5. List of antibodies employed in the different immunoassays performed in this study and respective experimental conditions.

Antibody/ Lectin	Application	Dilution	Origin	Immunogens/ Targets
Rabbit Monoclonal to CD276	WB, IHC, PLA	1/500, 1/1500, 1/1500	ab219648 (Abcam)	Recombinant fragment within human CD276 aa 29-466
Rabbit Polyclonal to CD276	WB	jan/50	PA5-141121 (Thermo Fisher Scientific)	Recombinant protein within human CD276 280-500 aa
Rabbit Polyclonal to CD276	IP, IF	3 µg, 1/250	PA5-80426 (Thermo Fisher Scientific)	Recombinant protein within human CD276 1-461 aa
Biotinylated VVA lectin	WB, IHQ	1/10000, 40 µg/mL	B-1235-2 (Vector Laboratories)	α- or β-linked terminal N-acetylgalactosamine structures
FITC-labeled VVA lectin	FC, IF	0.01 µg/µL, 40 µg/mL	FL-1231-2 (Vector Laboratories)	α- or β-linked terminal N-acetylgalactosamine structures
FITC-labeled PNA lectin	FC	0.02 µg/µL	FL-1071 (Vector Laboratories)	Gal (β-1,3) GalNAc structures
Mouse monoclonal to tag 72	FC, IHC, PLA	0.01 µg/µL, 0.5 µg/mL, 0.5 µg/mL	ab199002 (Abcam)	Tag-72

Anti-CD3	FC	10 µg/mL	300313 (BioLegend)	T-cell surface glycoprotein CD3 delta chain
Anti-CD28	FC	2 µg/mL	302913 (BioLegend)	T-cell-specific surface glycoprotein CD28
Fixable Viability Stain 780 dye	FC	0,73611111	565388 (BD Bioscience)	-
Anti-CD4-PB	FC	01:25	B49197 (Beckman Coulter)	CD4
Anti-CD25-PE	FC	4 in 50 µL	341011 (BD Bioscience)	Human Phytohemagglutinin-activated T Cells
Anti-CD8-PerCP-Cy5.5	FC	3.5 in 50 µL	341050 (BD Bioscience)	Human Peripheral Blood T Cells
Anti-CD69-APC	FC	01:25	310910 (BioLegend)	Early activation antigen CD69
Anti-CD3-APC-H7	FC	1.5 in 50 µL	641415 (BD Bioscience)	T-cell surface glycoprotein CD3 epsilon chain
Alexa Fluor 488 Anti-Mouse IgG	FC	1/300	A11001 (Thermo Fisher Scientific)	-
Alexa Fluor 594 Anti-Rabbit IgG	IF	1/300	A11012 (Thermo Fisher Scientific)	-
Rabbit IgG isotype	IP	same as anti-CD276	LTI-02-6102 (Thermo Fisher Scientific)	-
Anti-Rabbit IgG HRP	WB	1/60000	656120 (Thermo Fisher Scientific)	-

Anti-Mouse IgG HRP	WB	1/70000	115-035-205 (Thermo Fisher Scientific)	-

WB – Western Blot; IHC – Immunohistochemistry; FC – Flow Cytometry; PLA – Proximity Ligation Assay; IF – Immunofluorescence; IP - Immunoprecipitation

P.PORTO

ESCOLA SUPERIOR DE SAÚDE

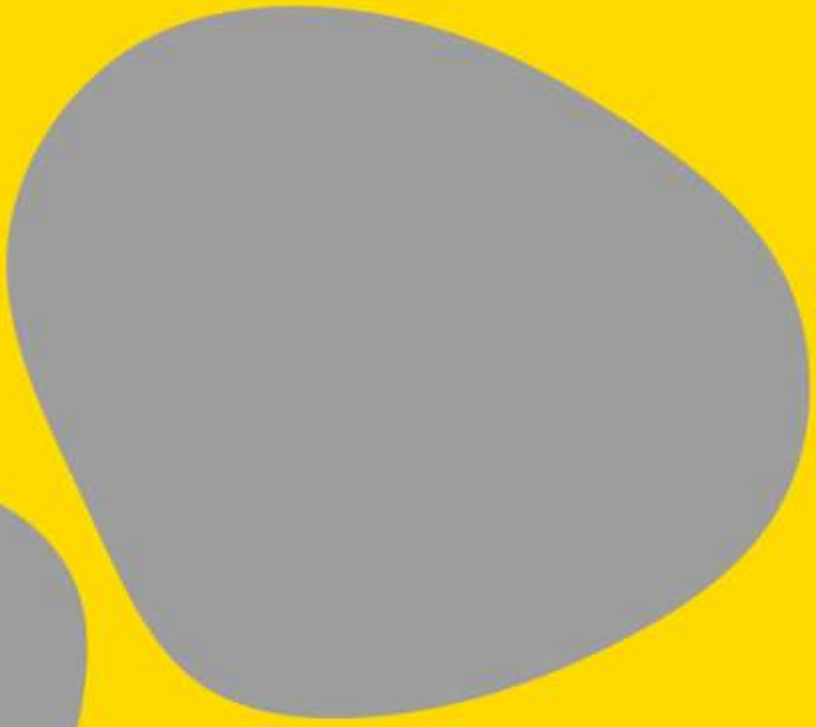

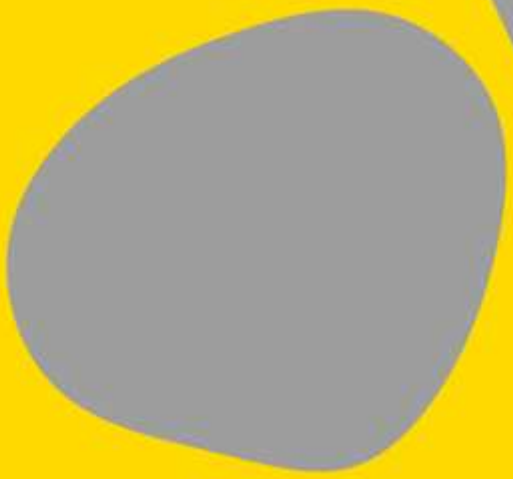

M MESTRADO

DESIGNAÇÃO DO MESTRADO